A METHODOLOGY FOR OPTIMAL PLACEMENT OF DISTRIBUTED GENERATION ON MESHED NETWORKS TO REDUCE POWER LOSSES FOR TIME VARIANT LOADS

S Malapermal

Student Number: 891131229

Dissertation submitted in partial fulfilment of the requirements for the degree of

Master of Science in Power and Energy

College of Agriculture, Engineering and Science

University of KwaZulu - Natal

Academic Supervisor: Dr IE Davidson

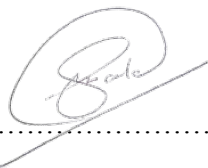Industrial Supervisor: Mr MM Bello

2015

COLLEGE OF AGRICULTURE, ENGINEERING AND SCIENCE

DECLARATION 1 - PLAGIARISM

I, Sanjian Malapermal student number 891131229 declare that:

1. The research reported in this dissertation, except where otherwise suggested is my original research.

2. This dissertation has not been submitted for any degree or examination at any other university.

3. This dissertation does not contain other persons' data, pictures, graphs or other information, unless specifically acknowledged as being sourced from other persons.

4. This dissertation does not contain other persons' writing, unless specifically acknowledged as being sourced from other researchers. Where other written sources have been quoted, then:
a. Their words have been re-written but the general information attributed to them has been referenced
b. Where their exact words have been used, then their writing has been placed in italics and inside quotation marks, and referenced.

5. This dissertation does not contain text, graphics or tables copied and pasted from the Internet, unless specifically acknowledged, and the source being detailed in the dissertation and in the References sections.

Signed

…………………………………………

S Malapermal Pr. Eng. (20000326)

24 November, 2015

Durban, South Africa

COLLEGE OF AGRICULTURE, ENGINEERING AND SCIENCE

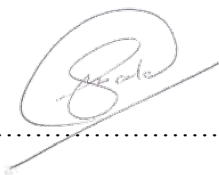# DECLARATION 2 - PUBLICATION

Publication presented at SAUPEC 2016

Session 2D1

A Methodology for Optimal Placement of Distributed Generation on Meshed Networks to Reduce Power Losses for Time Variant Loads

S. Malapermal, M.M. Bello, I.E. Davidson

Signed

…………………………………….

S Malapermal Pr. Eng. (20000326)

24 November 2015

Durban, South Africa

ACKNOWLEDGEMENTS

ABSTRACT

In the 21st century, humanity's thirst for an energy intensive lifestyle has led to the saturated expansion of the modern day power system. As the power system expands, centralised generation philosophies are rapidly being constrained due to increased technical losses. The inability to balance technical, economic and environmental conventional generation needs place further strain on the power system. This constraint has catalysed the emergence of decentralized renewable energy sources. Distributed generation supplements the electrical needs of a rapidly expanding demand for energy and minimises the adverse environmental impact of fossil fuel power stations.

Distributed Generation is defined as electric power generation units connected close to load centres. Distributed generation can be classified according to rating, purpose, technology, environmental impact, mode of operation and penetration. Optimally connected distributed generation have many advantages over classically supplied power systems. Such as reduced power losses, improve voltage support and reliability to the system. Deferring network upgrades by relieving congestion and reducing greenhouse gas emission being some of the benefits of integrated distributed generation.

This research delivers an optimal placement method of solar photovoltaic distributed generation on a 56 bus utility network to reduce power losses. Critical electrical factors for optimal placement of distributed generation to reduce power losses are defined. A practical loss optimization technique for optimal placement of distributed generation on meshed networks is defined. The technique follows an approach of ranking, profiling, activating, evaluating and finally selecting the optimally placed distributed resources. The importance of reactive power compensation is examined when integrating distributed generation onto meshed networks. Pre and post distributed solar photovoltaic generation placement shows the worsening phase angles leading to poorer power factors. The research demonstrates the impact of penetration and concentration of distributed generation on power system losses. Highly concentrated placement of non-dispatched distributed generation units lead to increase in power losses.

Results conclude that the placement of distributed generation for loss reduction on a meshed power system is optimally located to match load-profiled centres. This research is significant as power utility engineers can now benefit from a wider range of skills to assess the impact of DG connections.

TABLE OF CONTENTS

LIST OF TABLES

LIST OF FIGURES

LIST OF ACRONYMS

Acronym	Description
BW	Bid Window
CCGT	Closed Cycle Gas Turbine
CO2	Carbon Dioxide
CREZ	Competitive Renewable Energy Zones
CSP	Concentrated Solar Power
DFIG	Doubly Fed Induction Generator
DG	Distributed Generation
DOE	Department of Energy
DPF	DIgSILENT Power Factory
DPL	DIgSILENT Programming Language
EG	Embedded Generation
EHV	Extra High Voltage
ERCOT	Electric Reliability Council of Texas
EWS	Efficient World Scenario
GCCA	Generation Capacity Connection Assessment
GW	Giga Watt
HV	High Voltage
ICT	Information and Communication Technology
IEA	International Energy Agency
IEC	International Electrotechnical Commission
IEEE	Institute of Electrical and Electronic Engineers
IPP	Independent Powr Producer
IRP	Integrated Resource Plan
MOPI	Multi Objective Performance Index
MPSI	Maximum Power Stability Index
MTS	Main Transmission Station
MV	Medium Voltage
MVA	Mega Volt - Amp
MVAr	Mega Volt - Amp reactive
MW	Mega Watt
OCGT	Open Cycle Gas Turbine
p.u	per unit

Acronym	Description
PEV	Plug-in Electric Vehicle
POC	Point of Connection
PSO	Partical Swarm Optimization
PV	Photo-Voltaic
QDS	Quasi-Dynamic Simulation
R/X	Resistance / Reactance
RE	Renewable Energy
REDZ	Renewable Energy Development Zones
REFIT	Renewable Energy Feed in Tariff
REI4P, REIP4, REIPPPP	Renewable Energy Independent Power Producer Procurement Programme
RPCC	Reactive Power Capability Curve
RPPs	Renewable Power Plant
SIL	Surge Impedance Loading
TSS	Time Simulation Study
USD	United States Dollar
ZIP	Constant Impedance, Current, Power Load

1   INTRODUCTION

This introductory chapter highlights the importance of renewable energy (RE) to power utilities. Renewable energy have two main drivers; to reduce greenhouse gas and in the South African Electricity Supply Industry to speed up the shortfall of generation capacity. Pursuant sections provide a global and local outline of renewable energy developments. This highlights the rate and impact of RE for which power utilities must display their readiness to connect alternate forms of generation onto the power system.

1.1   World energy outlook

The International Energy Agency (IEA) developed three energy outlook scenario plans. These plans consider perpetuating fossil fuel as a source of energy and the impact on greenhouse gas (GHG) that threatens global warming. These are "Current Policy Scenario", the "New Policy Scenario" (NPS), and the "450 ppm CO_2 equivalent" scenario (450). These scenarios are based on World Energy Models and replicate the dynamics of energy markets [1].

Figure 1-1 shows the demand base - share of primary energy sources in the world as recorded in 2010 with two future model predictions for 2020 and 2035.
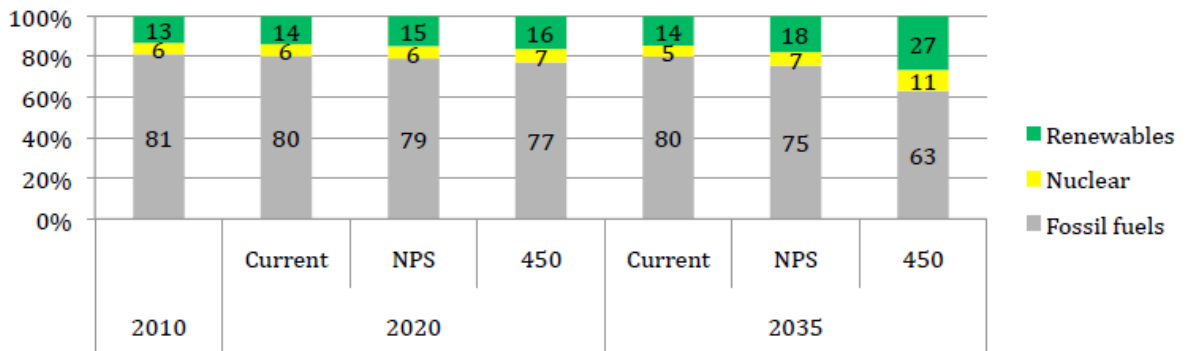
Figure 1-1 – Demand Base – Share of Primary Energy Sources: Source [1]

Predictions from the "450" scenario to reduced greenhouse gas by 2035 requires renewable energy sources grow from 13% to 27%. The share of energy sources translates from the scenario prediction to the technology mix for each scenario as shown in Figure 1-2.
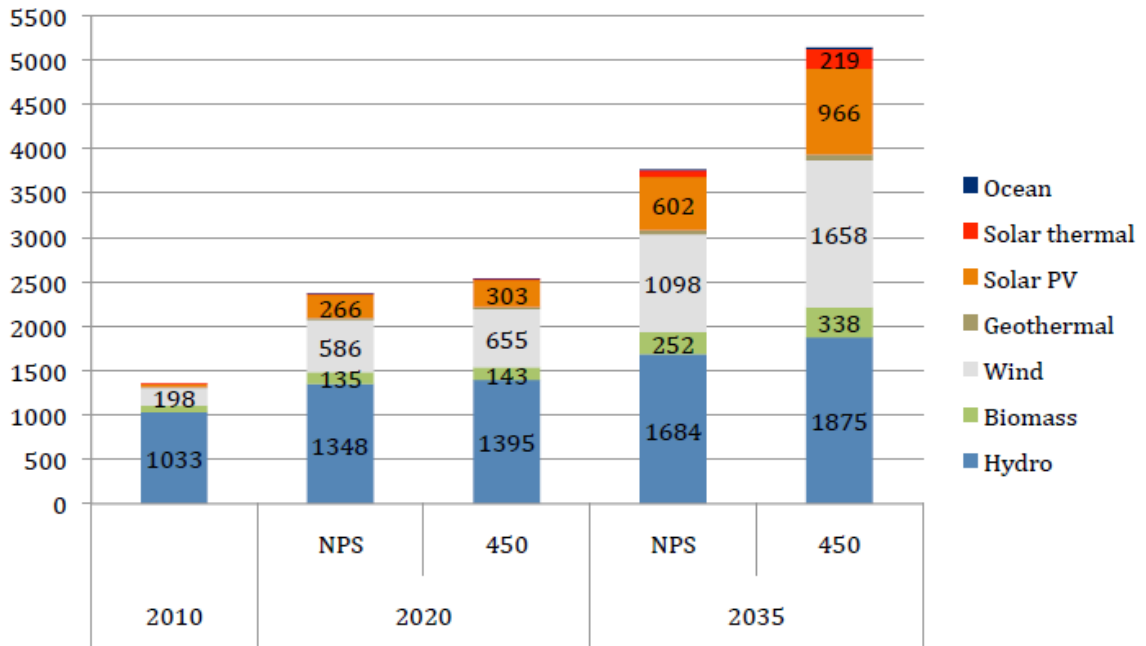
Figure 1-2 Global Cumulative Renewable Energy Capacity (GW) : Source [1]

1.2 International demand for renewable energy

The UN Secretary-General's initiative "Sustainable Energy for All" mobilises global action to achieve universal access to modern energy services. This resulted in launch of "Decade of Sustainable Energy for All (2014 – 2024)". The Renewable Energy Policy Network for the 21st Century (REN21) aims to document the "Sustainable Energy for All" initiative towards achieving these objectives [1].

In 2013 renewable energy provided an estimated 19.1% of global energy with growth in capacity and generation continuing to expand in 2014. The power sector dominated this growth increase with wind, solar PV and hydropower making up the mix.

Table 1-1 shows the global RE technology mix delivered up to 2014, with $270 billion USD invested in 657 GW of installed capacity.

Table 1-1: Global Investment and Capacity (GW) Commitment: [1]

		Started 2004	2013	2014
Investment				
New Investment (annual) in renewable power and fuels	Billion USD	45	232	270

Power				
Renewable power capacity (total, excl. Hydro)	GW	85	560	657
Renewable power capacity (total, excl. Hydro)	GW	800	1,578	1,712
Hydropower capacity	GW	715	1,018	1,055
Bio-power capacity	GW	<36	88	93
Geothermal capacity	GW	8.9	12.1	12.8
Solar PV capacity (total)	GW	2.6	138	177
Concentrated solar thermal	GW	0.4	3.4	4.4
Wind power capacity (total)	GW	48	319	370

1.3   South African demand for renewable energy

The Department of Energy (DOE) governs the South Africa's energy market. Initial attempts to integrated the monopolized power utility through the launch of the Renewable Energy Feed in Tariff (REFIT) [2], were unsuccessful. Technical considerations in the South African Grid Code Requirements for Renewable Power Plants [3] that ensure regulatory compliance. Bello describes [2] the changing power system landscape; technical skills needed by engineers to face the wave of independent power producer (IPP) applications to the power grid.

Department of Energy's RE policy launched the Renewable Energy Independent Power Producer Procurement Programme (REI4P) [4]. The Integrated Resource Plan (IRP 2010 – 2030) [5] defines the technology mix of energy for the power system over the next 20 years.

1.3.1   Capacity and sizing alternatives

Table 1-2 shows the provision of capacity (sizing) across the technology mix in the IRP 2010-2030. The IRP assigns renewable energy capacity (size) and the DOE adjudicates location through the preferred bidder's connection process. Plans have set in motion to connect more than 9770MW of solar PV to the grid by 2030.

Table 1-2 – Capacity Options for Technology Mix over IRP Horizon [5]

Technology Options	IRP 2010 – Capacity (MW)	IRP 2030 – Capacity (MW)
Existing Coal	34746	36230
New Coal	6250	2450
CCGT	2370	3550
OCGT / Gas Engines	7330	7680
Hydro Imports	4109	3000
Hydro domestic	700	690
PS (Incl. Imports)	2912	2900
Nuclear	11400	6660
PV	8400	9770
CSP	1200	3300
Wind	9200	4360
Other	915	640
Total	89532	81350

Table 1-3 integrates small-scale roof top PV generation and extends the intent of connecting 25GW of solar PV to the grid by 2050.

Table 1-3 Technology Options arising from the Rooftop PV [5]

Technology Options	Moderate Decline	Rooftop PV	Moderate Decline	Rooftop PV
Existing Coal	36230	36230	16120	16120
New Coal	2450	2450	12700	13450
CCGT	3550	2840	9230	10650
OCGT / Gas Engines	7800	13440	11400	17160
Hydro Imports	3000	3000	3000	3000
Hydro domestic	690	690	690	690
PS (Incl. Imports)	2900	2900	2900	2900
Nuclear	6660	3460	20800	17600
Embedded PV	-	21617	-	29778
PV (additional)	9630	8770	25000	24930
CSP	3300	700	10900	4000
Wind	4250	3790	10680	10870
Other	640	640	-	-
Total	81100	100527	123420	151148

These options form the basis of the IRP and cost efficiencies will impact supply chain resources.

1.3.2 Location options

Figure 1-3 shows the location options for preferred bidders in bid-window 1-3.
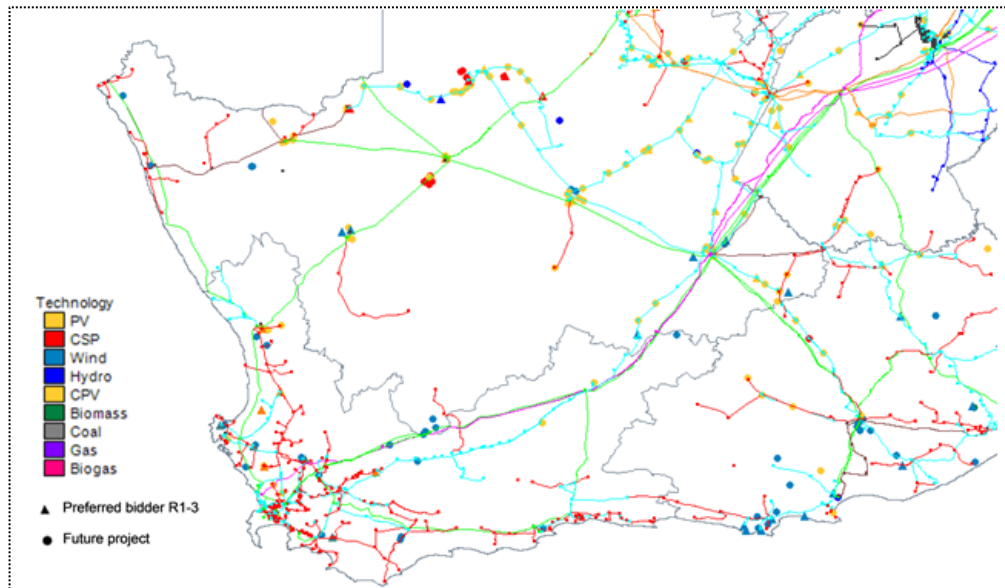
Figure 1-3 Independent Power Producers BW 1-3 [6]

Figure 1-3 shows the Eskom power system as a backdrop to the IPP technology mix. Scattered positioning of preferred bidders aggravates sustainable end-state planning. The Electric Reliability Council of Texas (ERCOT) [7] and Competitive Renewable Energy Zones (CREZ) [8] have chartered the way in REDZ development. Figure 1-4 define the South African equivalent Renewable Energy Development Zones (REDZ) [9] to mitigate multiple points of connection to the grid.
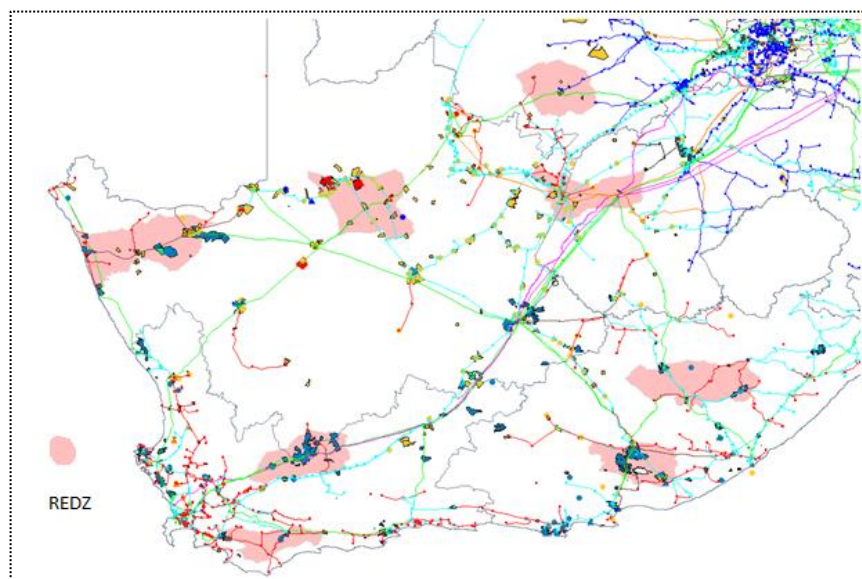
Figure 1-4 Development of REDZ [9]

1.3.3 South Africa's investment in renewable energy

Financial investment in Renewable Energy Bid Windows 1-3 has seen more that R192 billion [10] committed to the REIPP Procurement Programme.

1.3.4 Renewable power plant network assessment challenges

A challenging result of the REI4P is the scattered division of preferred bidders. This inhibits end-state capacity sizing and network planning. Current preferred bidder announcements as single entity connections to the grid are technically undesirable. Collective cluster announcements are preferred for sustainable long term planning. Long-term equipment sizing and rating vary for single entity connections compared with multiple connections. The uncertainty of future preferred bidder locations inhibit optimal power system planning and design.

Eskom's greatest challenge over the next decade will be the shortage of generating capacity. The current generation fleet is ageing. Eskom lack the ability to fund its new build programme. The DOE's acceleration of REI4P is commitment to bringing Renewable Power Plants (RPPs) on line to support the state owned utility. The accelerated connection plan and technical impact of RE capacity onto the Eskom power system has led to defining the following research questions 1.5.

1.4 Research hypothesis

Are the current IPPs optimally and strategically connected onto the electric grid to reduce power losses given the generation and financial constraints faced by Eskom?

1.5 Research questions

- What critical electrical factors determine the optimal placement of DG to reduce power losses?
- What practical loss optimization power flow method can be applied to place DG on meshed networks?
- What is the importance of reactive power control for the integration DG?
- How does DG penetration and concentration affect power system losses?

1.6 Objectives and approach

The research objective proposes a practical method for ideal sizing and placement of DG. The aim of this research is to extend on the current connection methods for adoption by utilities.

The research was approached by obtaining and analysing a meshed utility network in DIgSILENT Power Factory. The study case was used to develop the methodology and address the research questions.

1.7   Significance of research

Each research question will develop specific knowledge factors and technical power system planning abilities. Power utility engineers will benefit from a wider range of skills to assess the impact of DG connections. These skills will enable optimal placement of DG on meshed network to reduce losses for time variant loads.

1.8   Structure of dissertation

Chapter 1 provides the global and local perspective on the appetite for renewable energy and highlights the current challenges of the REI4P. Key questions will focus research to evaluate the hypothesis.

Chapter 2 develops a literature review of industry peers pertaining to the research questions.

Chapter 3 focuses on the technical analysis of grid connected distributed generation.

Chapter 4 defines the methodology employed in DIgSILENT Power Factory for optimal placement and sizing DG connections to reduce power losses.

Chapter 5 presents the result of the methodology employed on a typical utility network.

Chapter 6 summarizes the findings of the research and evaluates the hypothesis. The research concludes by discussing the relevance of the research, the research contribution, proposed further work and recommendations and conclusion.

1.9   Chapter in perspective

Chapter 1 has highlighted the awareness of the global demand for renewable energy to sustain the electrical supply industry. Conventional power generated from fossil fuel power stations is no longer environmentally sustainable. Renewable energy sources have radically changed the way power and energy engineers plan the power system. Innovative planning methods demand a rethink of power flow simulations. Unidirectional power flow from centralized generation pools need to be considered alongside non-dispatchable generation. Our future as we know it has changed. Power and energy engineers face a complex task of ensuring optimal placement and sizing of IPPs to ensure "Stainable Energy for all".

2   LITERATURE REVIEW

Chapter 2 is dedicated to scholarly literature in support of the research topic. This chapter aims to seek out scholarly works in the field of ideal placement of DG. The literature scan focuses on the key questions raised in chapter one. Section 2.1 introduces optimal placement techniques with section 2.2 to 2.5 addressing the key questions through the literary review.

2.1   Optimal placement techniques

Three optimized placement techniques are discussed in [11], each with their own advantages and disadvantages. A review of 20 techniques highlights the array of optimization algorithms available. These include the 2/3 Rule, Analytical Methods, Optimal Power Flow and Mixed Integer Nonlinear Programming. Conventional Methods; Artificial Intelligent Optimization Techniques and Hybrid Intelligent System classify placement techniques. Each technique promotes the application for optimal placement of distributed generation.

Sizing of renewable generation is inherently implicit in optimal placement. Techniques discussed in [11] addresses various network constraints and limits associate with DG integration. Figure: 2-1 shows the three categories of optimization techniques. Complexity in software simulations and modelling techniques increase from left to right. A review of these methods reveals that pragmatism is essential to ensuring widespread adoption.
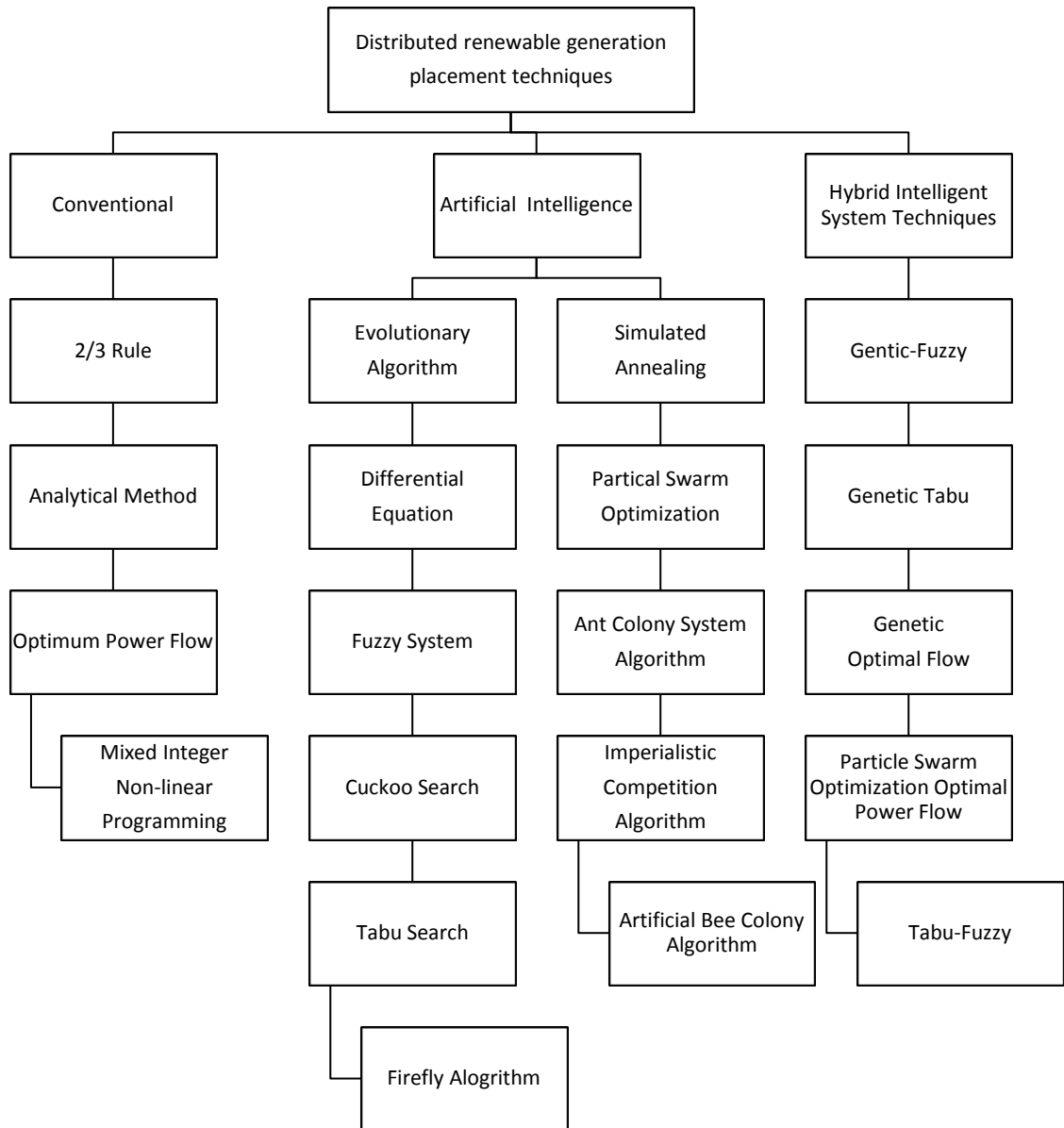
Figure: 2-1 Optimization Techniques for Distributed Renewable Generation [11]

The following review of scholarly works address the four research questions raised in chapter 1.

2.2   What critical electrical factors determine the optimal placement of DG to reduce power losses?

Power system topology [12] defined by impedance and interconnectivity affect optimal placement of DG. High voltage networks with high impedance to resistive ratios are more sensitive to reactive power losses compared with medium and low voltage networks[13]. Steady state voltage limits; reactive power support; fault level and evacuation of thermal capacity are critical factors for optimal placement of DG to reduce power losses.

An efficient optimal placement and sizing technique in a large scale radial distribution systems is presented in [14]. The objective of minimizing network power losses to improve the voltage stability was presented. A detailed performance analysis was carried out on a 33, 69, and 118-bus radial distribution system to demonstrate the techniques effectiveness. Voltage collapse was tested on the 118-bus system. The research highlights the importance of modelling the accurate load and generator profiles. Modelling load types were used assessed the impact of multiple DGs in small, medium and large radial distribution networks.

A loss sensitivity method determined optimal location and sizing for weakly meshed distribution networks. A study of time varying loads with ZIP load models were considered on a 38 bus UK distribution network [15]. Power loss sensitivity studies were conducted for various DG sizes and locations in [16].

A network de-meshing algorithm enabling radial protection to operate in the presence of DG was presented in [17]. The algorithm evaluates the number of switches to close compared with the number of conductors to reinforce. Optimization was achieved by selecting the cheapest option.

The placement of DG in meshed networks strongly depend on the network topology [18]. Optimum placement changes with penetration levels. Penetration levels [19] are represented by the ratio DG to load, expressed as a percent. Power losses will increase if the size of the DG is increased more than a threshold level [20]. Injecting currents into a network will increase the fault levels [21].

Distributed generation integrated into power systems have many advantages over classic power systems when connected optimally. These are to reduce power losses and improve the network voltage profile. The optimal integration of DG can defer costly network upgrades. Renewable energy DG can reduce greenhouse gases [22].

Weighting factors for optimal determination of size and location on an IEEE 24 bus mesh system were proposed in [23]. Factors included losses, voltage profile, short circuit level; thermal capacity and dynamic stability used in the algorithm.

DG integration challenges conventional unidirectional power flow thinking. Power flow can be sourced across previously weak networks, which carried tail end feeder currents.

2.3   What practical loss optimization power flow method can be applied to place DG on meshed networks?

Thirty-one techniques across 3 categories for optimal placement are summarised in [24]. A MATLAB algorithm proposed in [25] optimized losses for a 96-hour seasonally reduced load profile while sizing and integrating DG. Typical wind and PV profiles are used as controlled variables for testing the optimization algorithm. Load and generation profiles are critical for power loss management. Technical constrained parameters are listed for optimizing the location. These

relate to the utility standards for voltage control, power loss management and thermal loading management for both line and substation equipment [25]. The research in [25] assumes that more than one type of DG is connected to a busbar. Renewable DG units were operated at unity power factor. Dispatchable units were range bound between a power factor of 0.8 leading and 0.8 lagging. Dispatchable units were curtailed when generation power exceeded system demand.

Methods using PV and PQ models to determine optimal location of renewable and dispatchable generation were discussed in [26] and [27]. Distributed generation modelled as voltage controlled node behaves as voltage dependent current source as described in [25]. The amount of reactive current injected depends on the difference between the voltage magnitudes and the scheduled value, of the voltage controlled node. The proposed algorithm modelled DG as voltage controlled node, with the flexibility of being converted to PQ node in case of reactive power limit violation.

Optimal sizing of DG using average hourly variations of load was modelled in [28]. Adherence to technical and economic factors were incorporated. Technical factors include real power loss reduction; line load reduction and voltage profile improvement. Economic factors considered optimal DG investment cost. A voltage and power sensitive index was proposed for the identification of optimal location for DG placement.

An algorithm presented in [29] looped through a series of load flows using criteria for identification of DG placement. Violations in voltage, reactive power and losses limit the selection and placement of DG. While placement of DG improves the network voltage profile, optimal placement and sizing play a major role in reducing system losses [29].

A technique of linearly ramping-up the load was presented in [30]. A one-percent (1%) step size from 50% to 150% of load was applied to each optimal size and location of DG. This load flow technique proposed a new long term scheduling for optimal allocation and sizing of different types of DG. The tests were performed on a 33-bus IEEE radial distribution network. Loss minimization formed the core focus of the research paper.

A Maximum Power Stability Index (MPSI) considered voltage collapse based on maximum power transfer limits was derived in [31]. The MPSI was used to identify the optimal location and size of DGs based on the Particle Swarm Optimisation (PSO) algorithm. A PSO model with randomized loads optimized DG sizing in view of power losses developed in [31]. Optimum DG placement was identified through a voltage stability assessment method [31]. This was achieved by locating DG at the weakest bus in the system as the load demand randomly increased. Optimum sizing of DG considered the minimization of active power losses.

However [20] suggested an optimum sizing of DG that consumes locally serviced demand without exporting energy beyond the substation boundary.

Three-phase DG modelling on unbalanced radial systems were considered in [32]. Power system analysis and power flow fundamentals of power (P), voltage (V), reactive power (Q) and Cos (δ) were defined. Loss minimization through optimal placement of DG was displayed on a 69 bus network in [33].

Available headroom with thermal and voltage limits on a distribution feeder was introduced in [34]. Harrison and Wallace presented practical forward thinking about availability of capacity DG in [34].

2.4   What is the importance of reactive power control for the integration DG ?

Reactive power control is a key factor to supporting steady state voltage [35]. Decentralized voltage control through distributed generation highlights the divergent approaches to voltage management [36]. Reactive power regulation aligned with the philosophy of reactive power to support voltage control at DG connected busbars were demonstrated in [37], [38] and [39]. Further evidence of reactive power control in support of voltage control strategies were provided in [40].

Information and communication technologies (ICTs) have advanced power system towards smart grids with centralized voltage control [41]. This approach reduces voltage rise in the presence of high penetration of distributed generation [42]. In [43] and [44] centralized control of concentrated DG systems are controlled in real time by providing reference signals for reactive power injection.

Active distribution networks such as smart voltage control and intelligent distribution transformers can be implemented to provide voltage control. [45] Supports the decentralized philosophy in smart grids. Optimization of a voltage control strategy and a reactive control strategy enable an active power loss management strategy. Power loss management becomes an important consideration for the business operations and sustained energy management. With advances in industrial internet systems future networks may evolve to use online smart grid strategies [46].

Reactive power control on a radial network to maintain voltage within a predefined limit was discussed in [47]. A Volt - VAR sensitivity matrix was established to determine initial conditions for reactive power control. The optimization problem was to maintain voltages within a permitted range by using reactive power from DG connections. Voltage stability was critical in developing an optimized model for utility modelling and planning. Classifications of voltage stability into dynamic and static methods were introduced in [47]. Dynamic modelling relates to time domain and classic modelling is associated with steady state.

Dynamic stability is concerned with the ability of a power system to maintain acceptable busbar voltages after being subjected to a disturbance [48]. Steady state analysis is concerned with the proximity to voltage collapse of a power system. Voltage collapse occurs in heavily loaded power systems that operate too close to their voltage stability limits. Accurate modelling of load types

affect critical impedance points [49]. The main focus of voltage stability studies is the identification of weak or critical busbars. Voltage instability in power systems can be analysed based on P-V and Q-V characteristics.

A method of locating and sizing DG units to improve the voltage stability in the presence of probabilistic load and renewable DG generation was presented in [50]. Busbars that are sensitive to voltage change are prioritized for installation of DG. The DG unit placement and sizing was formulated using mixed-integer nonlinear programming aimed at improving stability margin. The constraints were listed as system voltage, feeder capacity, and DG penetration level.

A multi-objective performance index (MOPI) for enhancing voltage stability radial distribution systems was proposed in [29]. This index method was carried out using a 69 node radial IEEE distribution network to determine the optimal placement and sizing of DG units.

2.5   How does DG penetration and concentration affect power system losses?

Integrating distributed generation in distribution systems will voltage, power flow, power quality, voltage stability, reliability, and protection. DG units are relatively small in capacity compared to central power plants. The impact on the above criteria are minor if the penetration levels are low $(1\%-5\%)$ [51].

Targets laid down for renewable energy will see large amounts of embedded generation (EG) connected to power system. Linear programming was used to determine the optimal allocation of DG in [52]. The methodology was implemented and tested on a section of the Irish distribution network. Results demonstrated that optimal placement and sizing of DG was crucial to increased penetration levels. However, increasing penetration levels beyond anticipated level of $20\%-30\%$, resulted in increased losses. The effect on overall cost of optimum DG placement and size was studied in [53].

Increased penetration of the DG could increase or decrease voltage stability margin depending on their operation. DGs are operated at unity power factor to avoid interference with the voltage regulation devices connected to the system [54].

Probability models present in [55], optimized DG technology mix given high penetration levels. These models accounted for the stochastic nature of solar irradiance and wind speed. Stochastic nature of wind and solar renewable energy supply, for optimal siting and sizing was also discussed in [56]. Time varying loads and supplies affect power quality and impacts dispatchable generation operations.

Stochastic charging of plug-in electric vehicles (PEV) presents uncertainty in optimal sitting and sizing of distributed generators as recorded by [57], [58] and [59]. In networks with high

probability of PEV, dispersed DG along the feeder yields lower losses resulting from DG being closer to the load centre.

While conventional wisdom presumes, that DG will reduce losses. A characteristic U-shape trajectory for losses explored in [60], showed an increase in losses with increased penetration and concentration. Wind power also showed the worst behaviour for losses reduction.

3 TECHNICAL ANALYSIS OF GRID CONNECTED DISTRIBUTED GENERATION

Chapter 3 employs the literature surveyed from chapter 2 to address the key questions raised in the hypothesis. Dispatchable, non-dispatchable generation and load determine network behaviour. The characteristics of these sources and sinks through network impedance underpin the research questions leading to the hypothesis. Network behaviour intern determines characteristics of power loss. Sections 3.1 to 3.12 serve to support the fundamental knowledge base to addressing the key questions.

Section 3.13, communicates the technical requirements of grid connected DG for the Renewable Energy Independent Power Producer Procurement Programme (REI4P). Sections 3.14 and 3.15 provide the Eskom connection strategy for transmission and distribution. These sections introduce the South African REI4P and serves as a trigger for the research.

Section 3.16 addresses optimal sizing and location for loss reduction.

Chapter 3 concludes by addressing the key questions and framing the objective of the research.

3.1 Characteristics of time variant loads

Power systems require constant monitoring for adaptive operational control to meet the constant changing demand. However small these changes across the time [61], supply always need to balance demand to ensuring stability of frequency and voltage. Voltage limits are range bound and managed through the grid connection codes as proposed in [40].

Three main load types are connected to the power system, constant power, constant current and constant impedance (ZIP). These loads consume power and energy as a function of time.

3.1.1 Load types

Electric load resulting from electrical devices are rated at their nominal voltage. Electric loads vary as the supply voltage changes. These are grouped into three categories depending on how their demand varies as a function of voltage [62]. The following two fundamental equations can be used to interpret the relationship of the three load types.

$$P = I*V \qquad \dots (1)$$

$$V = I*R \qquad \dots (2)$$

A constant power load behaves such that demand is constant, regardless of voltage. A constant current load behaves such that demand is proportional to voltage. A constant impedance load behaves such that power is proportional to voltage squared [62].

Table 3-1 ZIP Load Model [62]

↔		↑		↓	
P	=	I	*	V	…Constant Power
↔		↑		↓	

↑		↔		↑	
P	=	I	*	V	…Constant Current
↓		↔		↓	

↑		↑↑		↔	
P	=	V^2	/	Z	…Constant Impedance
↓		↓↓		↔	

Aggregated busbar loads make up a combination of load types. As a rule of thumb, a ratio of 60/40 for (Power / Impedance) can be assumed [62].

3.1.2 Time variant loads

There are three variants of time varying load types namely, residential, commercial and industrial loads. Due to season variations and aggregation of loads, load summations are statistically modelled. Load curves with statistical single standard deviation based on season changes are used for load profiles [63]. This presents the utility planner with various likelihoods of load profiles. Complex permutations result in a standard set of load curves for planning purposes.

Utility planners must account for likely permutations of generation and load patterns when sizing and placing DG. Proprietary load management programs simplify load profiling, summation, aggregation and forecasting. Statistical representations of the current and future loads are studied in power system simulation tools such as DIgSILENT Power Factory. Studying time variant loads and generation patterns isolate four permutations as static time proxies. High Generation – High Load; High Generation – Low Load; Low Generation – High Load and Low Generation – Low Load scenarios represent the critical study points for generation and load profiles.

3.2   Characteristics of time variant sources of renewable generation

3.2.1   Global wind patterns

Wind patterns drives by global wind systems. The power from transforming kinetic wind energy to electric energy differs from location and across seasons. Medium and long-term forecasting is a restrictive. Short-term forecasting is probabilistic in nature. The unpredictable nature of wind patterns adds complexity to managing voltage stability and reactive power stability [64].

3.2.2   Weibull distribution

Weibull distribution functions statistically analyzed and categorized by varying location based wind speeds. These functions define the shape, average and median wind speeds [65]. The Weibull distribution function defines the percentage probability of the wind speed. Weibull distribution functions model the percentage probability for time varying wind speeds in power simulation programs.

3.2.3   Wind power equation

The wind power equation [66] represented by (3) is proportional to "air density" (ρ); "swept area (A)" and cube of the "wind speed" (v_w), and defined below.

$$P_w = \tfrac{1}{2} \, C_p \, \rho \, A \, V_w{}^3 \qquad (3)$$

Where, C_p is the Betz constant with a value of 0.59.

Wind power is only partly predictable when the wind blows and is unpredictable beyond a week [65].

3.2.4   Wind power curve

Fundamentally, all wind turbines have similar power curves. They have a cut-in wind speed at the lower end of the wind scale and a cut-out value at the higher end because of mechanical instability [66]. Overlaying the Weibull distribution function with the wind power curve presents a narrow margin at which full capacity is available. A theoretical comparison of the Weibull distribution function to the power curve, reveal that wind turbines have a 10% probability of delivering rated power. This presents an inefficient cost to benefit ratio for planning wind power connections to the grid.

3.3 Electrical characteristics of renewable wind generation

3.3.1 Real power

The real power output was presented by the power equation in section 3.2.3. Extracting wind power through four types of electrical generators can be achieved. These fall into two broad categories namely, fixed speed and variable speed [66]. Older technology fixed speed generators have no reactive power control [66].

3.3.2 Reactive power

Modern day variable speed wind turbines are able to inject and absorb reactive current from the power system [67]. Such capabilities ensure reactive power and power factor compliance to the grid connection code [3] and [68]. Doubly Fed induction Generators (DFIG), fully rated converter induction generators and synchronous generators are all representative of modern wind turbines. Stricter grid code requirements may require plants to operate along the constant Q or constant Power Factor (Cos φ) [69].

3.4 Solar PV - partially predictable source of renewable energy

3.4.1 Global solar irradiance

South Africa and Africa compare favourably on the world solar irradiance (W/m^2 – KW/m^2 – MJ/m^2) scale [70]. This highlights the potential for solar renewable energy in South Africa.
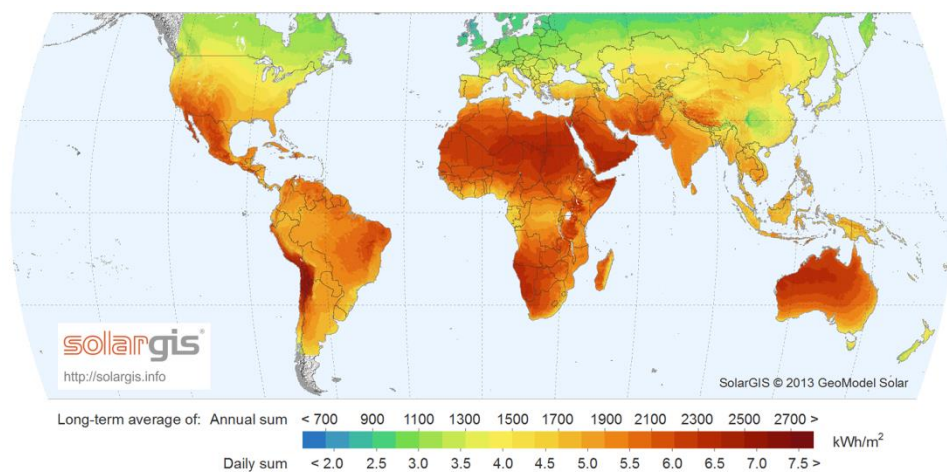
Figure 3-1 Global Solar Irradiance – KW/m^2 [70]

Although solar energy is more predictable than wind, solar irradiance can only be converted to electrical energy when the sun shines. In solar PV systems, no energy is stored, unlike in concentrated solar power plants. Daylight depends on the location on the earth and energy is extracted as shown by Figure 3-2.
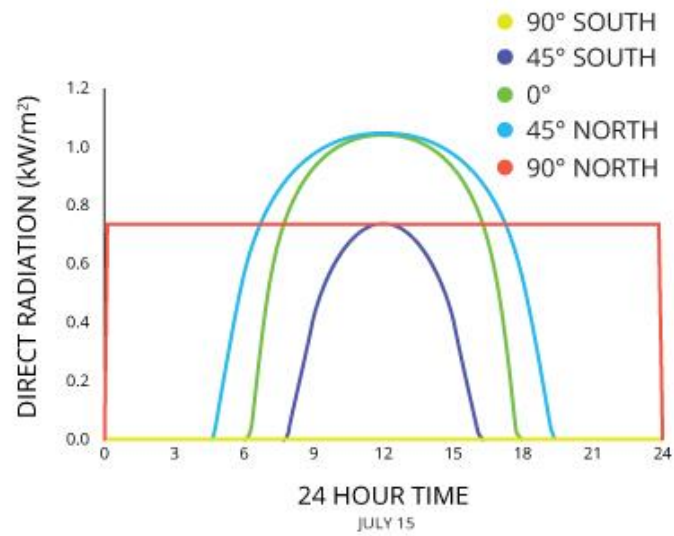
Figure 3-2 Direct Solar Radiation (KW/m2) – Southern Hemisphere [71]

In theory these curves are constant. In reality power output is affected by cloud cover interference as shown in Figure 3-3 below.
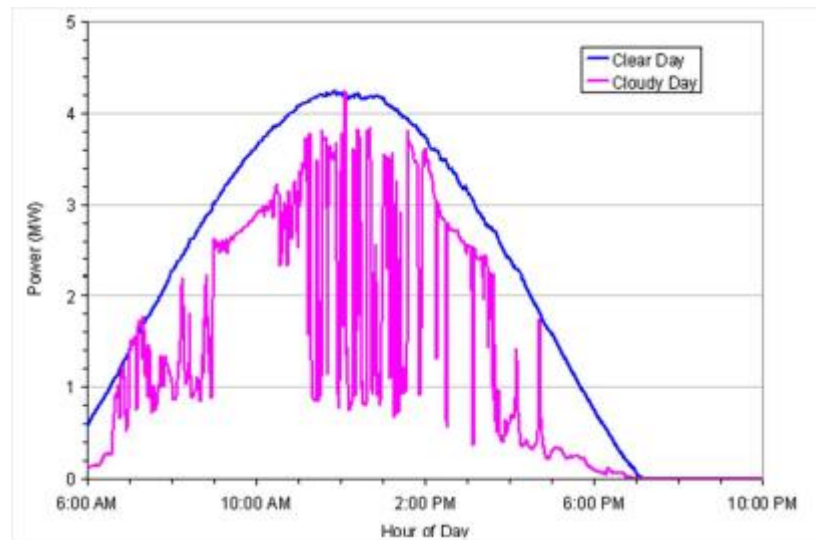
Figure 3-3 Show local example of solar farm output [72]

3.4.2   Solar power curve

Solar PV behave like a constant current source [73]. It displays short circuit currents at zero volts and open circuit voltage at zero current as shown along the V-I curve in Figure 3-4.
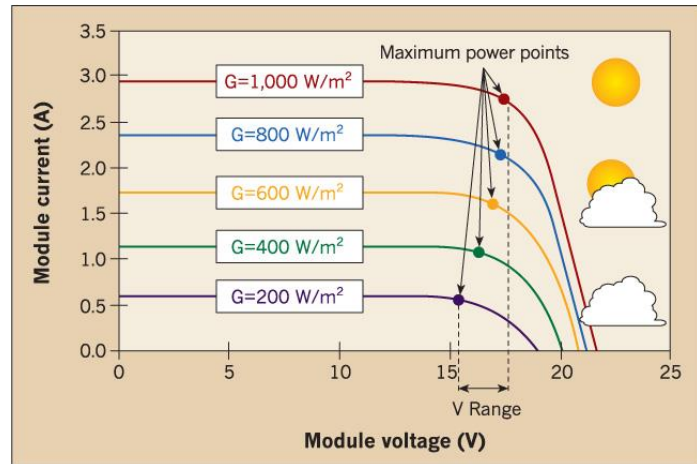
Figure 3-4 Show local example of solar farm output [74]

Based on the time of day and cloud cover, PV output varies as shown in Figure 3-3. Smart solar cell technology's optimizes the maximum power point. Figure 3-5 shows how maximum power is delivered for a given irradiance and ambient temperate.
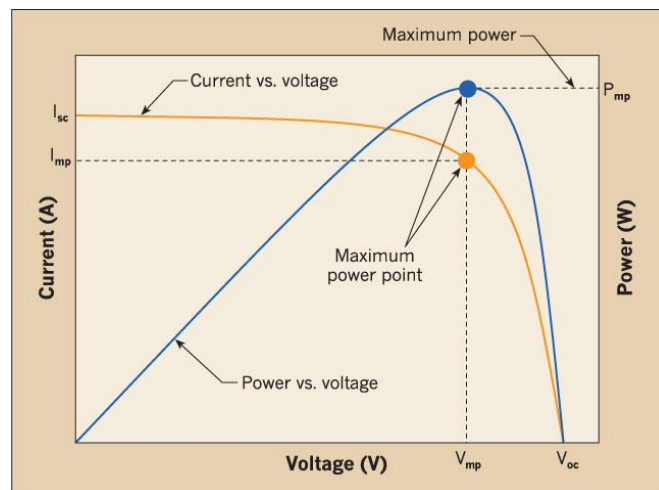
Figure 3-5 Show local example of solar farm output [74]
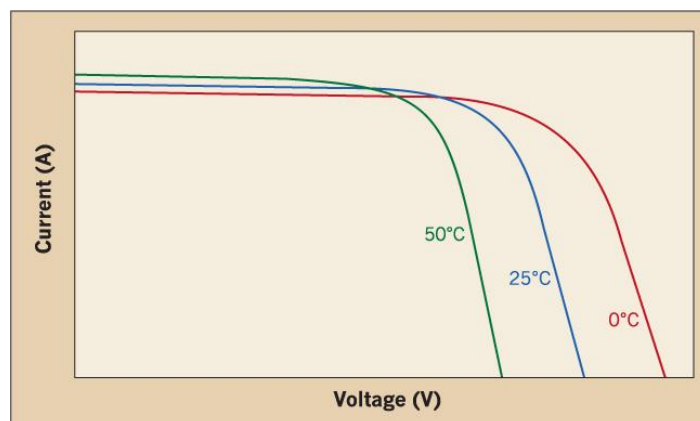
Figure 3-6 Show local example of solar farm output [74]

Higher surrounding temperatures have lower voltage ranges. Lower ambient temperatures have higher voltage ranges as shown in Figure 3-6. This explains why northern hemisphere countries benefit from solar PV installations.

3.5 Electrical characteristics of renewable solar PV generation

3.5.1 Real power

Real power is a function of the solar irradiance power curve as optimized through the maximum power point tracking.

3.5.2 Reactive power

Modern day PV inverters can inject reactive current into the power system as well as absorb reactive current from the grid. This electrical characteristic ensures compliance to the grid code [3]. Smart inverters can deliver or absorb reactive power (Q) at zero real power.

The South African renewables code does not distinguish by technology but rather by size of connecting to the grid. Wind and solar technologies therefore have the same reactive power capability requirement [3]. Figure 3-7 shows the reactive power capability of a PV inverter.
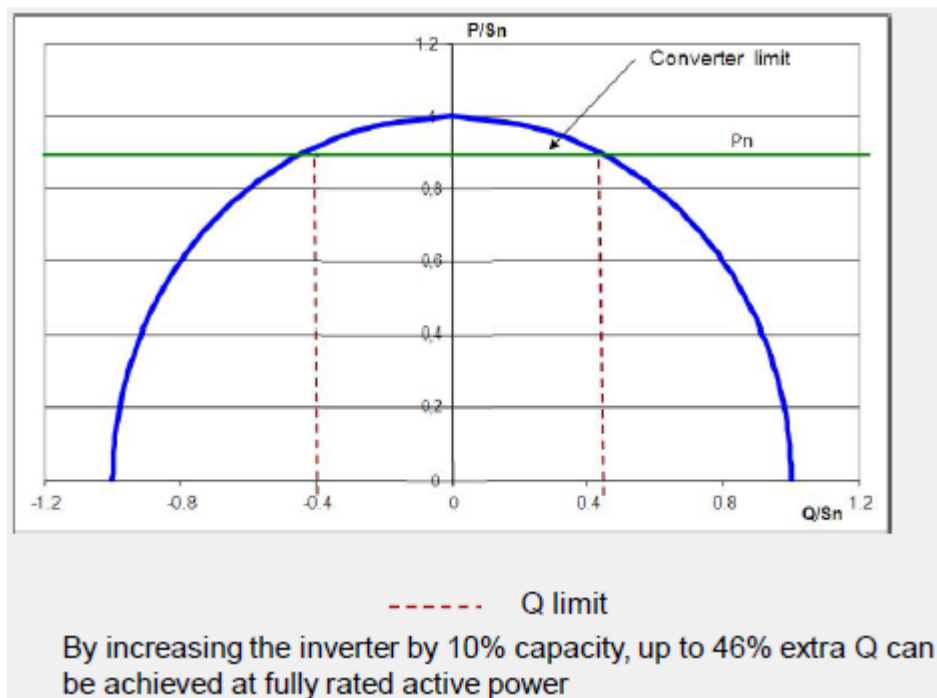
Figure 3-7 Reactive Capability Curve – PV Inverter [72]

3.6   Concentrated solar plants

Concentrated solar plants absorb the suns energy through collectors similar to solar PV. This technology uses molten salt to store solar energy and drive conventional synchronous generators through steam turbines. This technology is partially dispatchable and limited by its storage capacity.

3.7   Bagasse

Bagasse generation uses renewable biomass to drive a steam turbine and in turn drive conventional synchronous generators. DG driven by bagasse is dispatchable.

3.8   Hydro / pumped storage

Hydro and pumped storage plants run on flowing water and stored water respectively. They drive vertical orientated salient pole synchronous generators to produce electricity. Hydro-electric schemes are partially dispatchable limited by the flow of water and pumped storage is a dispatchable form of generation.

3.8.1   Electrical characteristics of renewable non-solar PV and non-wind generation

Concentrated solar plants, bagasse and hydro plants all have synchronous generators used to produce electrical energy. These generators differ only in size to the convention coal fired power stations and nuclear power base load power stations.

3.8.1.1   Real power

Active power is controlled by driving the prime mover to a maximum as rated by the generating capacity.

3.8.1.2   Reactive power

Reactive power is provided by RPCC governed by the generators excitation and stator currents as shown in Figure 3-8.
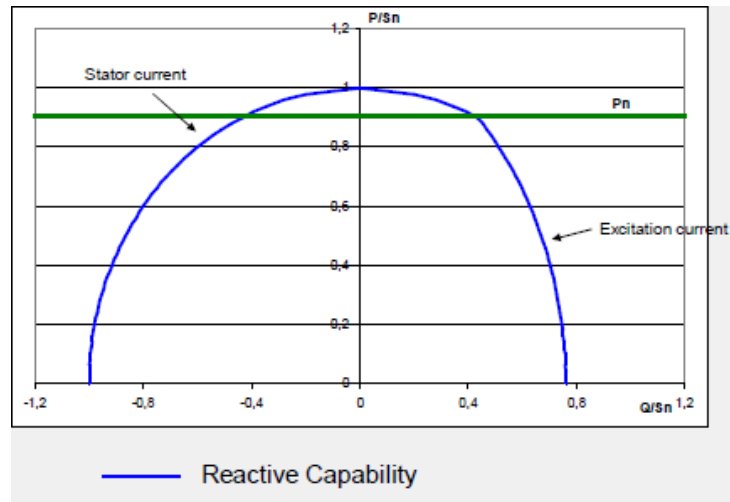
Figure 3-8 Reactive Capability Curve – Synchronous Generator [72]

The RPCC is limited by the excitation current on the capacitive scale; by the stator currents on the inductive scale. Reactive power is also limited by the machine rating on the active power axis. Unlike the PV inverter, the synchronous generator is a relative clean source of electrical energy as very little harmonics is injected into the network.

3.9   Dispatchable Vs non-dispatchable generation

Conventional generating technologies e.g., coal, gas-combined-cycle and nuclear are dispatchable forms of generation. Dispatchable generation is controlled by the system operator based the power systems supply and demand need. Generation is scheduled on a least economic cost "dispatch curve" [75]. Reactive power reserves [76] and [77], frequency regulation [78] and spinning reserves [61] are managed by the system operator to provide reliability services to the grid.

Non-dispatchable renewable generating technologies supply intermittent electricity. Electricity produced by these technologies is driven by the weather. Output power from intermittent sources can vary widely across time scale, location and technology [79]. These forms of renewable generation cannot be controlled or dispatched by system operators. Rather than controlling much power will be delivered to the grid. System operators must respond by dispatching generators to continuously balance supply and demand [80] and [61]. This makes the control of the power system with large installations of non-dispatchable generation very challenging.

3.10 Characteristics of power losses

3.10.1 Energy losses

Despite the inefficiencies in converting renewable energy to electrical energy, technical losses are also present which increases the demand to be supplied. Losses should be managed by optimal placement and sizing of equipment.

3.10.2 Power losses

Electrical losses represent the different between DG power generated and power consumed at the load [81]. Power losses are small when DG is consumed at the source. Large-scale DG is often connected to the power system at high voltages. Injection of large power flows at non-load centered busbars, will lead to increased power loss.

Power loss is a function of time. It changes continuously as the product of the square of the load current and impedance represented by $I^2 Z(t)$. Z is the vector sum of real resistance and imaginary reactance $(R + j X)$. Power losses are dependent on load current and the impedance of the network between the source and load [62].

Transmission networks have high X/R ratios and are more sensitive to changes in reactive power. Distribution network have high R/X ratios and are more sensitive to resistive changes. Accurate modelling of network parameters play a significant role in power loss determination [82].

Optimization of location and sizing of DG at load centers thereby ensure optimization of losses. Excessive penetration and concentration of DG above an optimal level will result in "U-shape" trajectory of losses [83].

3.11 Characteristics of distribution network topology

Medium voltage distribution network voltages range from 11kV to 33kV with high R/X ratios.

3.11.1 Typology of distribution networks

Distribution networks can either be radial, radial with tie-lines or meshed. Each topology will be discussed in relation to DG sizing, location and power losses in the following subsections.

3.11.1.1 Radial networks

Radial networks [84] are synonymous with rural where network load densities are low. These networks are designed on the trunk and branch philosophy [85] to minimize cost. Economic sizing of conductors follow a conductor tapering method based on the conventional power flow from the

substation to the load. Conductor sizing matches loading levels. As load tapers toward end-of feeder, so to do conductor size.

3.11.1.2   Tie line radial networks

For increased network reliability, radial network designs include switchable normally open tie-lines to support interconnection. They are placed at the beginning of a network, connected through a bypass breaker for maintenance purposes. Alternatively, at the midpoint of a traditional trunk designed network; or at the end of the feeder.

3.11.1.3   Meshed networks

Meshed networks are deployed in urban, high density load concentrated areas. Network designs allow for full transfer of load between source breakers. Network costs are high and reliability performance indices are demanding.

3.11.2   Voltage profile of distribution networks

The voltage profiles of radial and tie-line radial feeders taper from source to end-of-line. Long or heavily loaded feeders are designed with compensation to support voltage sag. Distribution networks have no inherent Volt - VAR support and need compensation for voltage support. DG can supply and absorb reactive power to support voltage control [86]. Regulatory codes may restrict the use of DG to solve existing voltage problems, as this may be too costly for this purpose alone [87]. This however forfeits a costs savings opportunity during optimal placement and sizing DG.

3.11.3   Thermal capability of distribution networks

Tapered conductor designs, implies tapered thermal transfer capacity to end-of-line. This causes tapered spare capacity or headroom [34], [88]. Strategic and optimal placement and sizing of DG on radial and tie-line radial networks can increase the thermal transfer on the network. Fully meshed networks provide an ideal topology for placing and sizing of DG.

3.11.4   Fault level characteristic of radial networks

Fault levels on radial lines decay rapidly because of high R/X ratios and are not conducive for connecting constant power loads. These loads dip the network voltage on startup resulting in large machines stalling [89]. Rotating renewable technology prove difficult to place on low fault current networks due to the exceedance of voltage variation. Solar DG is more plausible for these network topologies as their capability allows for the control of fault contributing currents.

3.12 Impact of distributed generation on distribution network topology

Sizing DG to reduce reverse power flow through the HV/MV transformer is ideally suited for distribution network topologies. Network topology designs can host small amounts of DG with minimal cost impact. Locating DG approximately halfway on the backbone will not negatively impact on the traditional trunked designed. Fully meshed networks suite this placement strategy [90].

Trunk topology's of radial and tie-line networks require upstream reinforcement for high levels of DG connection [91].

Distribution networks will experience improved voltage levels through DG connections as reactive power support can be supplied at source. Power losses will be minimized since the DG power is consumed at source. Loading cycles on HV/MV transformers will reduce, thereby reducing power losses across the transformer.

Penetration and concentration of DG should be managed to prevent reverse power flow leading to an increase in costly protection upgrades.

3.13 Department of energy's renewable energy requirement

The South African government has made its intent clear to diversity the energy mix to reduce greenhouse emissions by 34% by 2020. The government's Integrated Resource Plan (IRP) published in May 2011, sets out South Africa's required generation capacity for the next 20 years [5]. It is encouraging to see government's plan to diversify the energy mix and move away from fossil fuels.

This plan comes at a critical juncture in the local electricity supply industry as energy shortages plague economic growth.

In April 2015, the DOE concluded 4 rounds of preferred bidder's evaluations, totalling 96 power purchase agreements (PPAs). These agreements will add more than 6400 MW of installed RE capacity to the Eskom power system. In comparison, the Medupi power station [92] is a single coal fired power station with future generation capacity of 4764 MW. This highlights the speed and agility to connect renewable energy to the grid.

Successful bidders selected from a pool of applicant at least threefold in number. Bidders were assessed on an individual connection strategy to the grid. A critically assessing the connection strategy of bid rounds 1-4 show a flaw of not clustering bidders along power corridors. Sterilization of networks presented in [93], [94] will result from individually assessed DG applications.

3.14 Eskom transmission connection strategy

The IRP 2010-2030 [5] identifies 17 800 MW of RE grid connections by 2030. Eskom responded with the Generation Connection Capacity Assessment based on the transmission network in 2022 (GCCA - 2022) [95]. The GCCA - 2022 presumes completion of all transmission development plans (TDP) [96].

The Eskom transmission strategy provides for a collection of multiple IPPs through "Satellite" and "Collector" nodes. These nodes aim to maximize evacuation of RE through bulk power transport. The installed capacity at each of the 163 Main Transmission Stations (MTSs) will serve as injection points to host RE onto the grid. Generation hosted at the MTS will displace local load.

Figure 3-9 show 163 MTSs clustered into 27 zones with available capacity for RE integration.

Figure 3-9: GCCA 2022 Generation Connection Capacity Assessment for 27 Transmission Supply Areas [95]

The power system is not equipped to absorb and redistribute power from renewable energy and needs expansion in a cost-effective manner. Several connection strategies available depict themselves in Figure 3-10. Existing networks need to be expanded as marked by the red line to incorporate DG integration.

Figure 3-10: Transmission Connection Strategy – Option I [95]

Where concentrated sources of RE need to be evacuated through EHV networks, the following connection strategy is considered.
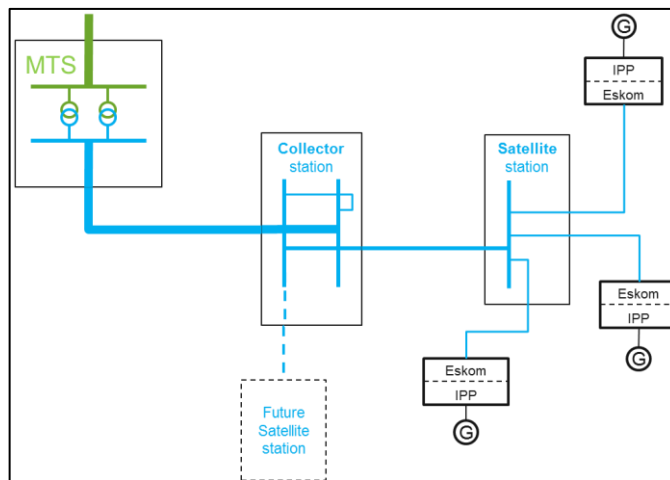
Source: Transmission Connection Strategy [95]

Figure 3-11 Transmission Connection Strategy Option II

DG integration in high generation areas, where load centres are remotely located, behaves like centrally located conventional generation. Caution must be exercised, as losses will increase as penetration levels increase. Passive voltage control through reactive power support is limited by the impedance of the sub-transmission lines between the satellite, collector and MTS.

Integration, shown in Figure 3-10 favours loss reduction as DG is consumed at the load centre. Connections for grid expansion, while managing voltage control; reactive power control and minimization of losses, should be robust.

3.15 Typical Distribution connection options

The Eskom Distribution Business has more than 3000 HV/MV substations. It is not reasonable to develop a distribution based GCCA. Point of connection options are at medium voltages, either at the substation busbar or within the medium voltage network.

3.16 Utility technical challenges

The following section addresses key questions aligned to technical challenges of optimum placement of DG on meshed networks to reduce losses.

3.16.1 Critical electrical factors that determine optimal location to reduce power loss

Section 2.2 provided scholarly reference to key electrical factors that determine optimal location to reduce power loss. Network topology affects system characteristics such as voltage; power flows; fault levels; reactive power margins for dynamic and steady state control. Transformer and line impedance defines system impedance and power flow.

Radial distribution overhead networks high R/X ratios. They are not sensitive to reactive power changes. They offer no reactive power support. They display high losses when operated at high thermal demands, resulting from I^2R losses.

High Thevenin equivalent source impedance on distribution networks limit fault levels and limit DG connection to the network.

Thermal construction limits of radial distribution lines curtail evacuation of DG power. Twenty-two kV systems limit these to 15MVA.

Wind, solar PV and synchronous DG should provide reactive support on high R/X impedance ratio networks. This will reduce reactive power loss and improve network power factors. Reactive power is optimally managed when supplied at the load.

Sizing DG at the high-end of category B on radial distribution networks has a greater probability of failing the rapid voltage change during loss of generation. This is because of the lower fault levels on radial distribution lines. This is unacceptable by the grid code standard. Sizing a connection at the lower-end of category B favours DG connection, while still limited by fault level.

Conversely, transmission overhead networks have high X/R ratios. They are sensitive to reactive power changes. They offer inherent reactive power support. They display high reactive power losses when operated at high thermal demands, resulting from I^2X losses.

Lower Thevenin equivalent source impedance provides higher fault levels and allows for larger DG capacity connections.

Thermal construction limits transmission lines reduce evacuation of DG capacity.

DG technologies such as wind, solar PV and synchronous machines should provide reactive support on high X/R impedance ratio networks. This will reduce reactive power loss and improve power factors. Reactive power is optimally managed when supplied at the load.

Economic viability limits sizing of category C [3] loads on transmission.

The following advantages and disadvantages [97] applies when considering "Category B" & "Category C" [3] for rated renewable plant.

Table 3-2: Extra High-Voltage (EHV) Point of Connection (POC)

Advantages	Disadvantages
Strong Fault Levels will ensure: Minimum impact to rapid voltage change Larger size plants can be connected	Cost are highly prohibitive Renewable energy sources may be far from load centres Technical losses will be costly as a result of the location of the meter

Table 3-3: High Voltage (HV) Point of Connection (POC)

Advantages	Disadvantages
Sufficiently High Fault Levels will ensure: reduced impact to rapid voltage change limited (network dependent) size plants can be connected Substations can be established closer to source of generation	Network integration and strengthening will add to the cost

Table 3-4: Medium Voltage (MV) Point of Connection (POC)

Advantages	Disadvantages
Supports smaller (less than) 10MW renewable plant connections	The connection criteria is dependent on the rapid voltage change, which is mostly the limiting factor on MV networks Evacuating power is limited to the MV line capacity, especially on 11kV networks Fault levels may be prohibitive and reduce size of connection Because of the issues above, network integration and strengthening will add to the cost

3.16.2 Practical power flow simulation methodology applied for placement of DG for loss optimization

Myriads of scholarly works present algorithms for optimum DG placement on radial networks and to a lesser extent on meshed networks. These were classified and discussed in chapter 2. These techniques are innovative and theoretically advanced. They lack practical application in the local environment because of inadequate data and models.

Utility engineers use a combination of power flow simulation methods to place DG [97]. Optimization techniques are limited to the closest available network. Location is dictated by large-scale integration of DG. Rapid growth in the DG landscape demands a long term optimum location; sizing and technology mix development plan, ensuring optimally operation of the power system.

This research aims to develop a practical approach for optimal placement and sizing of DG with the aim of reducing power losses. The methodology employs DIgSILENT Programming Language (DPL) [98] in Power Factory and tests a typical utility network with time varying loads.

3.16.3 The importance of reactive power support for integration of distributed generation

Reactive power generation from DG can manage voltage control on the grid. Fast acting PV inverter technology can boost voltage levels that may suddenly become depressed. This is achieved by injecting leading reactive currents to raise the voltage at the point of connection. Grid codes may restrict DG plants to operation at unity power factors.

Transmission networks with high X/R ratios provide inherent reactive support. Voltage rises during periods of low surge impedance loading. Renewable power plant can limit the voltage rise by absorbing reactive power. Conventional control is possible to manage reactive reserve margins. Smart grid integration with IPPs can operate their plant on Q-Control [3] to support the grid

without switching line inductors. Reactive power reserves can be supplied from Q-Controlled fully rated wind turbines.

Poor power factors loads supplied by reactive compensating DG minimize upstream reactive power reserves.

3.16.4 Penetration and concentration limits affecting losses

Ugranli proves that DG penetration levels of 30% or more increase losses as opposed to reducing losses [18]. During periods of low load, excess DG will reverse flow through the station transformer. Older technology transformers not equipped to allow reverse power flow will experience nuisance tripping. Upgrading the protection philosophy will be costly [99]. Sizing of DG at potential reverse power flow sites should ideally be relocated at higher load factors loads [100]. Integrating dispatchable DG technologies can mitigate reverse power flows especially on older protection technology networks.

3.17 Chapter in perspective

Chapter 3 reviews critical knowledge defining the complexity in dealing with the technical analysis of grid-connected generation. This provides an ideal basis for utility planners developing robust methods and algorithms to assess sizing and placement of DG to reduce power losses. Such methods will serve as a platform for developing a utility strategy for DG connection. A practical method for sizing and placing DG on meshed networks with the aim of reducing power losses is required.

4   ASSESSMENT METHOD

Chapter 4 proposes a method for placing DG on a meshed network to reduce power loss for time variant loads. The method reinforces technical knowledge assessed in chapter 2 and chapter 3. The method drives the need for a practical, repeatable, logical assessment for tactical decision making when sizing and placing of distributed generation. Load characteristics and load types drive power losses. RE generation patterns vary with weather and affect power flow and power losses [101]. Modelling these parameters to analyse optimal placement of DG are important factors in the assessment process. Section 4.7 presents the method.

4.1   Objective of method

Various methodologies to optimize the placement and sizing problem were cited in [11]. The objective is to provide utility engineers with a means of optimizing the DG placement problem. The functional objective is to minimize power loss in the presence of voltage, thermal and fault level limits [102].

4.2   Problem statement

Utility engineers must have complete oversight of the impact and constraints resulting from planned DG connections. Random connections result in poor power loss management. Multi-generation connections require reassessment as the first placement changes network limits for future connections. Availability of renewable energy sources dictates large-scale integration. Consideration to losses plays a minor role.

4.3   Technical constraints

The steady state voltage at each busbars shall remain within permissible ranges as defined by [102]. Thermal limits for line equipment shall not exceed 100% of line ampacity under normal operating conditions. Transformer loading shall not exceed 100% under normal operating limits. Voltage variation resulting from loss of solar PV is limited to 3% at point the of connection [3].

4.4   Scope of method

This method enables utility planners to work across all voltages on the power system. These voltages included medium voltage (MV) to high-voltage (HV) and extra high-voltage (EHV). Application applies to all voltage ranges and only category B [3] and C [3] were applied in the test utility network. Category B represents generation with maximum export capacity of less than 20 MVA and category C, greater than or equal to 20MVA.

4.5 Assumptions

The following assumptions are requisites apply in developing the method.

A. Power Factory version 15.1.4 was used.

B. The test grid is representative of a typical meshed EHV, HV and MV utility network.

C. DG was connected to only the HV and MV busbars.

D. Utility generation is supplied through two constant power and voltage (PV) bus and slack bus. These busbars made up the equivalence external grid.

E. No new loads were added over the study period.

F. Network topology remained unchanged over the study period.

G. MV feeders were not assessed for solar PV connection.

H. Twenty-four hour load profiles were assigned to each load bus based on the dominant nature of the downstream customer base.

I. Constant power load types were assumed for all busbars.

J. Network contingencies and maintenance outages were not considered during the assessment.

K. Wind power was not considered.

L. Solar PV was considered for all DG connection studies.

M. The following conditions were assumed for solar PV.

   a. Cloudless days were assumed for solar PV irradiance patterns

   b. Sunrise to sunset was assumed to be from 6am to 6pm following a normal solar irradiance pattern.

   c. All DG connections were applied on either the MV or HV busbar.

   d. Only one solar PV connection per busbar at a time was tested, section 4.3.

   e. All solar PV plants were modelled at and connected at unity power factor.

4.6 Exclusions

No dynamic studies in the milliseconds time range were performed.

4.7 Optimal placement methodology

4.7.1 Overview

Chapter three identified critical network factors that contribute to optimal DG placement. These factors were employed in the method and provide a single comparable overview for 3 ϕ fault levels; voltage levels; real and reactive power flow at each bus. Preventing voltage and thermal

violation of equipment is constantly managed throughout the selection process. The final selection of successful busbars is completed through assessing size of DG according to load demand.

The following flow diagram depicts the optimal placement method employed.

Pre-DG
- Set up pre-DG evaluation as described in section 4.7.2

Defining
- Defining busbar types as described in section 4.7.3

Ranking
- Ranking busbars based on fault levels as described in section 4.7.4

Profiling
- Profile power system busbars for DG sizing 4.7.5

Activating
- Activating DG for placement as described in section 4.7.6.

Evaluating
- Evaluating DG sizing for voltage variation testing as described in section 4.7.7.

Selecting
- Optimal selection of candidate busbars based on comparitive overview of optimal placement as described in section 4.7.8.

Figure 4-1: Optimum placement method

4.7.2   Pre-DG evaluation

Pre-DG evaluates and analyse a convergent DIgSILENT Power Factory © (DPF) version 15.1.4 utility network case file. Typical southern hemisphere summer months were selected for the study case time. Pre-DG study being prior to August 2015 and post-DG being during September and October 2015. A selection of three daily load profiles were selected for the research namely, a bulk load profile, municipality load profile and rural load profile. Daily load profiles were assigned to each load bus based on the dominant downstream load characteristics.

Quasi-Dynamic Simulations (QDS)[1] provide profile busbar load flow variations across the grid, for the 24-hour period. Variations in real and reactive power flow were recorded over a 24-hour period. Time static load flows informed by the QDS, were performed at maximum and minimum network load. This activity allows for assessment at time of high load and low load. Benefit is derived from aggregated profiled information rather than assumed high and low load approximations. Bus results together with real and reactive power flow results were recorded, through a grid summary report.

4.7.3   Defining power system busbars

The method of defining identifies load and non-load (network) busbars suitable for DG connection. Table 4-1 describes the convention applied for defining load and network busbars. This enables quick identification of suitable busbars on large utility networks.

Table 4-1: Defining Busbars for Optimal DG Placement

Code	Full Description of busbar	Description of Definition
MV **L**B	Medium Voltage **Load** Bus	Load directly on busbar
MV **N**B	Medium Voltage **Network** Bus	Supplies MV LB
HV **L**B	High Voltage **Load** Bus	Load directly on busbar
HV **N**B	High Voltage **Network** Bus	Supplies HV LB
EHV NB	Extra High Voltage Network Bus	Supplies EHV LB

4.7.4   Ranking power system busbars

Ranking the power system busbars was achieved by performing a 3-phase fault simulation, using the IEC 60909 [89] method. This provides a sign of busbar robustness to disturbances. Busbar ranking predicts DG sizing. Three to four percent of busbar fault level sizes the DG connection. The ratio of rated DG to system fault level is used as a proxy for percentage voltage disturbance. This ensures in-specification of voltage variation, subject to pre-DG loss voltages.

Table 4-2 presents busbars ranking based on fault level.

---

[1] A QDS is a time series load flow simulation performed at hourly intervals over a 24-hour period.

Table 4-2: Ranking Busbars

Code	3 ϕ Fault level	Max RE Size
MV LB	200 MVA	8 MVA
MV NB	300 MVA	12 MVA
MV NB	500 MVA	20 MVA
HV NB	625 MVA	25 MVA

4.7.5 Profiling power system busbars for DG sizing

Profiling load and network busbars to DG profiles classifies the expected impact of load and loss decrease. Profiling informs the degree of reverse power flow. Load busbars are assigned dominant downstream load profiles. Network busbars are assigned aggregated downstream load profiles. Prefixing "A" to the profile category supports analysis in large systems. QDS supports profiling.

Table 4-3: Profiling Busbars

Code	Load Profile	DG Profile
MV LB	Rural	Solar PV (SPV)
MV LB	Bulk	SPV
MV LB	Munic	SPV
HV NB	A_Rural	SPV
EHV NB	A_Bulk	SPV

Table 4-3 is populated with only SPV.

4.7.6 Activating DG for placement

Power Factory variation and expansion stages were configured using standardized solar PV generation models. DG connections arranged by voltage are connected to load and network busbars. Each bus was assigned a generation day. No two busbars had more than one generation connection. Size DG according to ranking. Match generator transformers to generation output. Configure the station controller to deliver unit power factor at the point of connection. Ensure solar PV farm delivers rated unity power (accounting for farm losses) at the point of connection.

DIgSILENT Programming Language (DPL) script ensured efficient and effective case file set up.

4.7.7 Evaluate DG sizing for voltage variation

Voltage variation tests carried out on load and network busbar confirms Grid Code requirement for loss of generation. Valid voltage variation results confirm continuation for QDS and static time based load flow. Results are generated by running a DPF grid and system summary report. Invalid voltage variation results warrant reduction in sizing of DG and repeating the activity.

4.7.8 Optimal selection process

Selection compared pre- and post-DG results aimed at optimum placement to reduce grid losses.

4.8 Analysis of results

Comparing pre-DG to post-DG losses for busbar selection identifies optimum location and sizing of DG to reduce losses. Table 5-3 to Table 5-8 in sections 5.6.1 to 5.6.7 show comparative results, based on the above method. A clear distinction of losses for DG placements on load centered busbars and network busbars are obvious. Study results and grid losses are presented in chapter five.

4.9 Chapter in perspective

This method allows for standardization of DG capacity sizing and placement when dealing with larger utility networks. Results present a clear and comparable means to making and informed selection to reduce technical losses. Utility engineers are empowered to improve the efficiency and effectiveness of DG integration planning. This methodology can be adapted and extended to downstream feeder networks.

5   ANALYSING THE UTILITY TEST GRID

The utility test grid displays interconnectivity of a typical network supplying industrial, commercial and rural load. The grid comprises of four sub-grids. A transmission grid; sub transmission grid; distribution grid and a distribution network feeder grid. This research will analyse the sub transmission grid to answer the research questions.

5.1   Transmission grid

The transmission grid shown in Figure 8-1 is sourced from three simulated external grids that represent the equivalent upstream network at each source. Source 1 models a slack bus [103] and supplies all real and reactive power swings as the load and loss needs varies. The slack bus model (V, δ) as known parameters and (P, Q) as unknown parameters. Source 2 models a constant power and voltage bus (P, V) that supplies a constant power of 100MW at a constant voltage of 1.03 per unit (p.u.). Constants (P, V) buses classified as generator buses model (P, V) as known parameters and (Q, δ) as unknown parameters. Source 2 has a maximum short circuit rating of 31.5 kA. Source 3 is a constant (P, V) source with a 50MW output at constant voltage of 1.03 per unit. The maximum short circuit rating of source 3 is 27 kA.

Source 1 and 2 feed into a 400kV Bus and Source 3 feeds into a 275kV bus. The 400kV bus supplies a step down to 88kV, 132kV and 275kV. The 275kV receives another infeed from external source 3. The 400kV, 275kV, 132kV and 88kV busbars show on both transmission grids and the sub transmission grids for easy of reference.

5.2   Sub-Transmission
5.2.1   Grid I and Grid II

Figure 8-2 and Figure 8-3 shows the sub transmission grid with two dominant HV networks. The 88kV network fed from the 400kV infeed at ST1 400kV. The 132kV network feed into both the 66kV via the 132kV Pluto substation and the 33kV network via the 132kV Pearl network.

The 88kV Basket substation steps down to 33kV and supplies the 11kV substations. The 33kV also receives support from the 132kV White infeed.

The 400kV steps down to 275kV and 132kV linking to the 66kV network. Figure 8-2 and Figure 8-3 with section 8.3.1 complete a full description of the networks that composes the sub transmission grid.

5.2.2   Line Parameters

The utility network was simulated with conductor impedances and line lengths shown in Table 8-1 and Table 8-2 in 8.3.1.

5.3   System overview prior to distributed generation

The methodology in chapter 4 warrants a thorough examination of the utility network prior to distributed generation (pre-DG). This establishes the base case for voltage limits and fault level. Fault level determines immunity to network disturbance. Real and reactive power flow and loss are recorded as the baseline for pre-DG. Section's 5.3.1 to 5.3.7 shows the pre-DG base case for the utility network. All equipment is within acceptable loading limits. All busbars are within voltage limits of 0.95p.u and 1.05p.u.

Pre-DG simulations were dated prior to 31 August and post-DG simulations after the 31 August. Twenty-four hour (QDS) time series load flows were performed using DIgSILENT Power Factory © (DPF). Aggregated downstream load profiles at the 132kV Diamond bus and ST1 Sub bus reveal similar profiles for real and reactive power. Figure 8-4 shows the QDS real and reactive power at Diamond 132kV busbar. Figure 8-5 shows the QDS real and reactive power at Sub 132kV. These two busbars represent the total load consumed over a 24 hour period.

Peaks and troughs are areas of interest on Time Series Simulations (TSS) / Quasi-Dynamic Simulations (QDS). Load flows converge with no voltage or thermal violations at peak and trough load times. All non-Quasi-Dynamic simulations are performed at 12 pm. This is deemed to be time of solar PV peak and used to compare pre- and post-DG results.

5.3.1   Load types and profiles

Constant power loads make up all loads types in the utility test grid. Three standard daily load profiles where used for the time series simulation load flow studies. A bulk load profile, municipality load profile and rural load profile shown in Figure 5-1. Rural profiles depict the classic twin-peaks, while bulk and municipality profiles present high demand during midday loading. Real and reactive power varies according to load profiles.
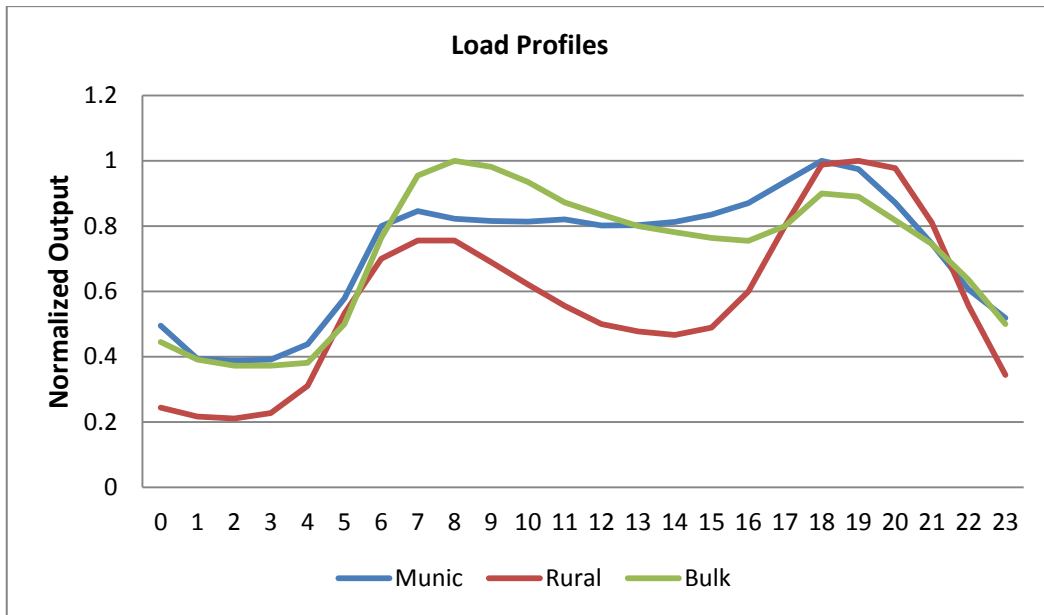
Figure 5-1 Daily Load Profiles

5.3.2 Sub – transmission grid loading

Table 8-3 shows 28 load centred busbars. Each load varies as the load profile changes over the course of the day. Higher voltage busbars that carry aggregated loads are not load centre busbars. They also carry losses to supply the loads at the remote load centres.

Table 8-3 shows the results of a 12pm load flow together with regulated busbar voltages and power factors for each load.

5.3.3 System fault level

Table 8-4 and Table 8-5 show three phase fault levels produced by the IEC 60909 method. These appear in descending order of voltage and fault level in MVA.

5.3.3.1 High-voltage fault level

Higher network voltages, positioned closer to the dominant source experiences lower impedance and have higher fault levels. High fault level busbars have higher tolerance to system disturbances. They also have a higher tolerance to DG injection with lower voltage variation during loss of generation.

5.3.3.2 Medium voltage fault level

Medium voltage busbars have lower fault levels because of the increased in Thevenin impedance. Medium voltage busbars have a lower tolerance to network disturbance compared with high-

voltage busbars. This reduces the potential for DG injection at MV busbars. Table 8-5 displays the medium voltage fault level for the utility test grid. Fault levels at netowrk busbars predicts maximum size of DG, such that the voltage variation limit is acceptable 5.5.

5.3.4 System voltage level

The system voltages vary continuously through the day. These voltages are determined by the supply of load, power losses and volt drop between source and sink. Load flow analysis allows comparison of pre- and post-DG at time of solar peak being 12pm. System voltages were recorded at time of solar peak. Table 8-6 and Table 8-7 documents per unit voltage and angles at each busbar. Evidence of voltage control philosophy can be seen in the p.u. voltage values of the Sapphire 66kV and 22kV busbars. Although the 66kV bus has dropped below 1 p.u., the 22kV bus is at 1.03 due to the transformer tapping.

5.3.4.1 High-voltage busbar system per unit values

Load flow studies for peak, off-peak and 12pm reveal no voltage violation. Table 8-6 shows record of pre-DG voltages at 12pm. No voltage violations were recorded on the HV bus system.

5.3.4.2 Medium voltage busbar system per unit values

Voltage control philosophy of HV transformers control medium voltage levels. Voltages change throughout the day within a bandwidth of the tolerance set points. Table 8-7 presents a snapshot of the pre-DG view at 12pm. Voltage studies conducted at times of high load; low load and at 12pm reveal no voltage violation of upper and lower limits of 0.95p.u and 1.05p.u. High load represents 6pm to 7pm and low load was at 2am and 11pm.

5.3.5 Active power load flow

Table 8-8 and Table 8-9 represent the active power load flow for both HV and MV networks at 12pm. Convention dictates that negative signs for active power, indicates flow into the busbar. Conversely positive signs, imply power flow out of the bus. The following relationship between the voltage angle and active power flow was observed. Active power flows from a smaller voltage angle to a larger voltage angle. The difference between the "from busbar" and "to busbar" are line losses due to line impedance. Reactance (X) and resistance (R) characterized impedance.

Various conductors have different ranges of X/R ratios. They present varying losses based on active and reactive currents. Table 8-13 shows varying active and reactive losses.

5.3.6   Reactive power load flow

Table 8-10 and Table 8-11 show the reactive power load flow for both HV and MV networks at 12pm. The same sign convention applies for reactive power. The relationship between the voltage magnitude and reactive power flow was observed. Reactive power flows from a larger voltage magnitude to a small voltage magnitude.

Apparent power represents the Pythagorean sum of real and reactive power. Solar PV plants do not have reactive purchasing power agreement and operate at unity power factor. Solar PV plants that generate reactive reduce their real power billed to the utility. Technically, solar PV plants have capability of supplying and absorbing reactive power. Economically and contractually they may not, unless called on by the utility control centre. The absence of reactive power from a solar PV plant implies other means of reactive compensation. This could be avoided during ramp-up and ramp-down cycles, as shown by the dashed line in Figure 5-2. Utilities can capitalize on inherent reactive power during these cycles not to negatively affect the maximum export capacity.

This is an important finding that seeks to optimize the reactive power flow through solar DG without additional reactive power compensation. Traditional shunt capacitors may still be employed where size exceeds the natural limit of the solar DG.

Reactive power losses recorded the difference in flows between the "from" and "to" busbars, shown in Table 8-10 and Table 8-11.

5.3.7   Sub-transmission phase angles – power factor

Table 8-12, reflects the pre-DG phase angle at each of the busbars excluding the load bus. The cosine of the phase angle represents the power factor at each bus. Examining the pre-DG phase angle of the 11kV Earth bus, obtained from Table 8-3 row 17, has record of the power factor at 0.965. The power factor at the load does not change as no customer compensation is applied. The power factor on the 11kV bus reflected through the transformer impedance onto the 66kV Earth bus as shown in Table 8-12. The 66kV Earth bus is supplied via two lines. The impedance of these supply lines affect the phase angle and power flow. Row 13 and 19 show the supplementary phase angles at the 66kV Earth busbar.

Table 5-1 Phase angle comparison pre and post DG

Table Ref Row	Terminal i Busbar	Terminal j Busbar	Magnitude Terminal i in p.u.	Magnitude Terminal j in p.u.	Angle between Voltage and Current Terminal i in deg.	Angle between Voltage and Current Terminal j in deg.
Table 8-12 13	Earth 66kV	Mercury 66kV	0.9647	0.9785	-135.1113	42.9492
Table 8-12 19	Sapphire 66kV	Earth 66kV	0.9794	0.9647	9.3246	-171.0584
Table 8-17 13	Earth 66kV	Mercury 66kV	1.005205	1.010247	-113.6103	62.93881
Table 8-17 19	Sapphire 66kV	Earth 66kV	1.01379	1.005205	18.65493	-160.8706

Comparison of row 13 from Table 8-12 (pre-DG) and row19 from Table 8-17 (post-DG) shows a widening phase angle, thus worsening the power factor. Active power is reduced from the supply of DG; reactive power remains unchanged, resulting in negatively affecting the upstream power factor. Reactive power compensation is required to support the change in phase angle.

Alternatively, compensation at the load busbar will reduce the reactive power requirement. Less upstream compensation is required to address the changes in phase angle.

5.3.8   Sub-transmission grid loss

Table 8-13, shows the active and reactive pre-DG line losses for each of the sub-transmission lines. Total grid losses, include transformer and line losses, are retrieved through a grid summary report. Grid losses in

Table 8-14 denotes the base case for pre-DG as at 12pm being the time of solar peak.

5.4   Distributed generation profile characteristic

Non-dispatchable RE sources constitute wind and solar PV, section 3.9. Since synchronous generation represents dispatchable DG due to a controlled RE source, it was not considered in this study. Unpredictability nature of wind excluded it for the study results. The method developed in chapter 4 will apply to all types of embedded generation.

The more predictable non-dispatchable solar PV generation pattern was used for research purposes. A southern hemisphere's solar PV irradiance curve without cloud cover was modelled in Power Factory as shown in the solid line in Figure 5-2. Further control limited solar DG to unity power factor.
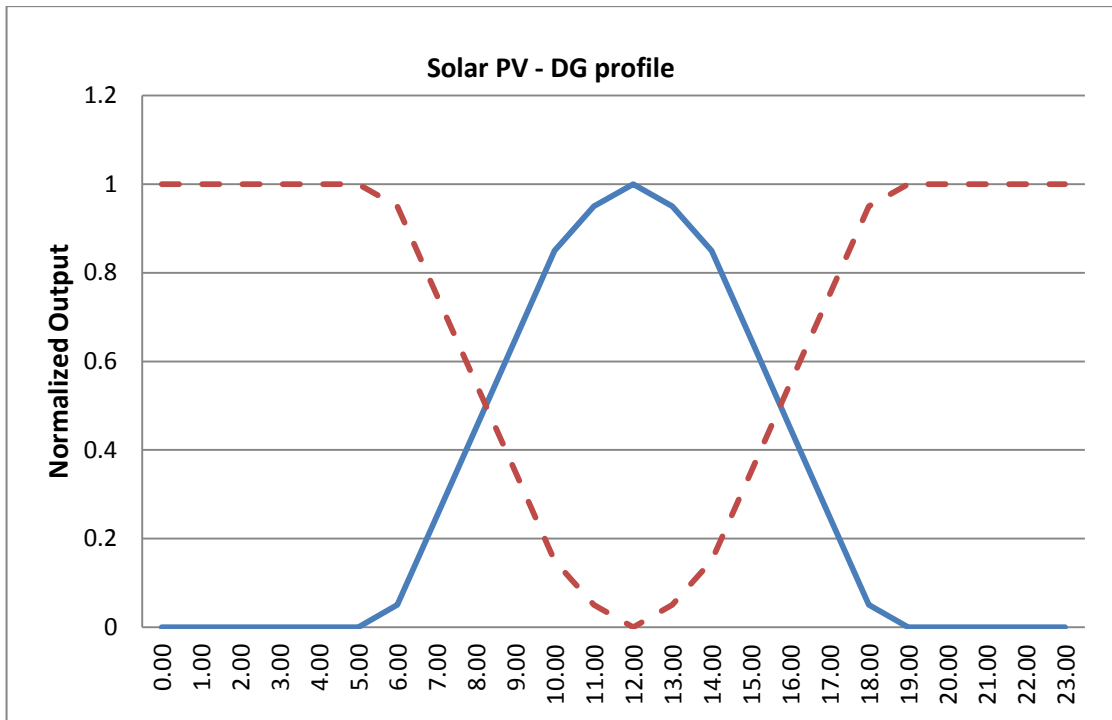
Figure 5-2 Solar PV Power Output

Subtracting the DG profile from the load profiles, results in a "duck" shaped resultant profile visualized in Figure 5-3. Negative real power represents surplus DG will flow upstream, from the point of connection, to supply neighbouring load centres. Reverse power flow will incur losses, when the mismatch between the load profile and DG profile is large.
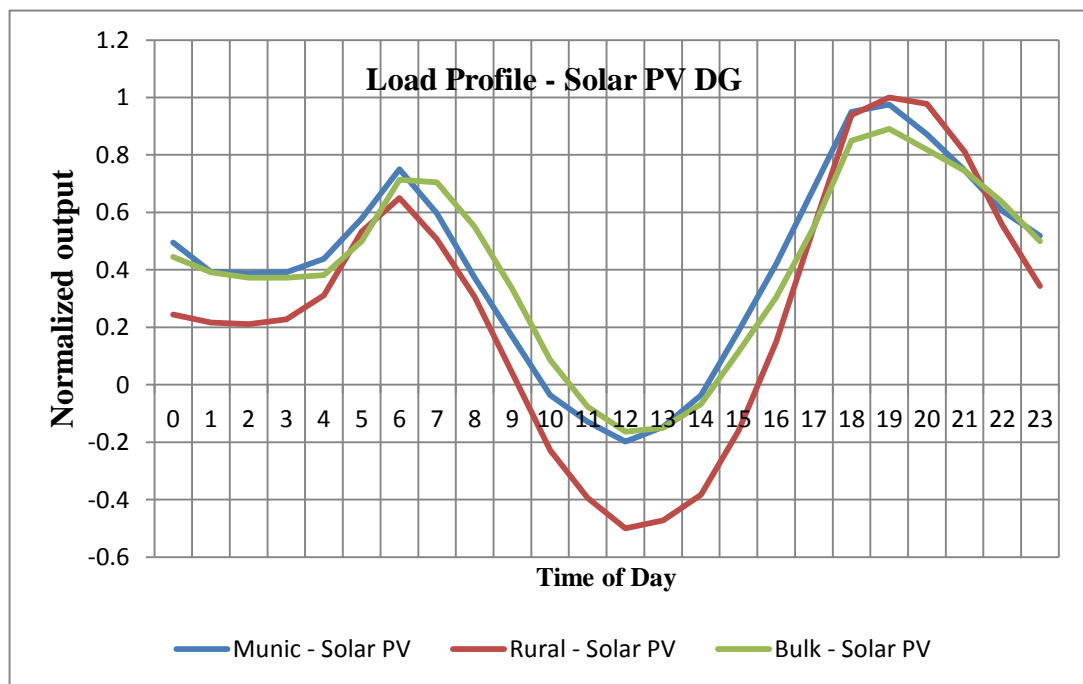
Figure 5-3: Resultant differential load VS Solar PV profile

5.5   Voltage variation results

Voltage variation analysis assesses the change in voltage at a busbar in the event of loss of generation. Two schools of thoughts define two approaches to the voltage variation test.

The first, aims to compare the pre-fault voltage to the post-fault voltage. Pre-fault load flows are executed with auto shunt and transformer tapping enabled. Post-fault voltages are determined by removing DG and locking all voltage compensation devices.

The second aims to record the change in busbar voltage at each ramp up of DG from 0MW to full load. This method has the advantage of monitoring the increase in busbar voltage (under locked transformer tap) to assess the continuous voltage change, resulting from increased DG injection.

Results of the second method are shown in 8.5.1.1 and 8.5.1.2. Tests were performed on the 132kV Diamond busbar and 33kV Basket busbar.

The test bus voltage rises as real power injected into the busbar reduces the upstream demand. The volt drop from the sending bus reduces, thereby raising the voltage at the receiving end. Voltage "bending" can be seen at higher voltage busbars shown in Figure 5-7. This is associated with diminishing voltage rise due to the non-linear load flow solution of meshed impedance networks. Voltage variation test results for the 11kV Earth busbar demonstrates the voltage increase.

5.5.1   11kV Earth busbar assessment for DG

5.5.1.1   Voltage variation results – Earth 11kV busbar

The fault level at the 11kV Earth busbar is 200 MVA therefore 8 MVA (8 MW Cos $\theta = 1$) solar PV was applied. Voltage variation noted in section 5.4, shows an increase in voltage due to the injection of real power at 11kV basket busbar Figure 5-4. Small DG sizing causes a linear increase in voltage. A total increase in voltage of 1.4% is noted. Sudden loss of generation would result in a volt-drop of 1.4 %. This is allowable according to [3].

Consequently, the rise in bus voltage at the 66kV Earth bus exceeds the 1.05 p.u limit by 0.0015p.u. A smaller solar PV generator is therefore recommended. Alternatively, the operational voltage philosophy needs to endorse the lowering of set-point voltages at the 66kV Earth busbar.

Additional voltage variation results shown at Sapphire and Diamond 132kV busbars, Figure 5-6 and Figure 5-7, respectively. The 132kV Diamond busbar displays the diminishing voltage rise.
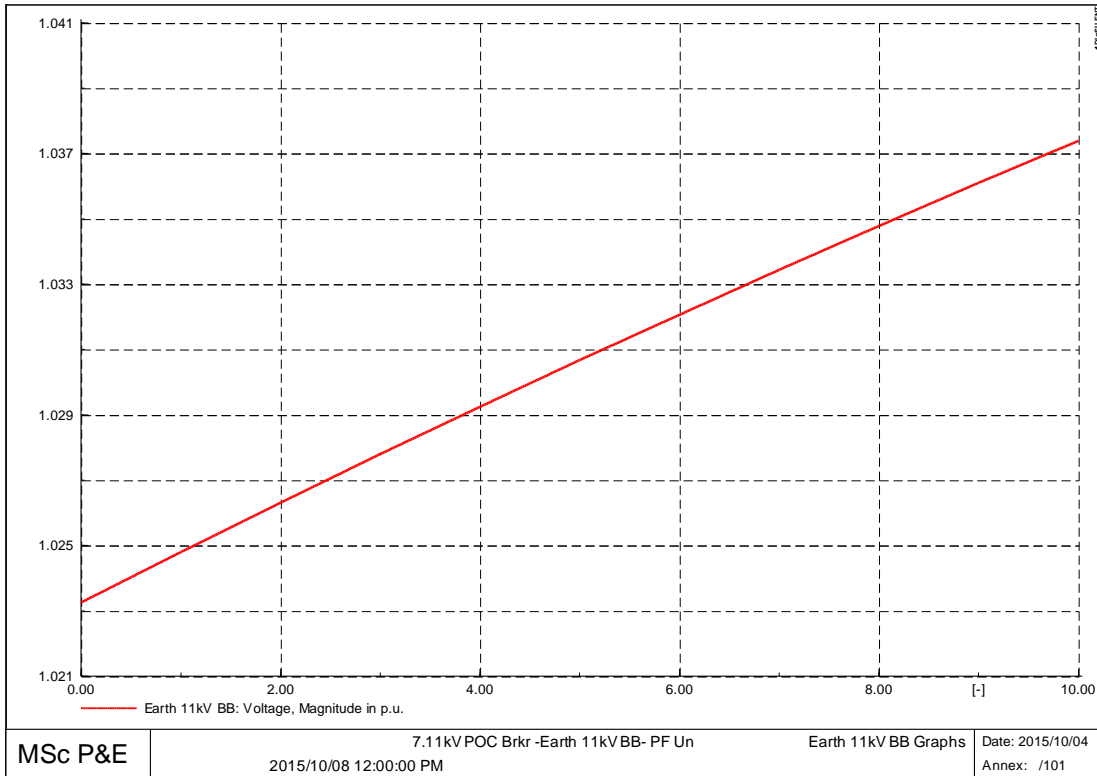
Figure 5-4 11kV Earth Busbar Voltage Variation Result
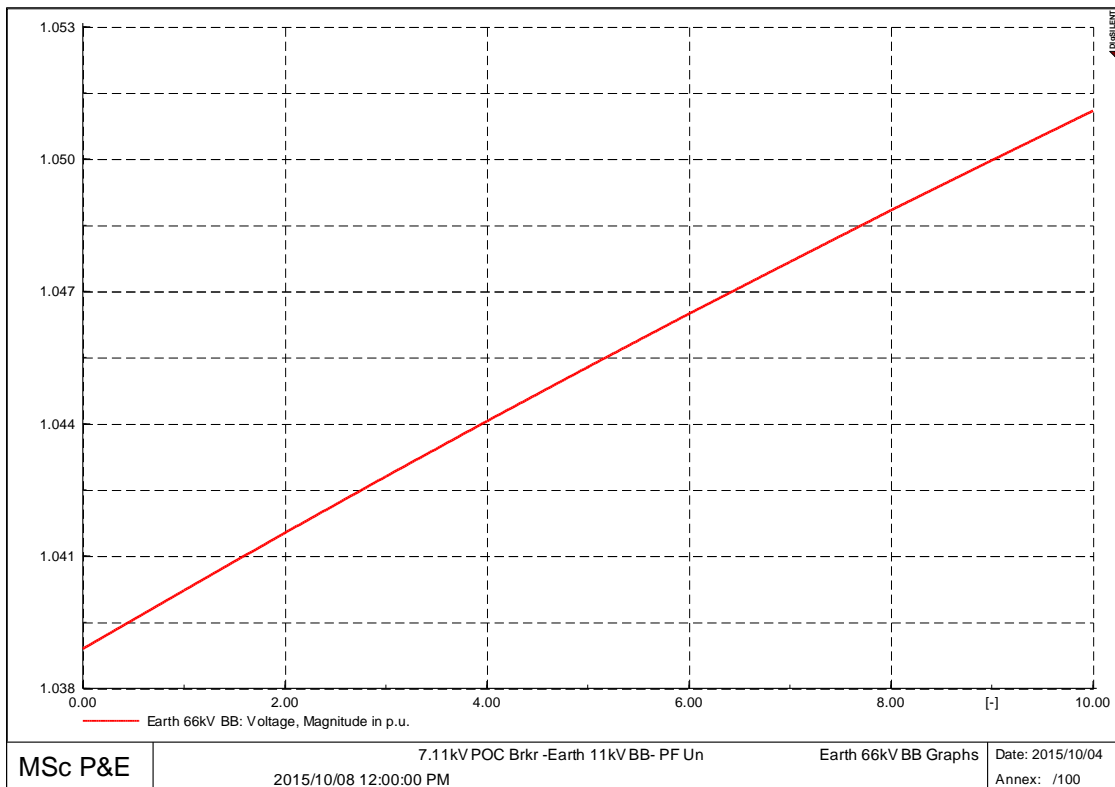
Figure 5-5 Voltage Variation Result of 66kV Earth Bus response to 8MW injection at 11kV Earth Busbar
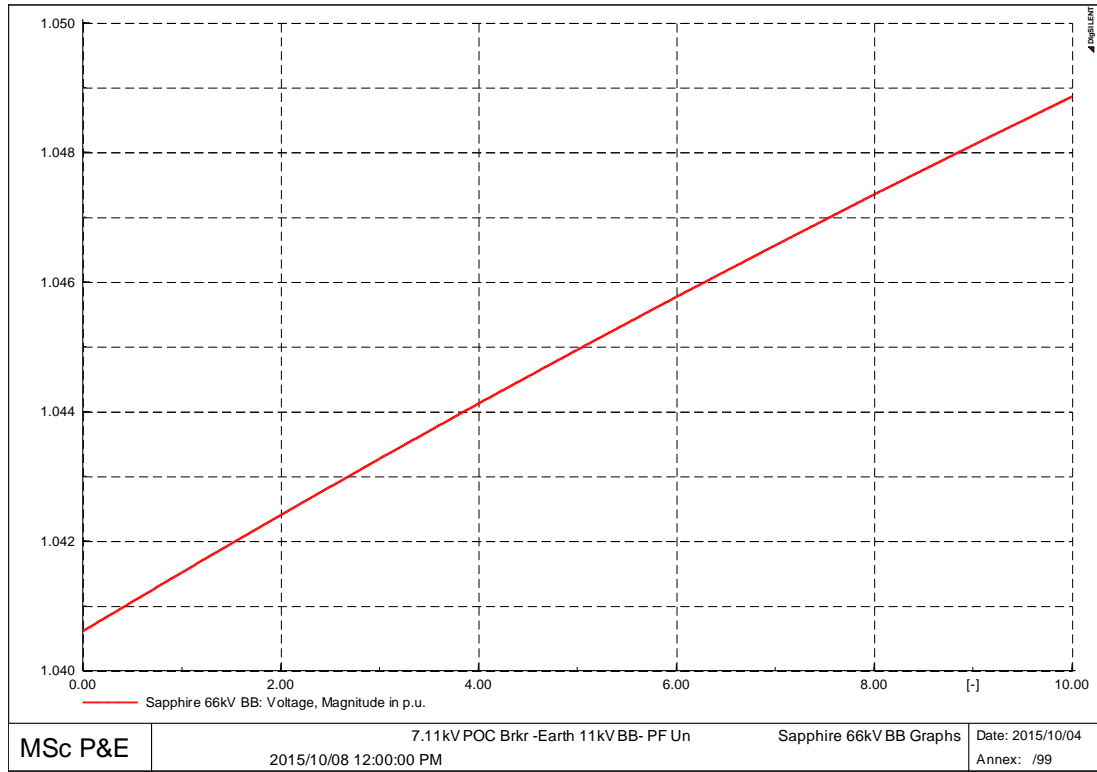
Figure 5-6 Voltage Variation Result of 66kV Sapphire Bus response to 8MW injection at 11kV Earth Busbar
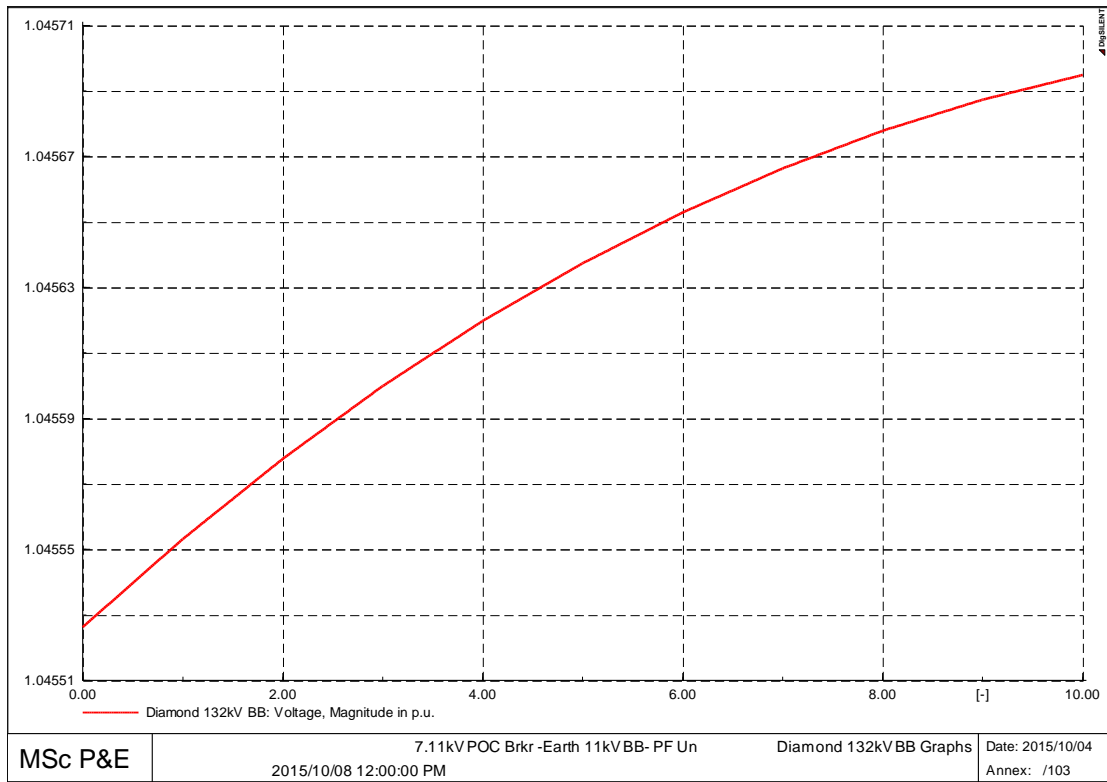
Figure 5-7 Voltage Variation Result of 132kV Diamond Bus in response to 8MW injection at 11kV Earth Busbar

5.5.1.2   Sub-transmission load flow – post DG 11kV Earth bus

The fault level at the 11kV Earth busbar is 200 MVA therefore 8 MVA (8 MW Cos θ = 1) solar PV was applied. Real and reactive power flows are shown in Figure 5-10. Prior to DG, Figure 5-8 and Figure 5-9, show two similar profile shapes at 11kV and 66kV busbars. Post-DG results are shown in Figure 5-10. Comparison of the pre- and post-DG at the 66kV Earth bus shows the deepening of midday profile as DG injection increases. The "commercial" Earth load profile has been altered to a "twin peak", residential profile.
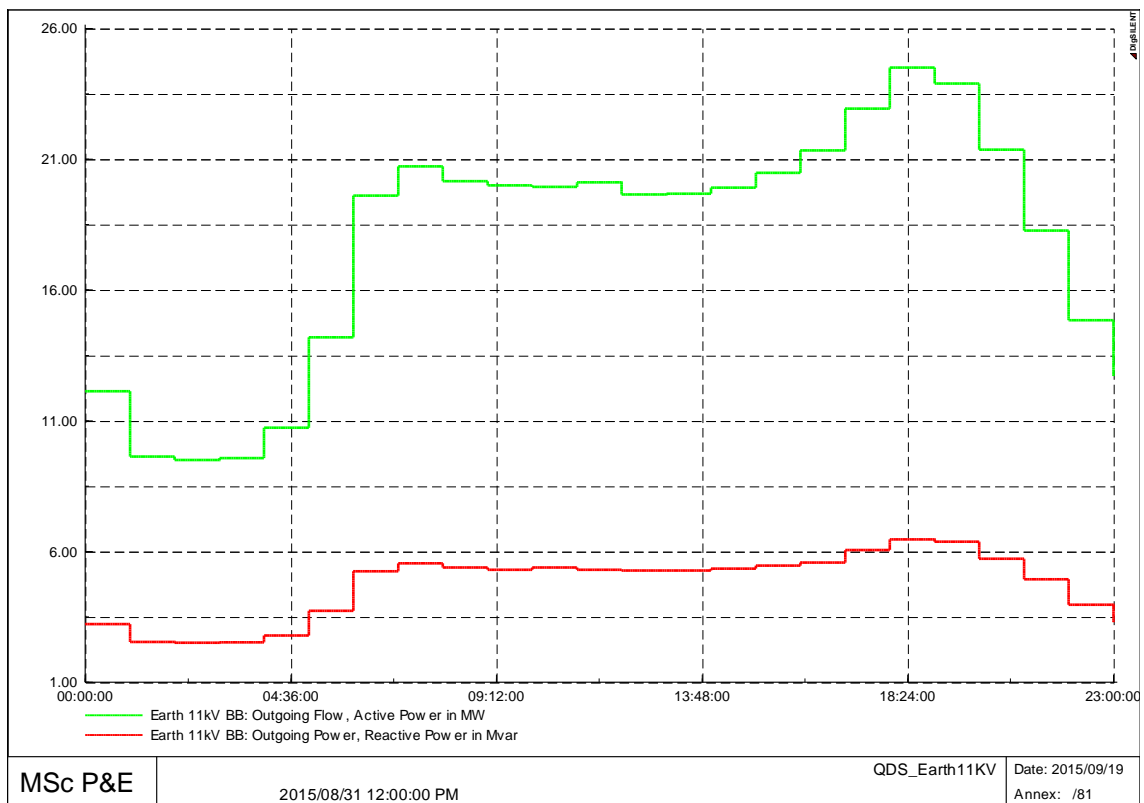
Figure 5-8 11kV Earth Busbar at 12PM – Pre–DG
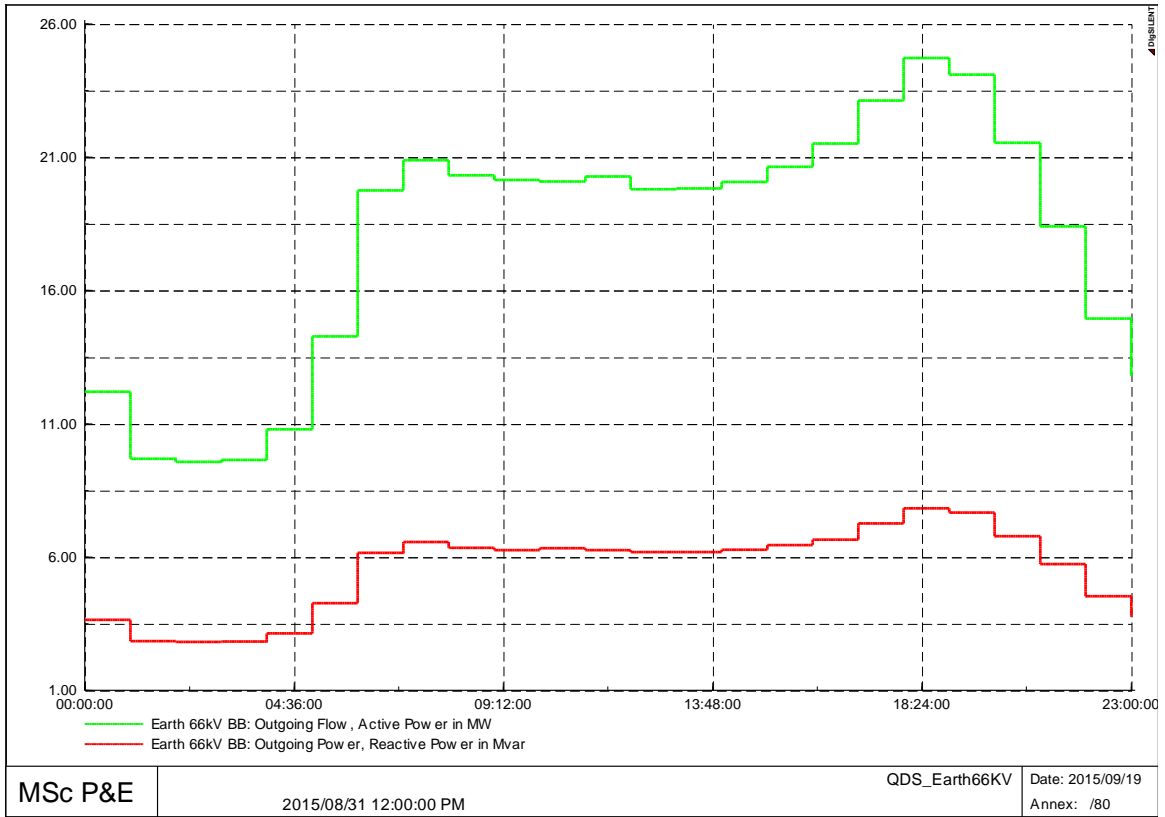
Figure 5-9 66kV Earth Busbar at 12PM – Pre–DG
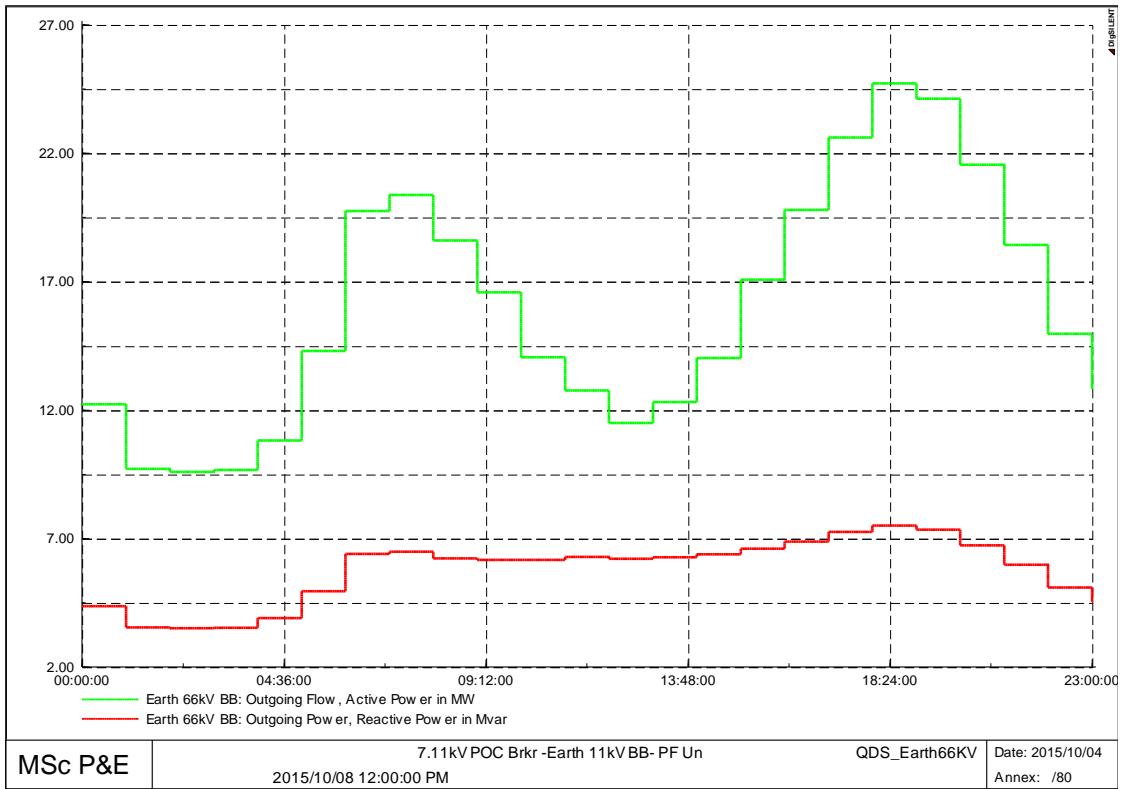
Figure 5-10 66kV Earth Busbar at 12PM – Post–DG

5.5.1.3   Sub-transmission grid loss – post DG 11kV earth

The 11kV Earth busbar hosted a relatively small solar DG plant, due to its relatively low fault level. Introducing 8MWs of DG reduced grid losses by 9.5% for real power and 13% for reactive power. Loss reduction results from DG being consumed at the load. The 11kV Earth bus load profile makes it ideal for solar PV. Table 5-2 shows a summary of the post-DG grid loss reported extracted from DPF.

<p align="center">Table 5-2 Grid Loss Result after 8 MW of DG applied to 11kV Earth bus</p>

2015/10/08 12:00:00 PM
Grid Summary Post DG on 11kV Earth 12pm
Grid Losses = 7.03 MW 16.24 Mvar

Two additional post-DG assessments results are presented. In 5.5.1, solar DG was connected to a load centre busbar. In 8.5.1.1 and 8.5.1.2 solar DG was connected to network (non-load) busbars. Analysis showed varying degrees of grid losses experienced based on load profile; load type; fault level.

5.6   Summary of post-DG on utility network

Table 5-3 to Table 5-8 list a full set of results for all load and network busbars. Tables report maximum allowable DG based on fault level in MVA, pre- and post-DG power flows and losses. Percentage change in real and reactive power losses concludes the reporting.

5.6.1   Utility grid – post-DG

Three voltage levels were selected to report the impact of post-DG connection to the utility network. Figure 8-8 show the effect of injecting active power into the 132kV Diamond busbar. Source profile flattens is observed due to the PV injection. Similarly Figure 8-20, shows the impact on the 88kV Basket busbar due to the injection of active solar power at the 33kV Basket bus. A deepening of the midday profile is observed as the solar DG profile increases. Figure 5-9 and Figure 5-10 compared, with explanation, the pre- and post-DG connection to the 11kV Earth busbar.

5.6.2   11kV busbar - post-DG results

Table 5-3 confirms the placement of DG to reduce losses is optimized when located close to or at load centres. The placement of solar PV at the 11kV Earth busbar yields optimum load loss

reduction. The 11kV Earth busbar carries a characteristic municipality load profile. This load is ideally suited for DG connections.

Application of solar PV to typical rural "twin peak" profiles may not yield optimum results, due to reverse power flow incurring further losses.

Table 5-3: 11kV Busbar - Post-DG Results

Bus Name Voltage	Max RE (MVA)	Pre DG load MW @ 12PM	Pre DG load MVAr @ 12PM	Sub Tx Grid Loss MW	Sub Tx Grid Loss MVAr	Delta Grid Loss MW	Delta Grid Loss MVAr
Earth 11kV BB	8	19.6490	5.3359	7.03	16.24	-9.5%	-13.3%
Nandos 11kV BB	7	18.2617	-5.2482	7.56	16.82	-2.7%	-10.2%
Yellow 11kV BB	6	13.7973	2.9603	7.56	16.41	-2.7%	-12.4%
Blou 11kV BB	6	7.6028	2.5667	7.58	16.73	-2.4%	-10.7%
Pink 11kV BB 2	6	3.8021	0.7822	7.6	16.82	-2.2%	-10.2%
Pink 11kV BB 1	6	5.3897	1.1892	7.6	16.94	-2.2%	-9.6%
Orange 11kV BB	6	6.5435	2.1442	7.63	17.03	-1.8%	-9.1%
Basket 11kV BB	7	4.6455	1.0742	7.64	16.87	-1.7%	-9.9%
Green 11kV BB	6	4.8667	1.4457	7.65	17.16	-1.5%	-8.4%
Black 11kV BB	4	6.0242	1.1620	7.66	17.45	-1.4%	-6.8%
Ruby 11kV BB	4	2.5650	1.5333	7.82	18.31	0.6%	-2.2%
Linkedln 11kV BB	9	18.5820	-7.0437	7.87	17.42	1.3%	-7.0%

Review of Table 5-3 nominates all negative real and reactive grid loss for selection. Two busbars in this voltage range do not qualify for selection being Ruby and LinkedIn.

5.6.3 22kV busbar - post-DG results

Table 5-4 shows the 22V Sapphire Mercury busbars are close contenders for DG selection, resulting from their municipality and bulk load profiles respectively. Fault level ranking Earth, sapphire and Mercury, reveals 200MVA, 175MVA and 100MVA, respectively.

Table 5-4: 22kV Busbar Post-DG Results

Bus Name Voltage	Max RE (MVA)	Pre DG load MW @ 12PM	Pre DG load MVAr @ 12PM	Sub Tx Grid Loss MW	Sub Tx Grid Loss MVAr	Delta Grid Loss MW	Delta Grid Loss MVAr
Sapphire 22kV	7	10.3217	1.8484	7.34	16.97	-5.5%	-9.4%
Mercury 22kV	4	3.4761	0.6682	7.45	17.72	-4.1%	-5.4%
Saturn 22kV	4	4.3228	1.1534	7.59	17.91	-2.3%	-4.4%
Emerald 22kV	6	5.1609	0.9708	7.59	17.61	-2.3%	-6.0%
Jupiter 22kV	5	2.6357	0.7419	7.62	17.88	-1.9%	-4.5%
Uranus1 22kV	4	3.9600	0.7314	7.63	17.94	-1.8%	-4.2%
Uranus2 22kV	4	2.9700	0.5679	7.64	17.99	-1.7%	-4.0%
Pluto 22kV	4	2.8350	-1.7034	7.66	18.28	-1.4%	-2.4%
Topaz 22kV	3	2.3520	0.9373	7.66	18.16	-1.4%	-3.0%
Pearl 22kV	6	6.2208	1.7326	7.7	17.7	-0.9%	-5.5%
Jade 22kV	3	2.9400	0.7462	7.75	18.19	-0.3%	-2.9%
Ruby 22kV	4	3.0240	1.1291	7.8	18.28	0.4%	-2.4%
Mars 22kV	10	4.7700	-2.6984	8.05	18.06	3.6%	-3.6%

Review of the 22kV post-DG results nominates all negative real and reactive grid losses for selection. Two busbars do not qualify being Ruby and Mars as there real power losses are higher than network losses without DG.

5.6.4   33kV busbar - post-DG results

Network topology shows all 33kV busbars feed 11kV loads. Comparison of loss studies shows a higher loss reduction. Reduced demand at 33kV reduces upstream load requirements, thereby reducing the losses. Higher 33kV fault levels hosts larger DG sources, which are more effective at supplying load centres. Comparing Table 5-3 and Table 5-5 shows the 33kV busbars supporting least twice DG hosting capacity and having approximately one-third more in loss reduction.

Table 5-5: 33kV Busbar - Post-DG Results

Name	Max RE (MVA)	Pre DG load MW @ 12PM	Pre DG load MVAr @ 12PM	Sub Tx Grid Loss MW	Sub Tx Grid Loss MVAr	Delta Grid Loss MW	Delta Grid Loss MVAr
Blou 33kV	12	7.6447	2.8427	7.53	15.66	-3.1%	-16.4%
Yellow 33kV	12	20.1666	7.0702	7.53	15.68	-3.1%	-16.3%
Red 33kV	5	5.1815	1.8465	7.54	17.03	-3.0%	-9.1%
Pink 33kV	12	7.6447	1.8237	7.57	15.87	-2.6%	-15.3%
Orange 33kV	13	6.5795	2.3599	7.58	15.73	-2.4%	-16.0%
Green 33kV	14	8.1242	0.0022	7.6	15.64	-2.2%	-16.5%
Basket 33kV	16	19.4249	9.8507	7.6	15.26	-2.2%	-18.5%
Black 33kV	14	9.0460	0.4092	7.61	15.69	-2.1%	-16.2%
White 33kV	15	17.1908	0.4541	7.62	15.57	-1.9%	-16.9%

Review of Table 5-5 nominates all negative real and reactive grid losses for selection.

5.6.5   66kV busbar - post-DG results

Larger sizing of DG showed larger grid losses when not placed close to load busbars. The 66kV Earth and Mercury busbars shows reduced post-DG loss. Table 5-6 show the results for DG integration with 66kV busbars.

Table 5-6 66kV Busbar - Post-DG Results

Name	Max RE (MVA)	Pre DG load MW @ 12PM	Pre DG load MVAr @ 12PM	Sub Tx Grid Loss MW	Sub Tx Grid Loss MVAr	Delta Grid Loss MW	Delta Grid Loss MVAr
Earth 66kV	13	19.7955	6.2409	7.52	16.88	-3.2%	-9.9%
Mercury 66kV	11	7.2681	4.2762	7.69	17.28	-1.0%	-7.7%
Saturn 66kV	6	4.3491	1.2512	7.88	18	1.4%	-3.9%
Sapphire 66kV	16	26.6554	4.8990	7.96	17.3	2.4%	-7.6%
Topaz 66kV	7	2.3664	0.9944	8	18.1	3.0%	-3.4%
Uranus 66kV	13	6.9671	1.4930	8.15	17.77	4.9%	-5.1%

Name	Max RE (MVA)	Pre DG load MW @ 12PM	Pre DG load MVAr @ 12PM	Sub Tx Grid Loss MW	Sub Tx Grid Loss MVAr	Delta Grid Loss MW	Delta Grid Loss MVAr
Emerald 66kV	13	5.1798	1.1598	8.17	17.8	5.1%	-5.0%
Jade 66kV	5	2.9563	0.8204	8.25	18.71	6.2%	-0.1%
Jupiter 66kV	16	10.2016	4.7614	8.28	17.76	6.6%	-5.2%
Pluto 66kV	16	29.1642	8.7594	8.28	17.77	6.6%	-5.1%
Ruby 66kV	9	5.6245	2.8332	8.5	18.74	9.4%	0.1%
Diamond 66kV	41	77.4664	17.3212	10.93	20.13	40.7%	7.5%

Review of 66kV post-DG results nominates Earth and Mercury busbars for selection. These two busbars were also contenders at 22kV.

5.6.6   88kV busbar - post-DG results

Increased power losses for larger DG sizing are note for 88kV busbar voltages shown in Table 5-7.

The pre-DG load flowing through Sub 88kV is 57MWs with 45MWs of solar DG connected. DG is not being consumed at this bus and requires to flow to the load centre. This flow insures losses as DG is injected at a sub-optimal location affecting the power flow balance shown in Table 5-7.

Similarly, 88kV Basket shows an increase in losses compared to the base case, but a reduction compared to Sub 88kV. Reduced reactive losses lie in the supply line and transformer impedance of 88kV networks. Reduce real power losses are attributed to the 88kV Basket bus, being closer to the load centre.

Table 5-7: 88kV Busbar - Post-DG Results

Bus Name Voltage	Max RE (MVA)	Pre DG load MW @ 12PM	Pre DG load MVAr @ 12PM	Sub Tx Grid Loss MW	Sub Tx Grid Loss MVAr	Delta Grid Loss MW	Delta Grid Loss MVAr
Sub 88kV	45	57.7221	0.9387	11.26	21.75	44.9%	16.1%
Basket 88kV	20	19.5157	11.0402	8.67	18	11.6%	-3.9%
Nandos 88kV	10	18.2781	-4.4193	8.01	17.67	3.1%	-5.7%
Linkedln 88kV	17	18.5985	-6.1468	8.86	18.97	14.0%	1.3%

Review of the post-DG 88kV summary results does not nominate any busbar selection.

5.6.7   132kV busbar - post-DG results

Increased power losses for even larger 132kV DG sizing were observed. Similar to 88kV explanations explain the reasoning. Where local load exists, these are serviced first and surplus power flows to adjacent load centres. The 132kV Pearl and Yellow busbars fits this description and have relatively smaller losses. Injection at Diamond 132kV and ST1 SUB 132kV present alternate centralized distributed generation. These cases represent suboptimal concentration of DG. Table 5-8 shows the grid loss for 88kV test busbars.

Table 5-8: 132kV Busbar - Post-DG Results

Bus Name Voltage	Max RE (MVA)	Pre DG load MW @ 12PM	Pre DG load MVAr @ 12PM	Sub Tx Grid Loss MW	Sub Tx Grid Loss MVAr	Delta Grid Loss MW	Delta Grid Loss MVAr
Pearl 132kV	25	43.7958	10.6134	8.25	18.71	6.2%	-0.1%
Yellow132kV	20	20.1839	8.2596	8.55	17.62	10.0%	-5.9%
Pluto 132kV	23	32.1047	8.4864	8.73	19.18	12.4%	2.4%
White 132kV	24	37.4567	8.7442	8.83	17.9	13.6%	-4.4%
Diamond 132kV	89	77.7192	21.2553	15.43	30.17	98.6%	61.1%
ST1 Sub 132kV	98	78.1757	17.4836	16.61	31.44	113.8%	67.9%

Review of post-DG table for 132kV busbars does not nominate any busbar for selection.

Results in Table 5-3 to Table 5-8 confirms optimization of DG to reduce losses can be achieved when placed close to load centres.

6 CONCLUSION

6.1 Overview

This chapter summarises the findings of the research and evaluates the hypothesis in relation the key questions raised in chapter 1. The importance and relevance of the research is demonstrated in section 6.2 followed by future work with recommendation and conclusions.

6.2 Summary of findings

The research has been guided by the literature peer review of previously published scholarly works. Analysing the topic led to the hypothesis statement, stated in 1.4 and restated below.

Are the current IPPs optimally and strategically connected onto the Eskom grid to reduce losses, considering the generation and financial constraints faced by South Africa?

Deconstructing the hypothesis into research questions addressed four research questions, posed in 1.5.

- What critical electrical factors determine the optimal placement of DG to reduce power losses?
- What practical loss optimization power flow method can be applied to place DG on meshed networks?
- What is the importance of reactive power control for the integration DG?
- How does DG penetration and concentration affect power system losses?

6.3 Assessing the research questions

The following sections will address each research question in relation to the result observed in chapter 5.

6.3.1 What critical electrical factors determine the optimal placement of DG to reduce power losses?

Critical electrical factors were identified and are discussed in sub sections 6.3.1.1 to 6.3.1.6.

6.3.1.1 Network topology

Section 2.2 identifies critical electrical factors in assessing the optimal placement of DG to reduce power losses. Network topology describes the extent to which the power system is meshed or radial. Inherent strengths and weaknesses are ingrained in each topology. Meshed topologies favour urban densification of loads and a robust grid. Meshed networks are disadvantaged by transferring disturbances across the grid due their interconnectivity.

Network configuration affects network topology through reconfiguration from radial to mesh through interconnectors. Provided the protection can accommodate these changes, reconfiguration can improve sizing and placement of DG.

Certain maintenance or fault conditions can alter network topologies. Where generation sizing has reduced negotiated curtailment is to be communicated with the IPP. These conditions may have the effect of limiting the DG connection to the network.

6.3.1.2   System impedance and system fault level

System impedance defined by reactance and resistance affects network topology and determines fault level "robustness" of the network. Networks with weak fault levels have high upstream impedance. Conversely, stronger fault levels are experienced closer to the source. Meshed networks with multiple sources have lower Thevenin equivalent impedance, resulting in higher fault current. Systems with high fault levels are invulnerable to disturbances. These systems can sustain larger disturbances resulting load or generation loss.

The short circuit ratio [48] equation expressed in (4) assesses the percentage voltage disturbance (U_{max}). Equation (4) expresses the ratio of rated generation power S_{Gen} (MVA) to system fault level S_{sys} (MVA), shown below.

$$U_{max}(\%) = \frac{S_{Gen}}{S_{Sys}} x100 \qquad (4)$$

System fault level and network impedance is thus critical sizing factors. Results in chapter five shows low fault levels accommodate low levels of rated DG. Proportionately high fault levels accommodate high levels of DG.

The utility test network considered system healthy conditions in accordance with the grid code for supplies less than one-thousand megawatts [3]. Certain contingencies and maintenance will reduce fault levels. These cases require curtailment in the IPPs maximum export capacities.

6.3.1.3   Equipment rating

Equipment rating of transformers and line capacity is equally importance for evacuating DG from the injected busbar. Insufficient sizing of transformer and line capacities will overload resulting in increased real and reactive power losses. Section 5.6.5 to 5.6.7 document the increase in losses (I^2R and I^2X) due to increased currents injected at high voltage busbars.

6.3.1.4   Voltage control of active and reactive power flow

Voltage control second only to frequency control, balance the flow of power across a system. Real power flows based on increasing voltage angle between sending end (V_s) and receiving end (V_r) described in [48]. Reactive power flows based on difference in voltage magnitude [48]. Equation (5) shows the power - impedance relationship and that of power – voltage angle. Equation (6) shows the relationship between reactive power and voltage. When Q decreases, voltage drops as the square, citing reasons for voltage slide under low reactive power reserves. This makes voltage critical for power flow.

$$P_{sr} = \frac{V_r V_s}{X} \sin \delta \qquad (5)$$

$$Q = -\frac{V^2}{X} \Delta V \qquad (6)$$

Pre and post-fault voltages determined by voltage variation, limits the size distributed generation. Voltage control through transformer tap changers and reactive power compensation manage steady state voltage within prescribed limits. This makes voltage control critical for DG integration to the grid.

Sections 5.5 demonstrate the extent to which voltage limits are used to restrict DG size. Voltage increase beyond the control limit (1.05p.u) due to loss of generation impacts sizing of DG at that location.

6.3.1.5   Load types and characteristics

Chapter 3 discussed three load models, viz., constant impedance, constant current and constant power and their responses to varying voltage Table 3-1 in 3.1.1. Constant power loads cover a wide approximation of load types on a power system. Load flow studies were controlled by modelling all load types as constant power loads.

Typical load profile shapes shown section 5.3.1 demonstrate the time varying nature over a 24-hour period. Modelling realistic profile characteristics for load types are important for calculating power losses. They become more important as the power output of DG varies for the different technologies.

The most favourable load profile for DG application was found to be municipality and bulk loads. High load factor profiles present ideal characteristics for maximum solar PV absorption. Reducing surplus injected power and reverse power flow favours these profiles.

Distributed generation characteristics are explored in 6.3.1.6.

Oversizing solar plants to leverage broad peak times accounting for cloud cover and future maintenance within the solar farm. Smart inverters with fast-run-back-schemes limiting DGs export capacity can be employed on oversized solar farms. Reduced pre-fault voltages can manage voltage variation from generation loss under fault conditions. Smart grid technology can integrate smart DG connections to the grid.

6.3.1.6   Solar PV characteristics

Solar output is affected by cloud cover as described in chapter 3. This affects the net power flow from solar DG. Consistent comparison requires all solar PV plants to have the same cloudless weather conditions. Results in 5.4 demonstrate the importance of solar DG and profile.

The net power flow (P_{Net}) from a DG injected busbar is the algebraic difference between active power (P_{Load}) and distributed generated power (P_{Gen}). When (P_{Net}) is negative, surplus DG power flows back through the transformer to supply neighbouring load centres. When (P_{Net}) is positive, all DG power has been consumed by the load. Distributed generation technology selection plays a pivot role in sizing DG for loss reduction.

The natural and predictable phenomenon of sun-rise and sun-set makes solar PV favourable. Storage and release of solar power can alter the DG solar profile, enabling supply beyond daylight hours. Technologies such as concentrated solar power (CSP) are preferred if cost effective. Alternative battery storage may also alter the solar PV daily profile. If applied optimally at load centres, will have an effect DG placement.

6.3.2   What practical loss optimization power flow method can be applied to place DG on meshed networks?

Chapter 4 presented a method of defining, ranking, profiling, activating, evaluating and selecting busbars for optimal placement. This method allows applies a logical and consistent approach to seeking out plausible busbars for DG connection. Confirmation of the method studied and reported in chapter 5. Future scholars and utility engineers can apply this approach to study their power systems for ideal busbar selection and DG placement.

6.3.3   What is the importance of reactive power control for the integration DG?

Reactive power compensation is critical for the integration of DG to address the reduction of reactive power flows. Solar PV injects unity active power into the grid. Reactive power is not compensated resulting in poor phase angles at higher busbar voltages. These lead to poorer power factors at upstream busbars.

Table 5-1 verifies the change in power factor from pre- to post-DG connection at the 66kV Earth busbar. Comparisons were made for each pre- and post- connected DG, validating the changes in phase angle; power factor and resulting reactive power flow.

Without reactive power compensation devices reactive power losses will increase. Sub-optimal DG placement will result in expensive life-cycle installations cost. As the penetration of DG increases to reduce active power, larger reactive power compensation devices must be added to the network. [104] provides a technique for optimum placement of reactive power compensation to reduce reactive power flows.

6.3.4   How does DG penetration and concentration affect power system losses?

Surplus power (P_{Net}) was discussed in 6.3.1.6 and is shown by equation (7).

$$(P_{Net}) = (P_{Load}) - (P_{Gen}) \qquad (7)$$

When (P_{Net}) is negative, (P_{Load}) < (P_{Gen}) and surplus DG power reverse flows to neighbouring load centres thereby incurring losses. Section 5.6.5 Table 5-6 results highlight larger losses associated with large DG injected at busbars where load is less than injected DG. A poor profile match between load and generation increases the losses. Penetration and concentration of DG was explained in chapter 2 and demonstrated chapter 5 section 5.6.5, 5.6.6 and 5.6.7 show the results for DG integration with 66kV busbars.

Table 5-6, Table 5-7 and Table 5-8, respectively confirms this effect. Overcrowding of DG by sub-optimal penetration and concentration will lead to undesirable losses.

6.4   Relevance of research

Addressing key research questions in sections 6.3.1 through to 6.3.4 provides holistic technical insight when connecting DG to the utility system. Utility engineers will benefit from the research results and apply these methods when analysing DG connections to the power system. Application of this methodology enables development of an integrated DG connection master plan for utilities.

The research methodology presented can be iterative to allow for multi-generation connections. Utility engineers can employ this multi-technology DG approach to develop future planning scenarios.

Tariff application on technical losses presents the cost of losses. Maximum losses are calculated at peak generation times. Loss load factors can be applied to determine the average and minimum loss values to generate a loss profile. Extension of daily losses can be fitted with the loss load profile for yearly and lifecycle determinations. Utility engineers account for lifecycle costing when planning for 20-year optimum placement strategies.

6.5 Assessing the hypothesis

Early adopting power utilities must act responsibly and account for the least economic cost connection of renewable power plants onto the grid. The research shows a significant increase in real and reactive power losses when nominating high voltage busbars that have no direct load connected. Eskom entered into 20-year power purchase agreements with IPPs connecting large installations to high voltage busbars. The long-term cost of losses resulting from these connections may place further financial burden on the utility. The resulting hypothesis is not positive when taking the long-term strategic view. Investor owned renewable power plants are partially responsible for these losses. They should be held to account in a manner that does not disadvantage the public prior to the DG installation. Busbar profiling favours municipality and bulk load and these should be the focus of the extended programme.

6.6 Future research

Several aspects of further research have emerged as follows. Wind energy impact on power systems with respect to quality of supply. Wind power output models for location based wind patterns. Optimizing mixed RE technologies for loss reduction. Load profile flattening through DG integration. Battery storage as a means to shift load peaks. Utility load peak flattening by integrating rooftop PV systems into the power system. The effects on power quality in highly concentrated solar DG during cloud cover. The effect of large power swings on voltage collapse, as renewable energy technologies penetrate the power system. Smart inverter technology with fast-run-back-schemes to reduce pre-fault voltage levels to allow oversizing of DG.

6.7 Conclusion

This research addressed the need for a practical methodology for optimal placement of DG on a meshed network to reduce power losses. A time variant model proposes an extension to the current high and low study method. Optimal placement of non-dispatchable solar PV distributed generation to optimize losses is critical to power loss reduction to sustain the economic longevity of the power utility.

6.8 Recommendation

This research is recommended for implementation to all utilities on the cusp of integrating DG into their power system. Reasons why increased power losses are experienced post DG integration will be addressed.

7 REFERENCES

[1]   J. L. Sawin, F. Sverrisson, and W. Rickerson, "Renewables 2015 Global Status Report," Paris, France, ISBN 978-3-9815934-6-4, 2015.

[2]   M Bello, R. Smit, C. . Carter-Brown, and I. E. Davidson, "Power Planning in a Smart Grid Environment-Case Study of South Africa," 2012.

[3]   "South African Grid Code Requirements for Renewable Power Plants," Eskom Transmission Division, South Africa, Version 2.8, Jul. 2014.

[4]   "IPP Renewables." [Online]. Available: http://www.ipprenewables.co.za/. [Accessed: 16-Jul-2015].

[5]   "Programmes: Integrated Resource Plan | Department: Energy | REPUBLIC OF SOUTH AFRICA." [Online]. Available: http://www.energy.gov.za/files/irp_frame.html. [Accessed: 16-Jul-2015].

[6]   "Guide to Independent Power Producer (IPP) processes." [Online]. Available: http://www.eskom.co.za/Whatweredoing/InfoSiteForIPPs/Pages/Guide_To_Independent_Power_Producer_IPP_Processes.aspx. [Accessed: 07-Nov-2015].

[7]   "Electric Reliability Council of Texas." [Online]. Available: http://www.ercot.com/. [Accessed: 16-Jul-2015].

[8]   "PUCT - CREZ Home Page." [Online]. Available: http://www.texascrezprojects.com/. [Accessed: 16-Jul-2015].

[9]   "REDZs." [Online]. Available: https://redzs.csir.co.za/. [Accessed: 16-Jul-2015].

[10]   "SA's mixed energy bag | Industry | Moneyweb Today," 24-Jun-2015. [Online]. Available: http://today.moneyweb.co.za. [Accessed: 09-Jul-2015].

[11]   W. Tan, M. Y. Hassan, M. S. Majid, and H. A. Rahman, "Optimal distributed renewable generation planning: A review of different approaches," *Renewable and Sustainable Energy Reviews*, vol. 18, pp. 626–645, Feb. 2013.

[12]   M. Kezunovic, "Monitoring of Power System Topology in Real-Time," in *Proceedings of the 39th Annual Hawaii International Conference on System Sciences, 2006. HICSS '06*, 2006, vol. 10, p. 244b–244b.

[13]   H. A. Khan, H. H. C. Iu, and V. Sreeram, "Active and reactive power control of the electronically interfaced DG sources for the realization of a Virtual Power Plant," in *IECON 2011 - 37th Annual Conference on IEEE Industrial Electronics Society*, 2011, pp. 808–813.

[14]   S. K. Injeti and N. P. Kumar, "A novel approach to identify optimal access point and capacity of multiple DGs in a small, medium and large scale radial distribution systems," *International Journal of Electrical Power & Energy Systems*, vol. 45, no. 1, pp. 142–151, Feb. 2013.

[15]   V. V. S. N. Murty and A. Kumar, "Mesh distribution system analysis in presence of distributed generation with time varying load model," *International Journal of Electrical Power & Energy Systems*, vol. 62, pp. 836–854, Nov. 2014.

[16]   T. Gözel and M. H. Hocaoglu, "An analytical method for the sizing and siting of distributed generators in radial systems," *Electric Power Systems Research*, vol. 79, no. 6, pp. 912–918, Jun. 2009.

[17]   M. -C. Alvarez-Herault, N. N'Doye, C. Gandioli, N. Hadjsaid, and P. Tixador, "Meshed distribution network vs reinforcement to increase the distributed generation connection," *Sustainable Energy, Grids and Networks*, vol. 1, pp. 20–27, Mar. 2015.

[18]   F. Ugranlı and E. Karatepe, "Convergence of rule-of-thumb sizing and allocating rules of distributed generation in meshed power networks," *Renewable and Sustainable Energy Reviews*, vol. 16, no. 1, pp. 582–590, Jan. 2012.

[19]   H. Hedayati, S. A. Nabaviniaki, and A. Akbarimajd, "A Method for Placement of DG Units in Distribution Networks," *Power Delivery, IEEE Transactions on*, vol. 23, no. 3, pp. 1620–1628, Jul. 2008.

[20]   N. Acharya, P. Mahat, and N. Mithulananthan, "An analytical approach for DG allocation in primary distribution network," *International Journal of Electrical Power & Energy Systems*, vol. 28, no. 10, pp. 669–678, Dec. 2006.

[21] C. L. T. Borges and D. M. Falcão, "Optimal distributed generation allocation for reliability, losses, and voltage improvement," *International Journal of Electrical Power & Energy Systems*, vol. 28, no. 6, pp. 413–420, Jul. 2006.

[22] J. A. Hernandez, D. Velasco, and C. L. Trujillo, "Analysis of the effect of the implementation of photovoltaic systems like option of distributed generation in Colombia," *Renewable and Sustainable Energy Reviews*, vol. 15, no. 5, pp. 2290–2298, Jun. 2011.

[23] M. M. Elnashar, R. E. Shatshat, and M. M. A. Salama, "Optimum siting and sizing of a large distributed generator in a mesh connected system," *Electric Power Systems Research*, vol. 80, no. 6, pp. 690–697, Jun. 2010.

[24] B. Singh, V. Mukherjee, and P. Tiwari, "A survey on impact assessment of DG and FACTS controllers in power systems," *Renewable and Sustainable Energy Reviews*, vol. 42, pp. 846–882, Feb. 2015.

[25] A. Y. Abdelaziz, Y. G. Hegazy, W. El-Khattam, and M. M. Othman, "Optimal allocation of stochastically dependent renewable energy based distributed generators in unbalanced distribution networks," *Electric Power Systems Research*, vol. 119, pp. 34–44, Feb. 2015.

[26] S. Khushalani, J. M. Solanki, and N. N. Schulz, "Development of Three-Phase Unbalanced Power Flow Using PV and PQ Models for Distributed Generation and Study of the Impact of DG Models," *IEEE Transactions on Power Systems*, vol. 22, no. 3, pp. 1019–1025, Aug. 2007.

[27] C. S. Cheng and D. Shirmohammadi, "A three-phase power flow method for real-time distribution system analysis," *IEEE Transactions on Power Systems*, vol. 10, no. 2, pp. 671–679, May 1995.

[28] S. R. Gampa and D. Das, "Optimum placement and sizing of DGs considering average hourly variations of load," *International Journal of Electrical Power & Energy Systems*, vol. 66, pp. 25–40, Mar. 2015.

[29] N. Mohandas, R. Balamurugan, and L. Lakshminarasimman, "Optimal location and sizing of real power DG units to improve the voltage stability in the distribution system using ABC algorithm united with chaos," *International Journal of Electrical Power & Energy Systems*, vol. 66, pp. 41–52, Mar. 2015.

[30] P. Karimyan, G. B. Gharehpetian, M. Abedi, and A. Gavili, "Long term scheduling for optimal allocation and sizing of DG unit considering load variations and DG type," *International Journal of Electrical Power & Energy Systems*, vol. 54, pp. 277–287, Jan. 2014.

[31] R. Ishak, A. Mohamed, A. N. Abdalla, and M. Z. C. Wanik, "Optimal placement and sizing of distributed generators based on a novel MPSI index," *International Journal of Electrical Power & Energy Systems*, vol. 60, pp. 389–398, Sep. 2014.

[32] S. M. Moghaddas-Tafreshi and E. Mashhour, "Distributed generation modeling for power flow studies and a three-phase unbalanced power flow solution for radial distribution systems considering distributed generation," *Electric Power Systems Research*, vol. 79, no. 4, pp. 680–686, Apr. 2009.

[33] G. Zareiegovar, R.R. Fesaghandis, and M.J. Azad, "Optimal DG location and sizing in distribution system to minimize losses, improve voltage stability, and voltage profile," in *2012 Proceedings of 17th Conference on Electrical Power Distribution Networks (EPDC)*, 2012, pp. 1–6.

[34] G.P. Harrison and A.R. Wallace, "Optimal power flow evaluation of distribution network capacity for the connection of distributed generation," *Generation, Transmission and Distribution, IEE Proceedings-*, vol. 152, no. 1, pp. 115–122, Jan. 2005.

[35] G. Kerber, R. Witzmann, and H. Sappl, "Voltage limitation by autonomous reactive power control of grid connected photovoltaic inverters," in *Compatibility and Power Electronics, 2009. CPE '09.*, 2009, pp. 129–133.

[36] K. Tanaka, M. Oshiro, S. Toma, A. Yona, T. Senjyu, T. Funabashi, and C.-H. Kim, "Decentralised control of voltage in distribution systems by distributed generators," *IET Generation, Transmission Distribution*, vol. 4, no. 11, pp. 1251–1260, Nov. 2010.

[37] R. Aghaterrani, "Reactive Power Management of a DFIG Wind System in Microgrids Based on Voltage Sensitivity Analysis."

[38]   V. Calderaro, G. Conio, V. Galdi, and A. Piccolo, "Reactive power control for improving voltage profiles: A comparison between two decentralized approaches," *Electric Power Systems Research*, vol. 83, no. 1, pp. 247–254, Feb. 2012.

[39]   V. Calderaro, V. Galdi, F. Lamberti, and A. Piccolo, "Coordinated local reactive power control in smart distribution grids for voltage regulation using sensitivity method to maximize active power," pp. 481–493, Dec. 2013.

[40]   V. Galdi, A. Piccolo, Calderaro, V, and F, Lamberti, "A Smart Strategy for Voltage Control Ancillary Service in Distribution Networks," *IEEE Transactions on Power Systems*, vol. 30, no. 1, pp. 494–502, Jan. 2015.

[41]   A. G. Beccuti and M. Morari, "A distributed solution approach to centralized emergency voltage control," in *American Control Conference, 2006*, 2006, p. 6 pp.–.

[42]   A. Keane, L. F. Ochoa, E. Vittal, C. J. Dent, and G. P. Harrison, "Enhanced Utilization of Voltage Control Resources With Distributed Generation," *IEEE Transactions on Power Systems*, vol. 26, no. 1, pp. 252–260, Feb. 2011.

[43]   A. Bracale, R. Angelino, G. Carpinelli, M. Mangoni, and D. Proto, "Dispersed generation units providing system ancillary services in distribution networks by a centralised control," *IET Renewable Power Generation*, vol. 5, no. 4, pp. 311–321, Jul. 2011.

[44]   A. Bracale, R. Angelino, G. Carpinelli, D. Lauria, M. Mangoni, and D. Proto, "Centralized control of dispersed generators providing ancillary services in distribution networks," in *Universities Power Engineering Conference (UPEC), 2009 Proceedings of the 44th International*, 2009, pp. 1–5.

[45]   C.-H. Lo and N. Ansari, "Decentralized Controls and Communications for Autonomous Distribution Networks in Smart Grid," *IEEE Transactions on Smart Grid*, vol. 4, no. 1, pp. 66–77, Mar. 2013.

[46]   A. Cagnano, E. De Tuglie, M. Liserre, and R. A. Mastromauro, "Online Optimal Reactive Power Control Strategy of PV Inverters," *IEEE Transactions on Industrial Electronics*, vol. 58, no. 10, pp. 4549–4558, Oct. 2011.

[47]   B. Gao, G. K. Morison, and P. Kundur, "Voltage stability evaluation using modal analysis," *IEEE Transactions on Power Systems*, vol. 7, no. 4, pp. 1529–1542, Nov. 1992.

[48]   "Power System Stability and Control: Prabha Kundur: 9780070359581: Amazon.com: Books." [Online]. Available: http://www.amazon.com/System-Stability-Control-Prabha-Kundur/dp/007035958X. [Accessed: 25-Jul-2015].

[49]   A. M. Chebbo, M. R. Irving, and M. J. H. Sterling, "Voltage collapse proximity indicator: behaviour and implications," *IEE Proceedings C Generation, Transmission and Distribution*, vol. 139, no. 3, p. 241, 1992.

[50]   R.S. Al Abri, E.F. El-Saadany, and Y.M. Atwa, "Optimal Placement and Sizing Method to Improve the Voltage Stability Margin in a Distribution System Using Distributed Generation," *IEEE Transactions on Power Systems*, vol. 28, no. 1, pp. 326–334, Feb. 2013.

[51]   Y. M. Atwa and E. F. El-Saadany, "Optimal Allocation of ESS in Distribution Systems With a High Penetration of Wind Energy," *Power Systems, IEEE Transactions on*, vol. 25, no. 4, pp. 1815–1822, Nov. 2010.

[52]   C. A. Canizares and F. L. Alvarado, "Point of collapse and continuation methods for large AC/DC systems," *IEEE Transactions on Power Systems*, vol. 8, no. 1, pp. 1–8, Feb. 1993.

[53]   N. G. A. Hemdan and M. Kurrat, "Distributed generation location and capacity effect on voltage stability of distribution networks," in *Student Paper, 2008 Annual IEEE Conference*, 2008, pp. 1–5.

[54]   R. A. Walling, R. Saint, R. C. Dugan, J. Burke, and L. A. Kojovic, "Summary of Distributed Resources Impact on Power Delivery Systems," *IEEE Transactions on Power Delivery*, vol. 23, no. 3, pp. 1636–1644, Jul. 2008.

[55]   P. Kayal and C. K. Chanda, "Optimal mix of solar and wind distributed generations considering performance improvement of electrical distribution network," *Renewable Energy*, vol. 75, pp. 173–186, Mar. 2015.

[56]   B. B. Zad, H. Hasanvand, J. Lobry, and F. Vallée, "Optimal reactive power control of DGs for voltage regulation of MV distribution systems using sensitivity analysis method and PSO algorithm," *International Journal of Electrical Power & Energy Systems*, vol. 68, pp. 52–60, Jun. 2015.

[57] S. Rahman and G. B. Shrestha, "An investigation into the impact of electric vehicle load on the electric utility distribution system," *IEEE Transactions on Power Delivery*, vol. 8, no. 2, pp. 591–597, Apr. 1993.

[58] K. Clement-Nyns, E. Haesen, and J. Driesen, "The Impact of Charging Plug-In Hybrid Electric Vehicles on a Residential Distribution Grid," *IEEE Transactions on Power Systems*, vol. 25, no. 1, pp. 371–380, Feb. 2010.

[59] S. Acha, T. C. Green, and N. Shah, "Effects of optimised plug-in hybrid vehicle charging strategies on electric distribution network losses," in *Transmission and Distribution Conference and Exposition, 2010 IEEE PES*, 2010, pp. 1–6.

[60] V.H.M. Quezada, J.R. Abbad, and T.G.S. Román, "Assessment of energy distribution losses for increasing penetration of distributed generation," *IEEE Transactions on Power Systems*, vol. 21, no. 2, pp. 533–540, May 2006.

[61] P. L. Joskow, "Comparing the Costs of Intermittent and Dispatchable Electricity Generating Technologies," *American Economic Review*, vol. 101, no. 3, pp. 238–41, 2011.

[62] H. Lee Willis, "Chapter 9. Load Reach and Volt- VAR Engineering," in *Power Distribution Planning Reference Book, Second Edition*, vol. 20044212, CRC Press, 2004.

[63] R. P. Broadwater, A. Sargent, A. Yarali, H. E. Shaalan, and J. Nazarko, "Estimating substation peaks from load research data," *IEEE Transactions on Power Delivery*, vol. 12, no. 1, pp. 451–456, Jan. 1997.

[64] "Global Wind Systems." [Online]. Available: http://earthguide.ucsd.edu/virtualmuseum/climatechange1/08_1.shtml. [Accessed: 02-Aug-2015].

[65] F. Vallee, J. Lobry, and O. Deblecker, "Impact of the Wind Geographical Correlation Level for Reliability Studies," *IEEE Transactions on Power Systems*, vol. 22, no. 4, pp. 2232–2239, Nov. 2007.

[66] T. Ackermann, Ed., *Wind power in power systems*. Chichester, West Sussex, England ; Hoboken, NJ: John Wiley, 2005.

[67] Y. Yang, W. Chen, and F. Blaabjerg, "Advanced Control of Photovoltaic and Wind Turbines Power Systems," in *Advanced and Intelligent Control in Power Electronics and Drives*, vol. 531, T. Orłowska-Kowalska, F. Blaabjerg, and J. Rodríguez, Eds. Cham: Springer International Publishing, 2014, pp. 41–89.

[68] J. Hu, J. Zhu, D. G. Dorrell, Q. Ma, Y. Zhang, and W. Xu, "Control strategies of variable-speed wind system under new grid code requirement #x2014; A survey," in *IECON 2010 - 36th Annual Conference on IEEE Industrial Electronics Society*, 2010, pp. 3061–3066.

[69] S. N. Singh, J. Østergaard, and B. Singh, "Reactive power capability of unified DFIG for wind power generation," in *2010 IEEE Power and Energy Society General Meeting*, 2010, pp. 1–7.

[70] "SolarGIS :: Online data and tools for solar energy projects." [Online]. Available: http://solargis.info/. [Accessed: 04-Aug-2015].

[71] "Fondriest Environmental, Inc." [Online]. Available: http://www.fondriest.com/. [Accessed: 24-Aug-2015].

[72] Geveen Moodley, "Introduction to Renewable Generation," Centurion, 30-Jul-2015.

[73] C.-H. Lin, W.-L. Hsieh, C.-S. Chen, C.-T. Hsu, and T.-T. Ku, "Optimization of Photovoltaic Penetration in Distribution Systems Considering Annual Duration Curve of Solar Irradiation," *IEEE Transactions on Power Systems*, vol. 27, no. 2, pp. 1090–1097, May 2012.

[74] R. Mayfield, R. E. C. | E. Construction, and Maintenance, "The Highs and Lows of Photovoltaic System Calculations." [Online]. Available: http://ecmweb.com/green-building/highs-and-lows-photovoltaic-system-calculations. [Accessed: 04-Aug-2015].

[75] "NREL - Aggregation of distributed generation assets in New York state."

[76] P. A. Ruiz and P. W. Sauer, "Reactive Power Reserve Issues," in *Power Symposium, 2006. NAPS 2006. 38th North American*, 2006, pp. 439–445.

[77] O. A. Mousavi, M. Bozorg, A. Ahmadi-Khatir, and R. Cherkaoui, "Reactive power reserve management: Preventive countermeasure for improving voltage stability margin," in *2012 IEEE Power and Energy Society General Meeting*, 2012, pp. 1–7.

[78] N. W. Miller, K. Clark, and M. Shao, "Frequency responsive wind plant controls: Impacts on grid performance," in *2011 IEEE Power and Energy Society General Meeting*, 2011, pp. 1–8.

[79] E. Haesen, J. Driesen, and R. Belmans, "Robust planning methodology for integration of stochastic generators in distribution grids," *IET Renewable Power Generation*, vol. 1, no. 1, pp. 25–32, Mar. 2007.

[80] Z. H. Rather, Z. Chen, and P. Thogersen, "Impact of wind energy integration on reactive power reserve and its smart solution: A Danish Power System case study," in *2012 IEEE International Conference on Power System Technology (POWERCON)*, 2012, pp. 1–6.

[81] H. Mortazavi, H. Mehrjerdi, M. Saad, S. Lefebvre, D. Asber, and L. Lenoir, "A Monitoring Technique for Reversed Power Flow Detection With High PV Penetration Level," *IEEE Transactions on Smart Grid*, vol. PP, no. 99, pp. 1–1, 2015.

[82] L. Grigsby, R. Thallam, and G. Joós, "Chapter 19. Reactive Power Compensation," in *Electric Power Generation, Transmission, and Distribution, Third Edition*, 5 vols., CRC Press, 2012, pp. 1–20.

[83] R. G. Wandhare and V. Agarwal, "Reactive Power Capacity Enhancement of a PV-Grid System to Increase PV Penetration Level in Smart Grid Scenario," *IEEE Transactions on Smart Grid*, vol. 5, no. 4, pp. 1845–1854, Jul. 2014.

[84] H. Lee Willis, "Power Delivery Systems," in *Power Distribution Planning Reference Book, Second Edition*, 0 vols., CRC Press, 2004.

[85] H. Lee Willis, "Chapter 11. Basic Line Segment and Transformer Sizing Economics," in *Power Distribution Planning Reference Book, Second Edition*, 0 vols., CRC Press, 2004.

[86] A. Hagehaugen, "Voltage Control in Distribution Network with Local Generation," 2014.

[87] H. L. Willis, *Power Distribution Planning Reference Book, Second Edition*. CRC Press, 2004.

[88] R. A. A. de Graaff, J. M. Myrzik, W. L. Kling, and J. H. R. Enslin, "Series Controllers in Distribution Systems - Facilitating Increased Loading and Higher DG Penetration," in *Power Systems Conference and Exposition, 2006. PSCE '06. 2006 IEEE PES*, 2006, pp. 1926–1930.

[89] T. N. Boutsika and S. A. Papathanassiou, "Short-circuit calculations in networks with distributed generation," *Electric Power Systems Research*, vol. 78, no. 7, pp. 1181–1191, Jul. 2008.

[90] M. Dilek and R. P. Broadwater, "Chapter 29. Real-Time Control of Distributed Generation," in *Electric Power Generation, Transmission, and Distribution, Third Edition*, 5 vols., CRC Press, 2012, pp. 1–14.

[91] A. P. Hanson, J. V. Grubbs, and C. A. Gross, "Chapter 7. Electric Power Utilization," in *The Electric Power Engineering Handbook*, 0 vols., CRC Press, 2000.

[92] "Eskom Integrated Annual Report 2014," 2014.

[93] A. Alarcon-Rodriguez, G. Ault, and S. Galloway, "Multi-objective planning of distributed energy resources: A review of the state-of-the-art," *Renewable and Sustainable Energy Reviews*, vol. 14, no. 5, pp. 1353–1366, Jun. 2010.

[94] S.S. Al Kaabi, H.H. Zeineldin, and V. Khadkikar, "Planning Active Distribution Networks Considering Multi-DG Configurations," *IEEE Transactions on Power Systems*, vol. 29, no. 2, pp. 785–793, Mar. 2014.

[95] "GCCA of the 2022 Transmission Network." [Online]. Available: http://www.eskom.co.za/Whatweredoing/GCCAReport/Pages/Default.aspx. [Accessed: 16-Jul-2015].

[96] "Transmission Development Plans." [Online]. Available: http://www.eskom.co.za/Whatweredoing/TransmissionDevelopmentPlan/Pages/Transmission_Development_Plans.aspx. [Accessed: 16-Jul-2015].

[97] "Eskom - Distribution Technology 172.31.250.214." [Online]. Available: http://scot.eskom.co.za:8080/. [Accessed: 05-Nov-2015].

[98] F. M. Gonzalez-Longatt and J. Luis Rueda, Eds., *PowerFactory Applications for Power System Analysis*. Cham: Springer International Publishing, 2014.

[99]   T. G. M. Alvin, I. Z. Abidin, and H. Hashim, "Changes in fault current levels due to renewable embedded generation in a distribution network," in *2013 IEEE Conference on Clean Energy and Technology (CEAT)*, 2013, pp. 254–258.

[100]   A. Gabash and P. Li, "Variable reverse power flow-Part I: A-R-OPF with reactive power of wind stations," in *2015 IEEE 15th International Conference on Environment and Electrical Engineering (EEEIC)*, 2015, pp. 21–26.

[101]   L. L. Grigsby, *Electric Power Generation, Transmission, and Distribution, Third Edition*, vol. 20124365. CRC Press, 2012.

[102]   "Electricity Supply - Quality of Supply - PART 2," National Rationalized Specification Ed. 3, Dec. 2007.

[103]   L. L. Grigsby and A. P. Hanson, "Power Flow Analysis," in *Power Systems, Third Edition*, 5 vols., CRC Press, 2012, pp. 1–12.

[104]   M. Ntusi, "Optimal placement of shunt capacitor banks on a sub-transmission network," Dissertation, 2009.

8   APPENDIX

8.1 Transmission grid
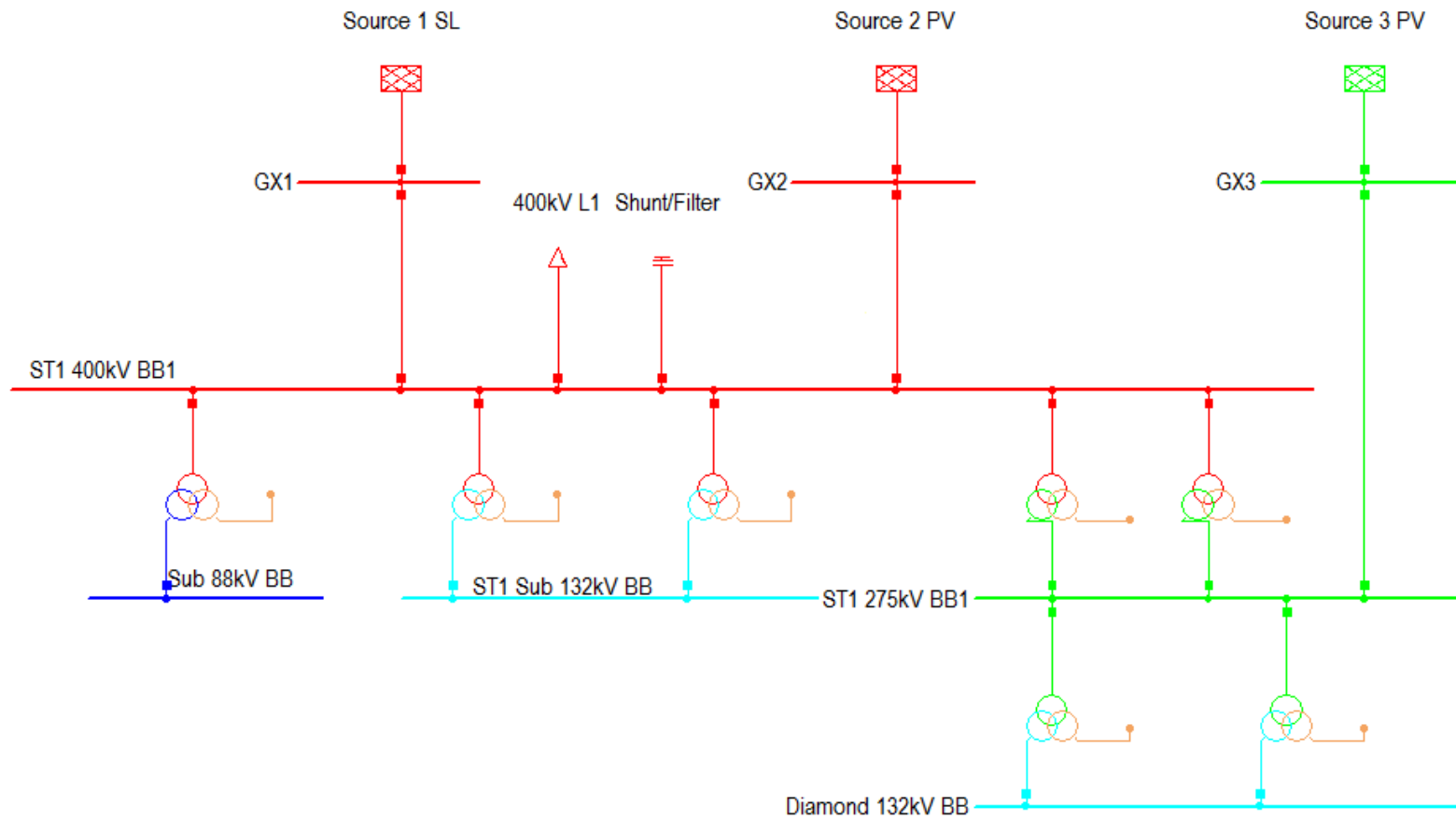
Figure 8-1 Transmission Grid

8.2 Sub-transmission grid I
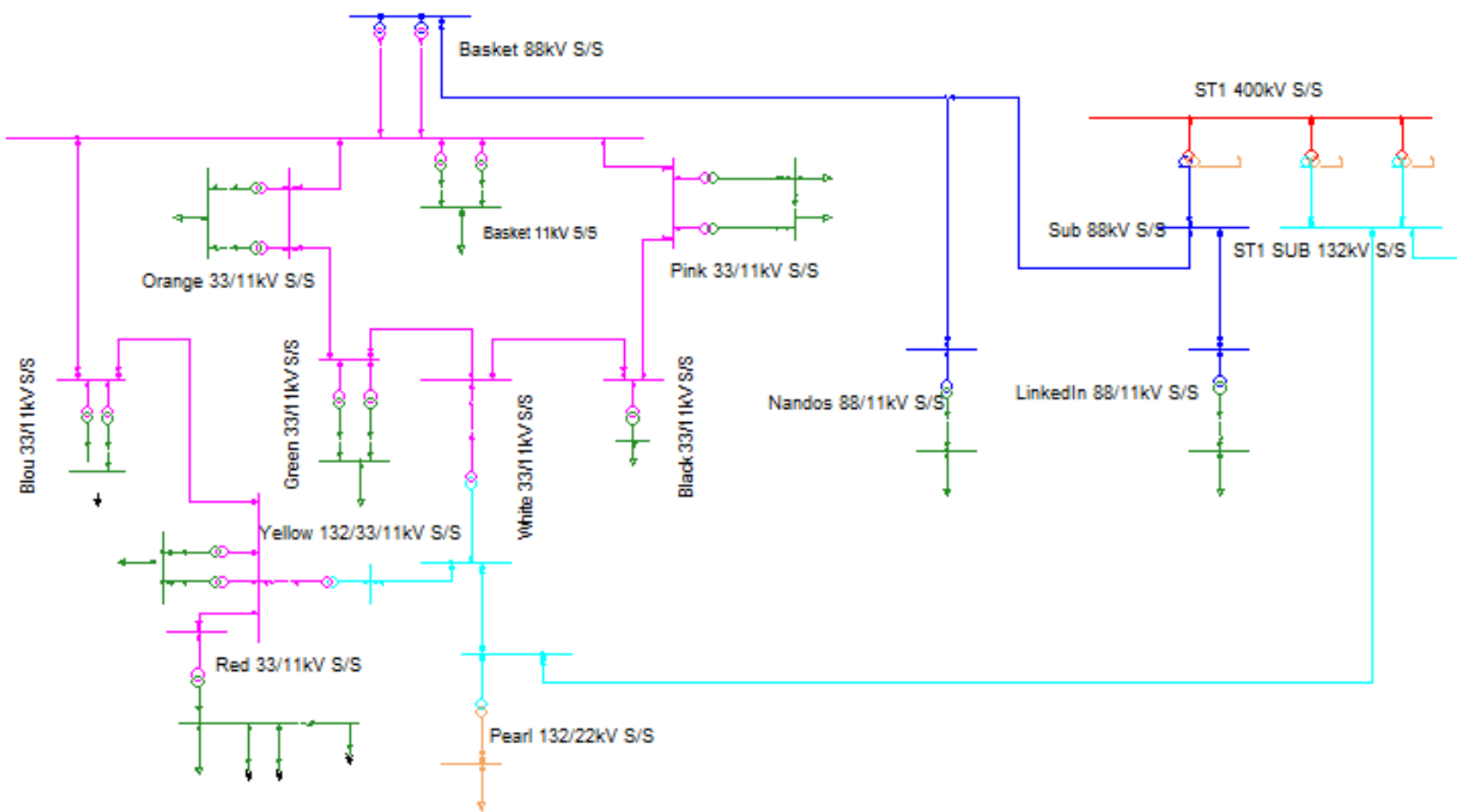
Figure 8-2 Network Overview – Part I

8.3 Sub-transmission grid II
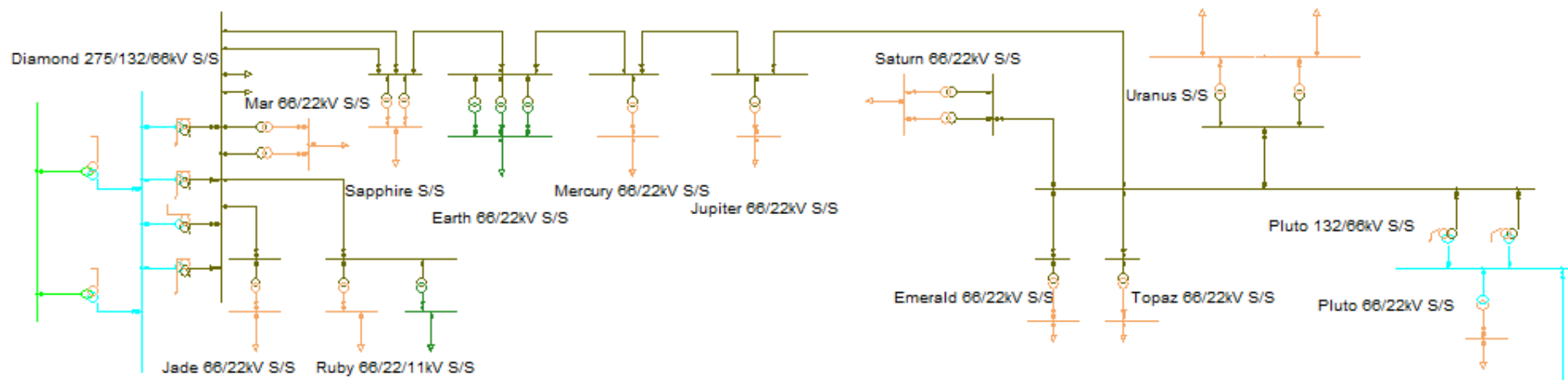
Figure 8-3 Network Overview - Part II

8.3.1 Line parameters

The network is constructed with the following conductor impedances as shown in Table 8-1. Table 8-2 shows line lengths.

Table 8-1: Line Parameters

Line Type	Z1 Ohm	phiz1 deg.	R1 Ohm	X1 Ohm	R0 Ohm	X0 Ohm
88kV CHICKADEE SC	7.636	68.112	2.847	7.086	7.125	27.506
33kV CHICKADEE SC	1.958	68.986	0.702	1.828	1.420	7.952
66 kV HARE SC	20.520	51.546	12.761	16.070	21.745	63.152
132 kV CHICKADEE SC	3.574	73.393	1.021	3.424	2.749	11.565

Table 8-2: Sub Transmission Grid Lines Lengths

Terminal i (From Bus)	Terminal j (To Bus)	Length – km		Terminal i (From Bus)	Terminal j (To Bus)	Length - km
Basket-88kV	Nandos 88 T-off	17.96		Red 11kV	T1-1	1.50
Basket-33kV	Orange 33kV	4.90		Red 11kV	T2-1	11.50
Diamond 66kV	Ruby 66kV	33.90		Mercury 66kV	Jupiter 66kV	54.00
Diamond 66kV	Sapphire 66kV	40.00		Megan Load	PointTerm1	0.62
Nandos 88 T-off	Sub 88kV	17.96		Uranus 66kV	Pluto 66kV	5.00
Pearl 132kV	White 132kV	8.62		Pluto 66kV	Emerald 66kV	5.00
Basket-33kV	Pink 33kV	5.60		Pluto 66kV	Topaz 66kV	32.60
Pink 33kV	Black-33kV	7.56		Red 33kV	Yellow 33kV	12.85
Basket-33kV	Blou-33kV	5.85		ST1 Sub 132kV	Pearl 132kV	62.20
Yellow 33kV	Blou-33kV	6.00		Pluto 132kV	ST1 Sub 132kV	61.50
Diamond 66kV	Sapphire 66kV	40.00		Nandos 88 T-off	Nandos 88kV	48.50
Diamond 66kV	Jade 66kV	73.50		Sub 88kV	LinkedIn 88kV	30.00
Earth 66kV	Mercury 66kV	22.00		Sapphire 66kV	Earth 66kV	10.00
Orange 33kV	Green-33kV	2.74		Saturn 66kV	Pluto 66kV	35.00
White 33kV	Green-33kV	1.40		White 33kV	Black-33kV	0.89
Jupiter 66kV	Pluto 66kV	1.00		White 132kV	Yellow132kV	19.86

8.4   Pre-DG system overview
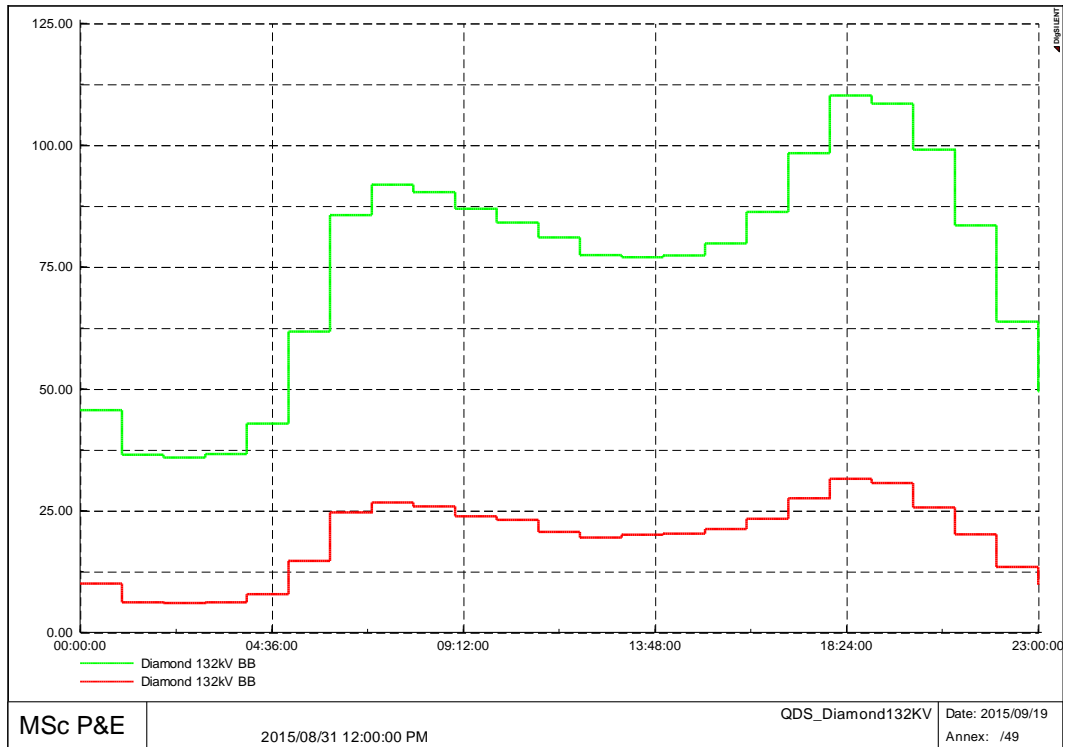
Figure 8-4 132kV Diamond Busbar at 12PM – Pre-DG
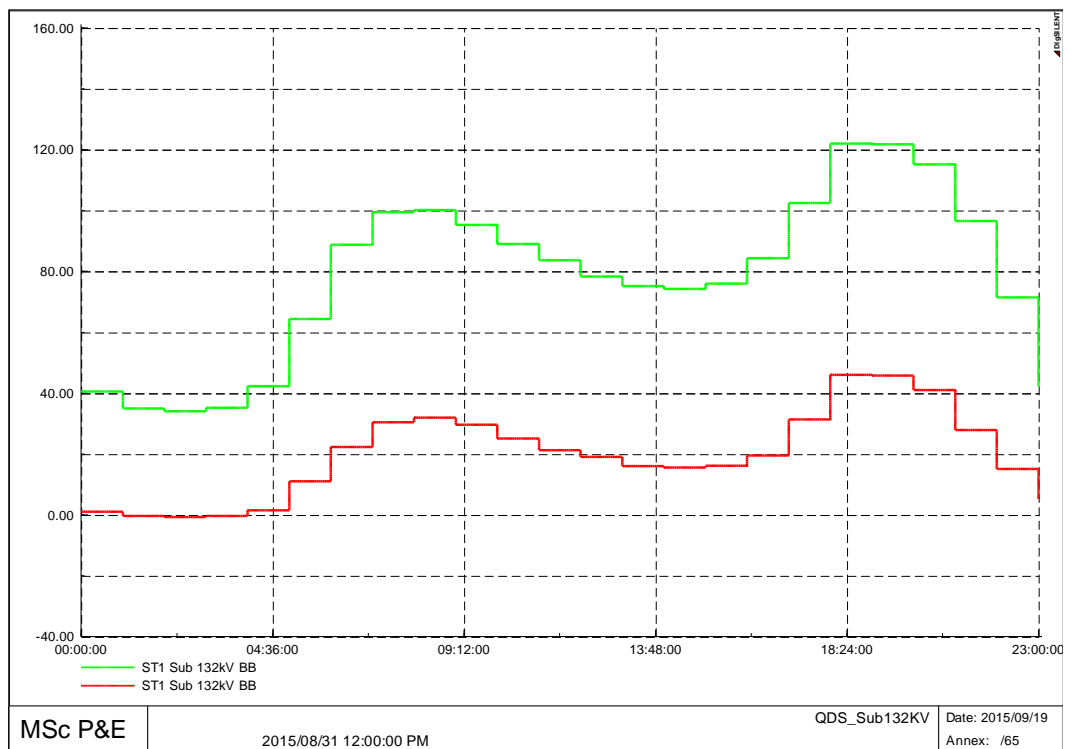
Figure 8-5 SUB 132 Busbar at 12PM – Pre-DG

8.4.1 Sub – transmission grid loading

Table 8-3: Sub – transmission grid loading at 12pm

Row	Bus Name	Voltage Magnitude p.u.	Active Power MW	Reactive Power Mvar	Apparent Power MVA	Power Factor	L-L Voltage Magnitude kV
1	Diamond 66kV BB	1.0285	7.3904	2.4790	7.7951	0.9481	67.8790
2	Diamond 66kV BB	1.0285	28.7838	9.6551	30.3600	0.9481	67.8790
3	Jade 22kV BB	1.0423	2.9400	0.7462	3.0332	0.9693	22.9312
4	Topaz 22kV BB	1.0398	2.3520	0.9373	2.5319	0.9290	22.8756
5	Pearl 22kV BB	1.0379	6.2208	1.7326	6.4575	0.9633	22.8341
6	Mecury 22kV BB	1.0366	3.4761	0.6682	3.5397	0.9820	22.8052
7	Ruby 22kV BB	1.0357	3.0240	1.1291	3.2279	0.9368	22.7861
8	Sapphire 22kV BB	1.0344	10.3217	1.8484	10.4859	0.9843	22.7571
9	Jupiter 22kV BB	1.0343	2.6357	0.7419	2.7381	0.9626	22.7547
10	Pluto 22kV BB	1.0336	2.8350	-1.7034	3.3074	0.8572	22.7382
11	Uranus 22kV BB2	1.0331	2.9700	0.5679	3.0238	0.9822	22.7289
12	Uranus 22kV BB1	1.0312	3.9600	0.7314	4.0270	0.9834	22.6870
13	Mars 22kV BB	1.0226	4.7700	-2.6984	5.4804	0.8704	22.4977
14	Saturn 22kV BB	1.0224	4.3228	1.1534	4.4740	0.9662	22.4920
15	Emerald 22kV BB	1.0207	5.1609	0.9708	5.2514	0.9828	22.4543
16	Red 11kV BB	1.0437	2.7450	0.6573	2.8226	0.9725	11.4809
17	Earth 11kV BB	1.0401	19.6490	5.3359	20.3606	0.9650	11.4407
18	Ruby 11kV BB	1.0334	2.5650	1.5333	2.9884	0.8583	11.3672
19	Pink 11kV BB 2	1.0313	2.2146	0.3753	2.2461	0.9859	11.3440
20	Pink 11kV BB 1	1.0313	5.3897	1.1892	5.5193	0.9765	11.3440
21	Blou 11kV BB	1.0283	7.6028	2.5667	8.0243	0.9475	11.3113
22	Yellow 11kV BB	1.0272	13.7973	2.9603	14.1114	0.9777	11.2995
23	Basket 11kV BB	1.0247	4.6455	1.0742	4.7681	0.9743	11.2716
24	LinkedIn 11kV BB	1.0229	18.5820	-7.0437	19.8722	0.9351	11.2515
25	Nandos 11kV BB	1.0187	18.2617	-5.2482	19.0009	0.9611	11.2061
26	Orange 11kV BB	1.0166	6.5435	2.1442	6.8859	0.9503	11.1823
27	Black 11kV BB	1.0131	6.0242	1.1620	6.1353	0.9819	11.1443
28	Green 11kV BB	1.0070	4.8667	1.4457	5.0769	0.9586	11.0765

8.4.2   High voltage fault level

Table 8-4: High voltage system fault level

Bus Name - Voltage (kV)	Line -Line Voltage (kV)	3 Phase Fault Current (kA)	3 Phase Fault Current (MVA)	Short Circuit Impedance Real Part - Rk, Re(Zk) Ohm	Short Circuit Impedance Imaginary Part - Xk, Im(Zk) Ohm
ST1 400kV BB1	400	11.98	8296.72	2.154	21.104
ST1 275kV BB1	275	9.66	4602.38	1.740	17.991
Pearl 132kV BB	132	2.79	637.27	7.595	29.101
Yellow132kV BB	132	2.16	494.55	9.890	37.472
Pluto 132kV BB	132	2.47	564.47	16.574	29.635
White 132kV BB	132	2.60	594.69	8.097	31.195
Diamond 132kV BB	132	9.74	2226.11	0.914	8.561
ST1 Sub 132kV BB	132	10.71	2448.85	0.340	7.819
Nandos 88kV BB	88	1.67	254.41	10.599	31.761
Basket 88kV BB	88	3.27	498.39	4.231	16.560
LinkedIn 88kV BB	88	2.78	424.27	5.573	19.289
Sub 88kV BB	88	7.46	1136.65	0.817	7.450
Earth 66kV BB	66	2.89	330.05	7.458	12.456
Mercury 66kV BB	66	2.32	265.53	9.698	15.218
Saturn 66kV BB	66	1.42	161.77	15.755	25.083
Sapphire 66kV BB	66	3.55	406.33	5.631	10.361
Topaz 66kV BB	66	1.48	168.74	14.989	24.119
Uranus 66kV BB	66	2.91	332.20	6.184	13.031
Emerald 66kV BB	66	2.91	332.20	6.184	13.031
Jade 66kV BB	66	1.00	113.78	23.949	34.642
Jupiter 66kV BB	66	3.43	391.82	4.818	11.240
Pluto 66kV BB	66	3.51	401.34	4.589	11.022
Ruby 66kV BB	66	1.94	221.46	11.293	18.456
Diamond 66kV BB	66	9.07	1036.54	0.459	4.600

8.4.3   Medium voltage fault level

Table 8-5: Medium voltage system fault level

Bus Name - Voltage (kV)	Line -Line Voltage (kV)	3 Phase Fault Current (kA)	3 Phase Fault Current (MVA)	Short Circuit Impedance Real Part - Rk, Re(Zk) Ohm	Short Circuit Impedance Imaginary Part - Xk, Im(Zk) Ohm
Blou 33kV BB	33	5.41	309.00	0.916	3.767
Yellow 33kV BB	33	5.46	312.12	0.743	3.765
Red 33kV BB	33	2.06	117.94	3.917	9.371
Pink 33kV BB	33	5.24	299.38	0.954	3.886
Orange 33kV BB	33	5.84	333.91	0.789	3.500
Green 33kV BB	33	6.08	347.30	0.698	3.378
Basket 33kV BB	33	7.07	404.36	0.594	2.902
Black 33kV BB	33	6.10	348.56	0.683	3.368
White 33kV BB	33	6.46	369.21	0.595	3.189
Sapphire 22kV BB	22	4.84	184.41	0.803	2.773
Mecury 22kV BB	22	2.72	103.61	1.432	4.935
Saturn 22kV BB	22	2.90	110.64	1.928	4.409
Emerald 22kV BB	22	3.76	143.17	0.825	3.626
Jupiter 22kV BB	22	3.05	116.24	0.890	4.493
Uranus 22kV BB1	22	2.91	110.78	1.041	4.692
Uranus 22kV BB2	22	2.91	110.78	1.041	4.692
Pluto 22kV BB	22	2.33	88.61	0.600	5.978
Topaz 22kV BB	22	2.23	85.07	2.020	5.924
Pearl 22kV BB	22	4.11	156.70	0.281	3.386
Jade 22kV BB	22	1.81	69.08	3.015	7.093
Ruby 22kV BB	22	2.52	96.21	1.609	5.295
Mars 22kV BB	22	6.51	248.18	0.228	2.133
Earth 11kV BB	11	10.59	201.69	0.243	0.614
Nandos 11kV BB	11	8.85	168.60	0.166	0.772
Yellow 11kV BB	11	7.72	147.06	0.127	0.896
Blou 11kV BB	11	7.69	146.57	0.146	0.896
Pink 11kV BB 2	11	7.58	144.38	0.150	0.910
Pink 11kV BB 1	11	7.58	144.38	0.150	0.910
Orange 11kV BB	11	7.97	151.84	0.132	0.867
Basket 11kV BB	11	8.65	164.77	0.110	0.800
Green 11kV BB	11	8.11	154.46	0.121	0.853
Black 11kV BB	11	5.21	99.34	0.164	1.330
Ruby 11kV BB	11	5.06	96.37	0.420	1.316
Linkedln 11kV BB	11	11.97	228.09	0.087	0.577

8.4.4   High voltage busbar system per unit values

Table 8-6: High voltage per unit values at 12pm

Bus Name - Voltage (kV)	Nominal Line - Line Voltage kV	Line - Line Voltage Magnitude kV	Line - Line Voltage per unit kV	Voltage angle degrees
ST1 400kV BB1	400	401.75	1.00	-14.46
ST1 275kV BB1	275	285.29	1.04	-14.76
Yellow132kV BB	132	130.16	0.99	-20.35
White 132kV BB	132	131.00	0.99	-19.88
ST1 Sub 132kV BB	132	136.88	1.04	-15.97
Pluto 132kV BB	132	130.90	0.99	-18.22
Pearl 132kV BB	132	131.52	1.00	-19.48
Diamond 132kV BB	132	135.91	1.03	-15.86
Sub 88kV BB	88	89.98	1.02	-17.45
Nandos 88 T-off Node	88	88.20	1.00	-19.28
Nandos 88kV BB	88	87.58	1.00	-22.17
LinkedIn 88kV BB	88	89.81	1.02	-19.23
Basket-88kV BB	88	86.66	0.98	-20.09
Uranus 66kV BB	66	67.73	1.03	-20.53
Topaz 66kV BB	66	67.42	1.02	-20.67
Saturn 66kV BB	66	66.99	1.02	-21.01
Sapphire 66kV BB	66	64.64	0.98	-20.90
Ruby 66kV BB	66	66.41	1.01	-19.11
Pluto 66kV BB	66	67.94	1.03	-20.38
Mercury 66kV BB	66	64.58	0.98	-21.59
Jupiter 66kV BB	66	67.86	1.03	-20.41
Jade 66kV BB	66	66.67	1.01	-19.49
Emerald 66kV BB	66	67.78	1.03	-20.49
Earth 66kV BB	66	63.67	0.96	-21.69
Diamond 66kV BB	66	67.88	1.03	-18.48

8.4.5   Medium voltage busbar system per unit values

Table 8-7: Medium voltage per unit values at 12pm

Bus Name - Voltage (kV)	Nominal Line - Line Voltage kV	Line - Line Voltage Magnitude kV	Line - Line Voltage per unit kV	Voltage angle degrees
Yellow 33kV BB	33	34.05	1.03	-53.23
White 33kV BB	33	33.95	1.03	-52.38
Red 33kV BB	33	33.24	1.01	-54.40
Pink 33kV BB	33	33.91	1.03	-52.99
Orange 33kV-BB	33	33.91	1.03	-52.79
Green-33kV BB	33	33.90	1.03	-52.60
Blou-33kV BB	33	33.94	1.03	-53.28
Black-33kV BB	33	33.91	1.03	-52.52
Basket-33kV BB	33	34.20	1.04	-52.62
Uranus 22kV BB2	22	22.73	1.03	-51.56
Uranus 22kV BB1	22	22.69	1.03	-51.91
Topaz 22kV BB	22	22.88	1.04	-51.46
Saturn 22kV BB	22	22.49	1.02	-51.77
Sapphire 22kV BB	22	22.76	1.03	-52.70
Ruby 22kV BB	22	22.79	1.04	-50.13
Pluto 22kV BB	22	22.74	1.03	10.06
Pearl 22kV BB	22	22.83	1.04	8.72
Mecury 22kV BB	22	22.81	1.04	-52.79
Mars 22kV BB	22	22.50	1.02	-49.41
Jupiter 22kV BB	22	22.75	1.03	-51.32
Jade 22kV BB	22	22.93	1.04	-50.49
Emerald 22kV BB	22	22.45	1.02	8.24
Yellow 11kV BB	11	11.30	1.03	-86.09
Ruby 11kV BB	11	11.37	1.03	10.09
Red 11kV BB	11	11.48	1.04	-86.46
Pink 11kV BB 2	11	11.34	1.03	-84.57
Pink 11kV BB 1	11	11.34	1.03	-84.57
Orange 11kV BB	11	11.18	1.02	-84.17
Nandos 11kV BB	11	11.21	1.02	-54.51
Megan Load Bkr	11	11.48	1.04	-86.46
Linkedln 11kV BB	11	11.25	1.02	-51.61
Green-11kV BB	11	11.08	1.01	-83.65
Earth 11kV BB	11	11.44	1.04	6.25
Blou-11kV BB	11	11.31	1.03	-84.84
Black-11kV BB	11	11.14	1.01	-85.10

8.4.6 High voltage active power load flow

Table 8-8: High voltage active power load flow at 12pm

Terminal i Busbar	Terminal j Busbar	Magnitude Terminal i in p.u.	Magnitude Terminal J in p.u.	Voltage Angle Terminal i in deg	Voltage Angle Terminal j in deg	Loading %	Nominal Line-Line VoltagekV	Active Power Terminal i in MW	Active Power Terminal j in MW
White 132kV BB	Yellow132kV BB	0.9925	0.9861	-19.8759	-20.3495	9.67	132	20.2489	-20.1839
ST1 Sub 132kV BB	Pearl 132kV BB	1.0370	0.9964	-15.9700	-19.4783	19.78	132	44.9110	-43.7958
Pearl 132kV BB	White 132kV BB	0.9964	0.9925	-19.4783	-19.8759	16.95	132	37.5445	-37.4567
Pluto 132kV BB	ST1 Sub 132kV BB	0.9917	1.0370	-18.2246	-15.9700	14.65	132	-32.1047	33.2647
Nandos 88 T-off Node	Nandos 88kV BB	1.0023	0.9952	-19.2847	-22.1666	12.58	88	18.6382	-18.2781
Sub 88kV BB	LinkedIn 88kV BB	1.0225	1.0206	-17.4491	-19.2309	12.75	88	18.8276	-18.5985
Basket-88kV BB	Nandos 88 T-off Node	0.9848	1.0023	-20.0903	-19.2847	14.94	88	-19.5157	19.7045
Nandos 88 T-off Node	Sub 88kV BB	1.0023	1.0225	-19.2847	-17.4491	25.44	88	-38.3427	38.8945
Diamond 66kV BB	Ruby 66kV BB	1.0285	1.0062	-18.4755	-19.1051	5.48	66	5.7191	-5.6245
Pluto 66kV BB	Topaz 66kV BB	1.0293	1.0215	-20.3824	-20.6682	2.20	66	2.3806	-2.3664
Pluto 66kV BB	Emerald 66kV BB	1.0293	1.0270	-20.3824	-20.4895	4.52	66	5.1896	-5.1798
Diamond 66kV BB	Sapphire 66kV BB	1.0285	0.9794	-18.4755	-20.9047	12.10	66	13.8852	-13.3277
Diamond 66kV BB	Sapphire 66kV BB	1.0285	0.9794	-18.4755	-20.9047	12.10	66	13.8852	-13.3277
Sapphire 66kV BB SM	Earth 66kV BB	0.9794	0.9647	-20.9047	-21.6937	14.75	66	16.2763	-16.0683
Diamond 66kV BB	Jade 66kV BB	1.0285	1.0101	-18.4755	-19.4938	2.66	66	3.0031	-2.9563
Earth 66kV BB	Mercury 66kV BB	0.9647	0.9785	-21.6937	-21.5853	4.77	66	-3.7272	3.7735
Mercury 66kV BB	Jupiter 66kV BB	0.9785	1.0282	-21.5853	-20.4145	7.54	66	-7.2681	7.5509
Jupiter 66kV BB	Pluto 66kV BB	1.0282	1.0293	-20.4145	-20.3824	9.58	66	-10.2016	10.2104
Saturn 66kV BB	Pluto 66kV BB	1.0150	1.0293	-21.0079	-20.3824	3.90	66	-4.3491	4.3988
Uranus 66kV BB	Pluto 66kV BB	1.0262	1.0293	-20.5276	-20.3824	6.07	66	-6.9671	6.9848

8.4.7 Medium voltage active power load flow

Table 8-9: Medium voltage active power load flow at 12 pm

Terminal i Busbar	Terminal j Busbar	Magnitude Terminal i in p.u.	Magnitude Terminal j in p.u.	Voltage Angle Terminal i in deg	Voltage Angle Terminal j in deg	Loading %	Nominal Line-Line Voltage kV	Active Power Terminal i in MW	Active Power Terminal j in MW
Pink 33kV BB	Black-33kV BB	1.0275	1.0277	-52.9928	-52.5168	5.39	33	-2.9760	2.9854
Orange 33kV-BB	Green-33kV BB	1.0277	1.0274	-52.7913	-52.5960	6.12	33	-3.2250	3.2294
Yellow 33kV BB	Blou-33kV BB	1.0319	1.0284	-53.2264	-53.2798	2.92	33	1.0125	-1.0103
Basket-33kV BB	Orange 33kV-BB	1.0362	1.0277	-52.6247	-52.7913	8.81	33	3.3708	-3.3545
Basket-33kV BB	Pink 33kV BB	1.0362	1.0275	-52.6247	-52.9928	9.34	33	4.6897	-4.6687
Basket-33kV BB	Blou-33kV BB	1.0362	1.0284	-52.6247	-53.2798	11.55	33	6.6679	-6.6344
White 33kV BB	Black-33kV BB	1.0289	1.0277	-52.3849	-52.5168	15.42	33	9.0550	-9.0460
White 33kV BB	Green-33kV BB	1.0289	1.0274	-52.3849	-52.5960	13.83	33	8.1358	-8.1242
Red 33kV BB	Yellow 33kV BB	1.0074	1.0319	-54.4035	-53.2264	9.55	33	-5.1815	5.2681

8.4.8 High voltage reactive power load flow

Table 8-10: High voltage reactive power load flow

Terminal i Busbar	Terminal j Busbar	Magnitude Terminal i in p.u.	Magnitude Terminal J in p.u.	Voltage Angle Terminal i in deg	Voltage Angle Terminal j in deg	Loading %	Nominal Line-Line VoltagekV	Reactive Power Terminal i in Mvar	Reactive Power Terminal j in Mvar
White 132kV BB	Yellow132kV BB	0.9925	0.9861	-19.8759	-20.3495	9.67	132	7.5057	-8.2596
ST1 Sub 132kV BB	Pearl 132kV BB	1.0370	0.9964	-15.9700	-19.4783	19.78	132	10.7900	-10.6134
Pearl 132kV BB	White 132kV BB	0.9964	0.9925	-19.4783	-19.8759	16.95	132	8.6125	-8.7442
Pluto 132kV BB	ST1 Sub 132kV BB	0.9917	1.0370	-18.2246	-15.9700	14.65	132	-8.4864	6.6936
Nandos 88 T-off Node	Nandos 88kV BB	1.0023	0.9952	-19.2847	-22.1666	12.58	88	-4.7116	4.4193
Sub 88kV BB	LinkedIn 88kV BB	1.0225	1.0206	-17.4491	-19.2309	12.75	88	-6.3456	6.1468
Basket-88kV BB	Nandos 88 T-off Node	0.9848	1.0023	-20.0903	-19.2847	14.94	88	-11.0402	11.0746
Nandos 88 T-off Node	Sub 88kV BB	1.0023	1.0225	-19.2847	-17.4491	25.44	88	-6.3630	7.2843
Diamond 66kV BB	Ruby 66kV BB	1.0285	1.0062	-18.4755	-19.1051	5.48	66	2.5207	-2.8332
Pluto 66kV BB	Topaz 66kV BB	1.0293	1.0215	-20.3824	-20.6682	2.20	66	0.5858	-0.9944
Pluto 66kV BB	Emerald 66kV BB	1.0293	1.0270	-20.3824	-20.4895	4.52	66	1.1063	-1.1598
Diamond 66kV BB	Sapphire 66kV BB	1.0285	0.9794	-18.4755	-20.9047	12.10	66	2.6495	-2.4495
Diamond 66kV BB	Sapphire 66kV BB	1.0285	0.9794	-18.4755	-20.9047	12.10	66	2.6495	-2.4495
Sapphire 66kV BB SM	Earth 66kV BB	0.9794	0.9647	-20.9047	-21.6937	14.75	66	2.6725	-2.5282
Diamond 66kV BB	Jade 66kV BB	1.0285	1.0101	-18.4755	-19.4938	2.66	66	-0.0631	-0.8204
Earth 66kV BB	Mercury 66kV BB	0.9647	0.9785	-21.6937	-21.5853	4.77	66	-3.7128	3.5126
Mercury 66kV BB	Jupiter 66kV BB	0.9785	1.0282	-21.5853	-20.4145	7.54	66	-4.2762	3.9554
Jupiter 66kV BB	Pluto 66kV BB	1.0282	1.0293	-20.4145	-20.3824	9.58	66	-4.7614	4.7593
Saturn 66kV BB	Pluto 66kV BB	1.0150	1.0293	-21.0079	-20.3824	3.90	66	-1.2512	0.8586

8.4.9 Medium voltage reactive power load flow

Table 8-11: Medium voltage reactive power load flow

Terminal i Busbar	Terminal j Busbar	Magnitude Terminal i in p.u.	Magnitude Terminal J in p.u.	Voltage Angle Terminal i in deg	Voltage Angle Terminal j in deg	Loading %	Nominal Line-Line VoltagekV	Reactive Power Terminal i in Mvar	Reactive Power Terminal j in Mvar
Pink 33kV BB	Black-33kV BB	1.0275	1.0277	-52.9928	-52.5168	5.39	33	1.0579	-1.0603
Orange 33kV-BB	Green-33kV BB	1.0277	1.0274	-52.7913	-52.5960	6.12	33	1.5790	-1.5773
Yellow 33kV BB	Blou-33kV BB	1.0319	1.0284	-53.2264	-53.2798	2.92	33	1.3728	-1.3887
Basket-33kV BB	Orange 33kV-BB	1.0362	1.0277	-52.6247	-52.7913	8.81	33	3.9637	-3.9389
Basket-33kV BB	Pink 33kV BB	1.0362	1.0275	-52.6247	-52.9928	9.34	33	2.9161	-2.8816
Basket-33kV BB	Blou-33kV BB	1.0362	1.0284	-52.6247	-53.2798	11.55	33	1.5203	-1.4540
White 33kV BB	Black-33kV BB	1.0289	1.0277	-52.3849	-52.5168	15.42	33	0.4269	-0.4092
White 33kV BB	Green-33kV BB	1.0289	1.0274	-52.3849	-52.5960	13.83	33	0.0271	-0.0022
Red 33kV BB	Yellow 33kV BB	1.0074	1.0319	-54.4035	-53.2264	9.55	33	-1.8465	1.9544
Megan Load Bkr	PointTerm1	1.0437	1.0405	-86.4563	-86.5264	6.92	11	0.7535	-0.7500
Red 11kV BB	T1-1	1.0437	1.0331	-86.4563	-86.5666	4.56	11	0.1738	-0.1710
Red 11kV BB	T2-1	1.0437	1.0116	-86.4563	-86.9932	1.85	11	0.0318	-0.0319

8.4.10 Phase angle results for pre-DG

Table 8-12: High and medium voltage busbar phase angle results – pre-DG

Row	Terminal i Busbar	Terminal j Busbar	Magnitude Terminal i in p.u.	u, Magnitude Terminal j in p.u.	Angle between Voltage and Current Terminal i in deg.	Angle between Voltage and Current Terminal j in deg.
1	ST1 Sub 132kV	Pearl 132kV	1.0370	0.9964	13.5095	-166.3776
2	Pluto 132kV	ST1 Sub 132kV	0.9917	1.0370	-165.1933	11.3773
3	Pearl 132kV	White 132kV	0.9964	0.9925	12.9198	-166.8597
4	White 132kV	Yellow132kV	0.9925	0.9861	20.3383	-157.7448
5	Basket-88kV	Nandos 88 T-off	0.9848	1.0023	-150.5029	29.3374
6	Nandos 88 T-off	Sub 88kV	1.0023	1.0225	-170.5776	10.6077
7	Nandos 88 T-off	Nandos 88kV	1.0023	0.9952	-14.1866	166.4079
8	Sub 88kV	LinkedIn 88kV	1.0225	1.0206	-18.6256	161.7114
9	Diamond 66kV	Ruby 66kV	1.0285	1.0062	23.7855	-153.2644
10	Diamond 66kV	Sapphire 66kV	1.0285	0.9794	10.8031	-169.5859
11	Diamond 66kV	Sapphire 66kV	1.0285	0.9794	10.8031	-169.5859
12	Diamond 66kV	Jade 66kV	1.0285	1.0101	-1.2033	-164.4901
13	Earth 66kV	Mercury 66kV	0.9647	0.9785	-135.1113	42.9492
14	Jupiter 66kV	Pluto 66kV	1.0282	1.0293	-154.9802	24.9912
15	Mercury 66kV	Jupiter 66kV	0.9785	1.0282	-149.5297	27.6470
16	Uranus 66kV	Pluto 66kV	1.0262	1.0293	-167.9053	11.7232
17	Pluto 66kV	Emerald 66kV	1.0293	1.0270	12.0338	-167.3796
18	Pluto 66kV	Topaz 66kV	1.0293	1.0215	13.8234	-157.2062
19	Sapphire 66kV	Earth 66kV	0.9794	0.9647	9.3246	-171.0584
20	Saturn 66kV	Pluto 66kV	1.0150	1.0293	-163.9505	11.0449
21	Basket-33kV	Orange 33kV	1.0362	1.0277	49.6215	-130.4189
22	Basket-33kV	Pink 33kV	1.0362	1.0275	31.8734	-148.3163
23	Pink 33kV	Black-33kV	1.0275	1.0277	160.4311	-19.5536
24	Basket-33kV	Blou-33kV	1.0362	1.0284	12.8440	-167.6382
25	Yellow 33kV	Blou-33kV	1.0319	1.0284	53.5899	-126.0377
26	Orange 33kV	Green-33kV	1.0277	1.0274	153.9131	-26.0317
27	White 33kV	Green-33kV	1.0289	1.0274	0.1912	-179.9848
28	Red 33kV	Yellow 33kV	1.0074	1.0319	-160.3859	20.3543
29	White 33kV	Black-33kV	1.0289	1.0277	2.6993	-177.4100

8.4.11 Sub-Transmission Grid Loss

Table 8-13: Active and reactive power losses

Terminal i Busbar	Terminal j Busbar	Nominal Line-Line Voltage kV	Losses (total) Terminal i in MW	Losses (total) Terminal j in MW	Reactive-Losses (total) Terminal i in Mvar	Reactive-Losses (total) Terminal j in Mvar
ST1 Sub 132kV BB	Pearl 132kV BB	132	1.1152	1.1152	0.1766	0.1766
Pluto 132kV BB	ST1 Sub 132kV BB	132	1.1601	1.1601	-1.7928	-1.7928
Pearl 132kV BB	White 132kV BB	132	0.0878	0.0878	-0.1317	-0.1317
White 132kV BB	Yellow132kV BB	132	0.0650	0.0650	-0.7539	-0.7539
Basket-88kV BB	Nandos 88 T-off Node	88	0.1888	0.1888	0.0344	0.0344
Nandos 88 T-off Node	Sub 88kV BB	88	0.5518	0.5518	0.9213	0.9213
Nandos 88 T-off Node	Nandos 88kV BB	88	0.3601	0.3601	-0.2923	-0.2923
Sub 88kV BB	LinkedIn 88kV BB	88	0.2291	0.2291	-0.1988	-0.1988
Diamond 66kV BB	Ruby 66kV BB	66	0.0946	0.0946	-0.3125	-0.3125
Diamond 66kV BB	Sapphire 66kV BB	66	0.5575	0.5575	0.2000	0.2000
Diamond 66kV BB	Sapphire 66kV BB	66	0.5575	0.5575	0.2000	0.2000
Diamond 66kV BB	Jade 66kV BB	66	0.0469	0.0469	-0.8835	-0.8835
Earth 66kV BB	Mercury 66kV BB	66	0.0463	0.0463	-0.2001	-0.2001
Jupiter 66kV BB	Pluto 66kV BB	66	0.0088	0.0088	-0.0021	-0.0021
Mercury 66kV BB	Jupiter 66kV BB	66	0.2828	0.2828	-0.3207	-0.3207
Uranus 66kV BB	Pluto 66kV BB	66	0.0176	0.0176	-0.0435	-0.0435
Pluto 66kV BB	Emerald 66kV BB	66	0.0098	0.0098	-0.0535	-0.0535
Pluto 66kV BB	Topaz 66kV BB	66	0.0142	0.0142	-0.4087	-0.4087
Sapphire 66kV BB	Earth 66kV BB	66	0.2080	0.2080	0.1443	0.1443
Saturn 66kV BB	Pluto 66kV BB	66	0.0497	0.0497	-0.3925	-0.3925
Basket-33kV BB	Orange 33kV-BB	33	0.0163	0.0163	0.0248	0.0248
Basket-33kV BB	Pink 33kV BB	33	0.0210	0.0210	0.0344	0.0344
Pink 33kV BB	Black-33kV BB	33	0.0094	0.0094	-0.0024	-0.0024
Basket-33kV BB	Blou-33kV BB	33	0.0336	0.0336	0.0663	0.0663
Yellow 33kV BB	Blou-33kV BB	33	0.0022	0.0022	-0.0159	-0.0159
Orange 33kV-BB	Green-33kV BB	33	0.0044	0.0044	0.0017	0.0017
White 33kV BB	Green-33kV BB	33	0.0115	0.0115	0.0250	0.0250
Red 33kV BB	Yellow 33kV BB	33	0.0867	0.0867	0.1079	0.1079
White 33kV BB	Black-33kV BB	33	0.0091	0.0091	0.0177	0.0177

Table 8-14: Pre-DG Sub Transmission Grid Loss

2015/08/31 12:00:00 PM
Grid Load = 204.05 MW, 27.11 Mvar, 205.84 MVA
Grid Losses = 7.77 MW, 18.73 Mvar

8.5   Post DG assessment

Two voltage levels are reported post DG connection as described in the following sections for 132kV Diamond busbar and 33kV basket busbar.

8.5.1   Diamond 132kV busbar assessment for DG

The fault level at the 132kV Diamond busbar is 2,226 MVA. Applying a maximum solar DG size to limit the voltage variation at the point of connection was selected. Solar PV connected to the 132kV point of connection requires double transformation capacity to meet the 132kV level from the 0.69kV generator terminals. This double transformation incurs internal losses of approximately 1%.

8.5.1.1   Sub-transmission load flow – post DG 132kV diamond bus

Figure 8-4 – Page 74, describes the pre-DG load flow of real and reactive power through the 132kV Diamond busbar. Network topology in Figure 8-1 – Page 70 shows the 132kV Diamond busbar being fed directly from the ST1 275kV busbar. This in turn fed from Source 3, a 50MW constant power source. Pre-DG load flow through the 275kV bus is shown in the Figure 8-6.
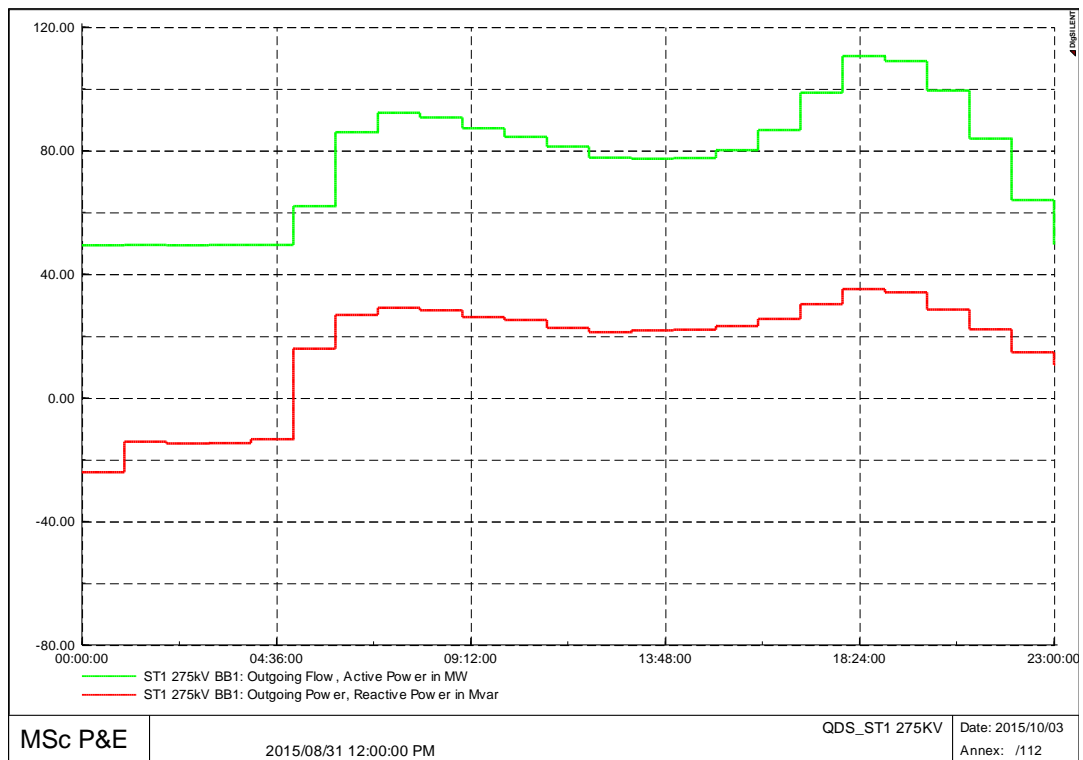
Figure 8-6 275kV Diamond Busbar at 12PM – Pre–DG

The maximum export capacity of 98MW is injected into the 132kV Diamond busbar and alters the load profile shown in Figure 8-7. The corresponding effect on the 275kV bus shows the reduced power during the mid-day peak of the solar PV generator, shown in Figure 8-8.
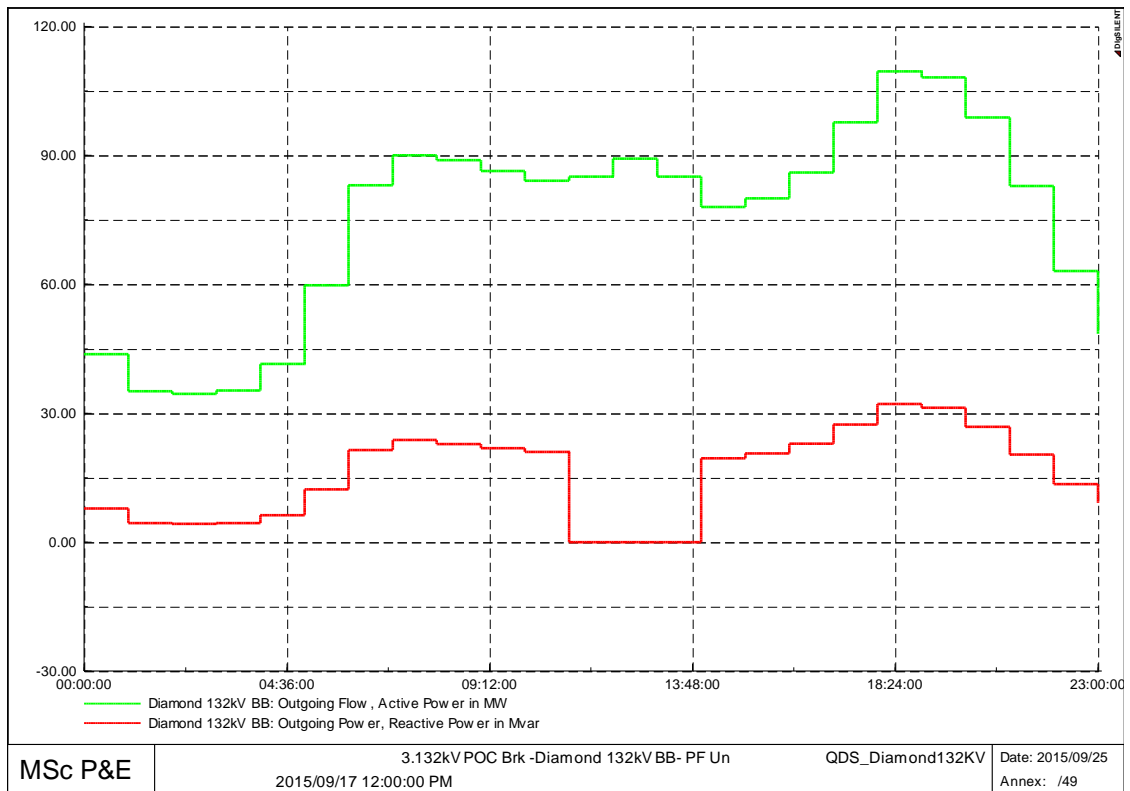
Figure 8-7 132kV Diamond Busbar at 12PM – Post – DG

The altered load profile provides additional power to the network that is not optimally timed and has the effect of increasing power flow and increasing losses.

Profile changes in Figure 8-6 and Figure 8-8 during the mid-day peak are observed. During the maximum export of 98 MW of the solar PV plant, less than 50MW is required from the 275kV bus connected to Source 3. Source 3 is a constant 50MW PV plant. Source 2 is a 100MW constant power source. The reduction in load due to the injection of 98 MW at the Diamond 132kV busbar will be seen at Source 1. Source 1 is the slack bus in the utility grid.
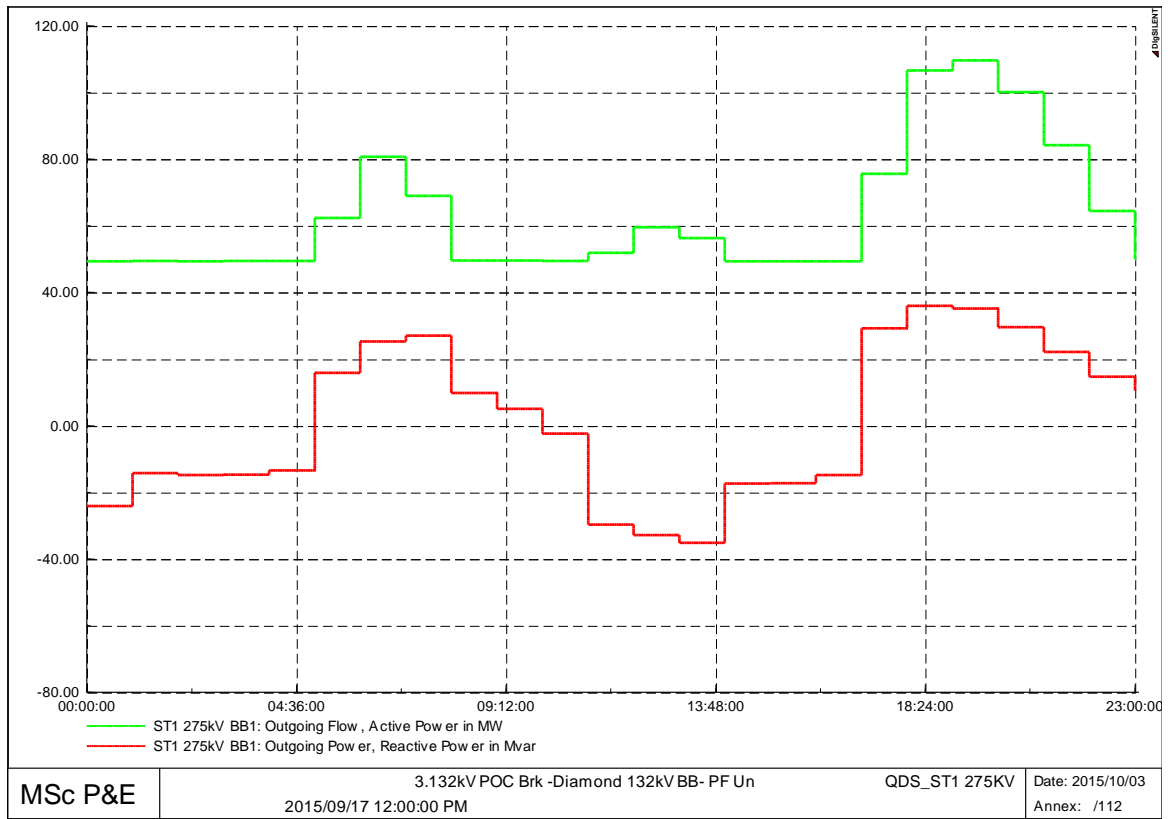
Figure 8-8 Sub 132kV Busbar at 12PM – Post – DG

Confirmation of reduction in load can be verified by the pre- and post- DG load profiles of the 400kV busbar. The reduction in the profile is not obvious due to the order of magnitudes differing.

8.5.1.2   Voltage variation results – diamond 132kV busbar

A DIgSILENT Programming Language (DPL) script was employed for the voltage variation test. The generators output was ramp-up from zero MW full capacity in ten steps of 10%. Each ramped step performed a "locked tap" load flow as described in Section 5.4.

The following series of graphs shows the impact of injecting 89 MW of real power into the Diamond 132kV bus in increments of 10% (X-axis). The (Y-axis) records the voltage change at the Diamond 132kV busbar and associated busbars. The injection of 89 MWs of solar PV while monitoring close proximity busbars yields results shown below.

MSc P&E	3.132kV POC Brk -Diamond 132kV BB- PF Un	Diamond 132kV BB Graphs	Date: 2015/09/25
	2015/09/17 12:00:00 PM		Annex: /100
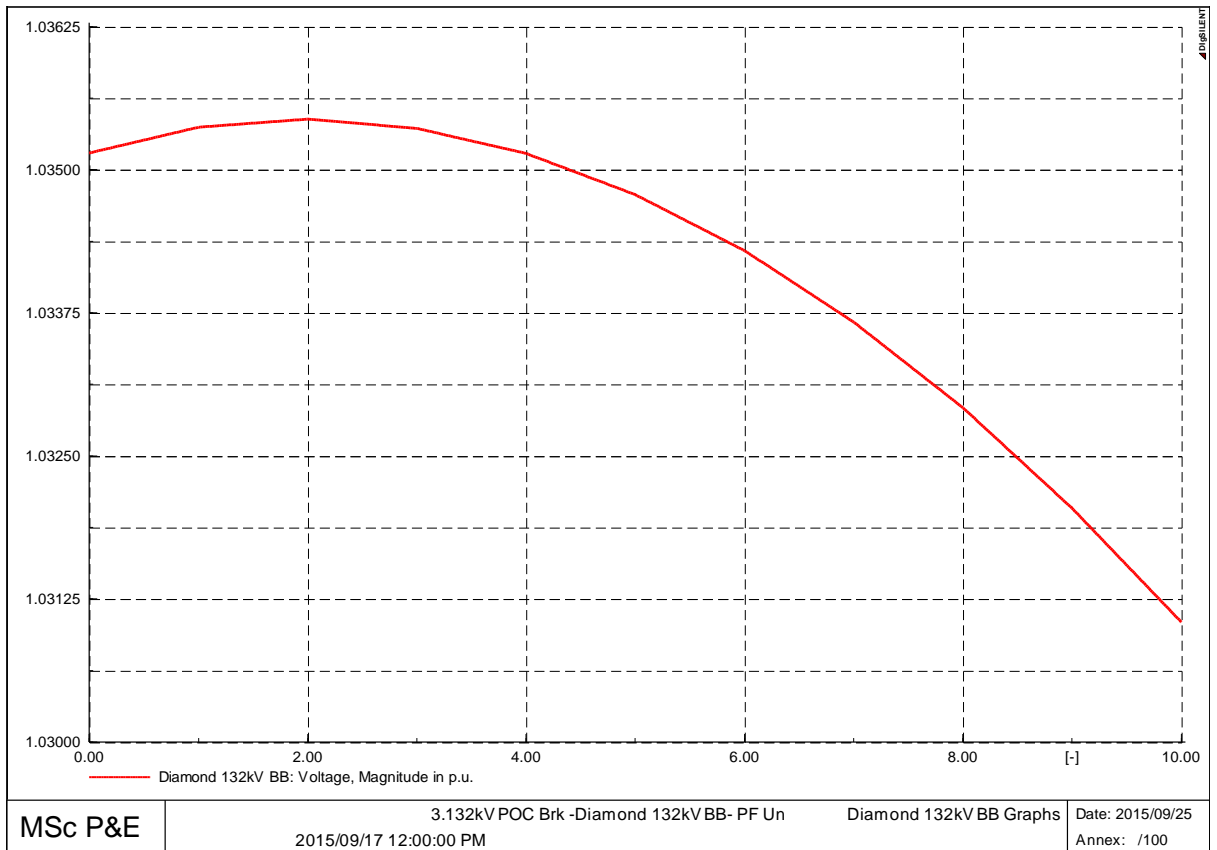
Figure 8-9 132kV Diamond Busbar Voltage Variation Result

The 132kV Diamond voltage variation test under method 1 reports, pre-DG voltage of 1.035p.u and post-DG voltage 1.031p.u. The preferred method displays the change in voltage at each stage of DG ramp-up from 0MW to 89MW of real power.

Figure 8-9 seems counter intuitive as voltage increase is expected with injection of power into the bus. The 132kV busbar is separated from source 3, only by the 275kV Diamond bus. Source 3 is a constant power and voltage source. The dominant nature of a voltage source is to controls voltage to a set point. With all transformer taps are locked during this simulation, the voltage is controlled down to the set point.

Referencing the topology of the sub-transmission network in Figure 8-3 and simultaneously monitoring each of the neighbouring busbars. The following voltage curves are derived from injecting 89MW into the 132kV Diamond busbar.
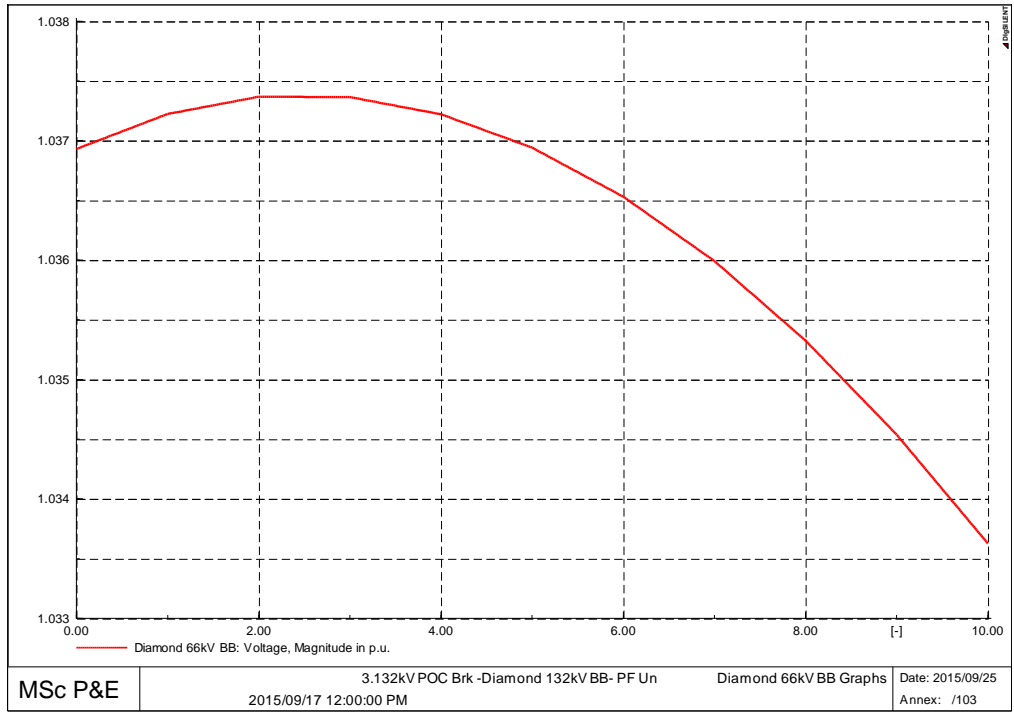
Figure 8-10 Voltage Variation Result of 66kV Diamond Bus response to 89MW injection at 132kV Diamond Busbar
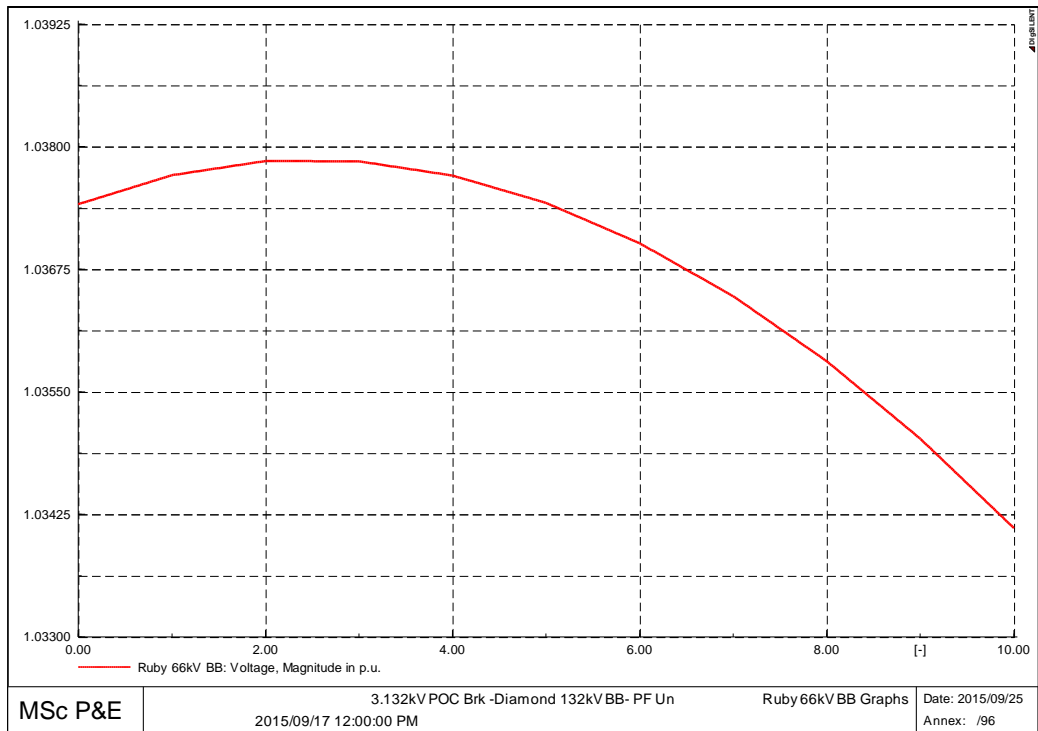

Figure 8-11 Voltage Variation Result of 66kV Ruby Bus response to 89MW injection at 132kV Diamond Busbar
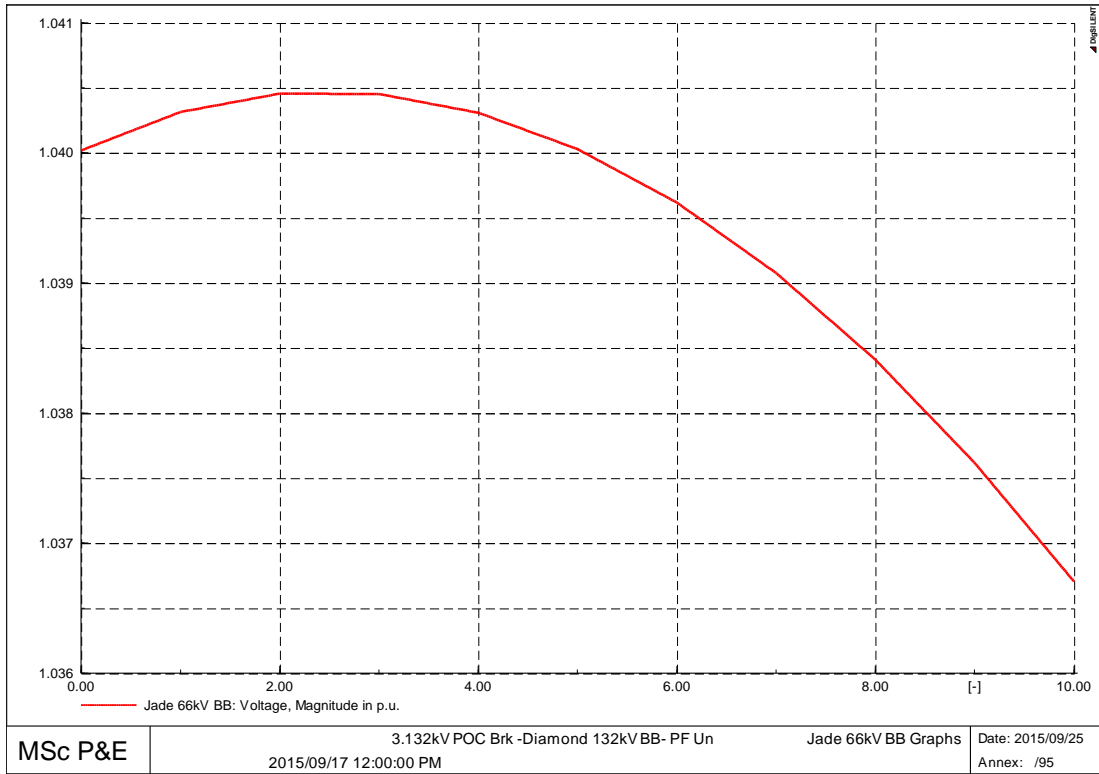
Figure 8-12 Voltage Variation Result of 66kV Jade Bus response to 89MW injection at 132kV Diamond Busbar
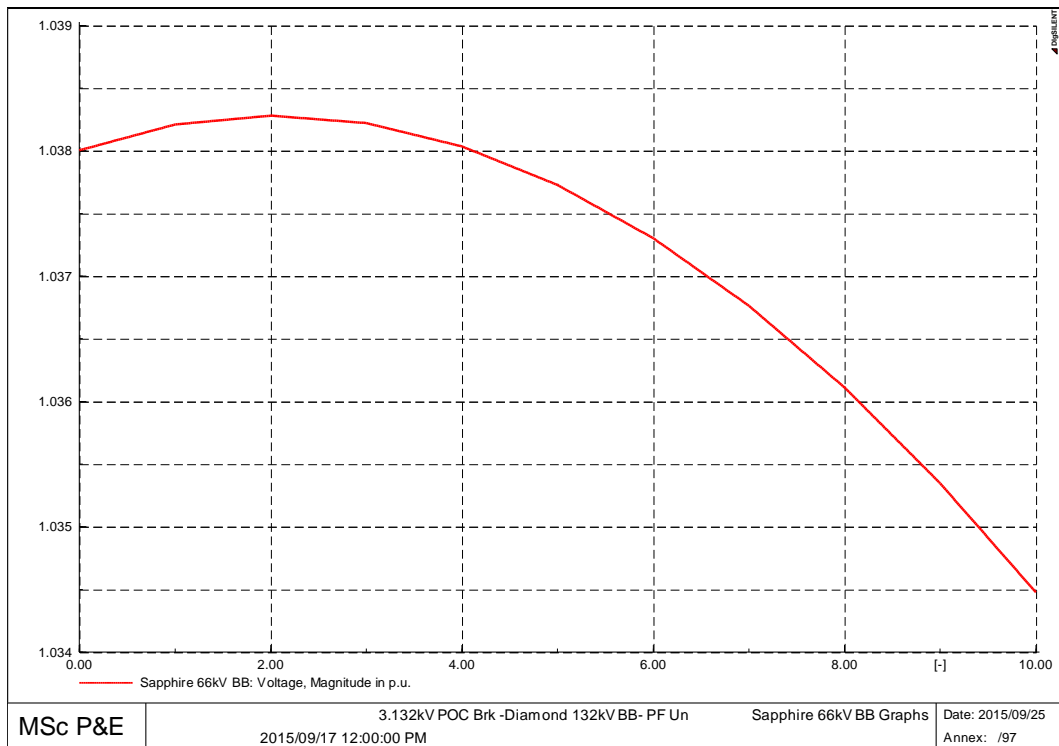

Figure 8-13 Voltage Variation Result of 66kV Sapphire Bus response to 89MW injection at 132kV Diamond Busbar
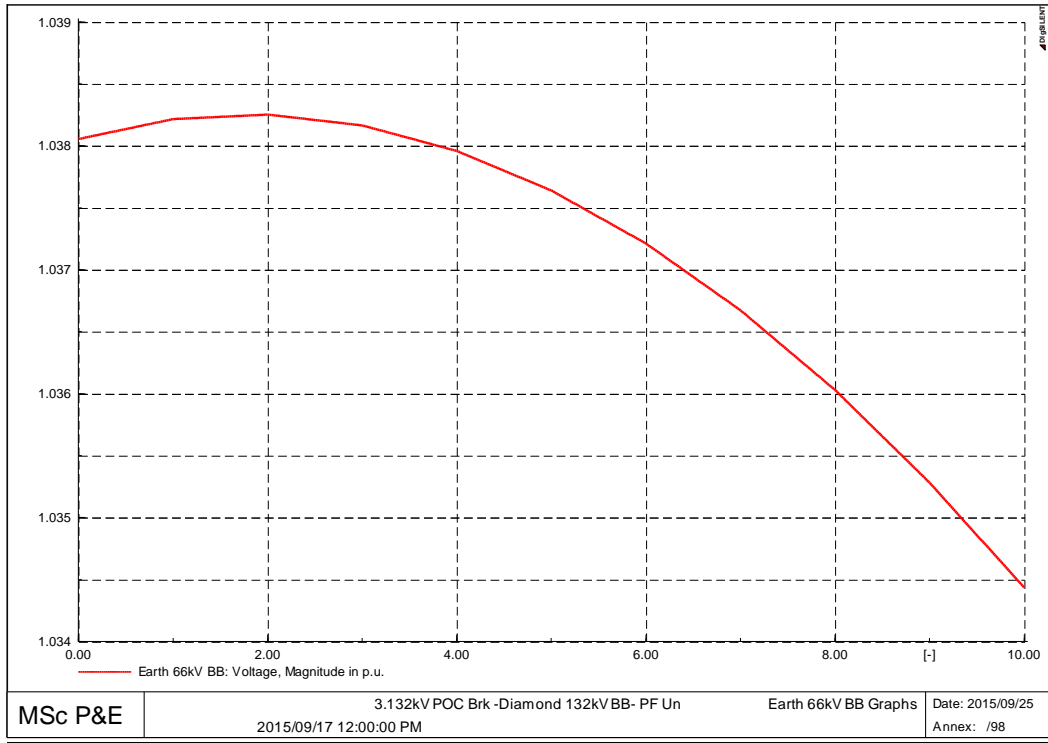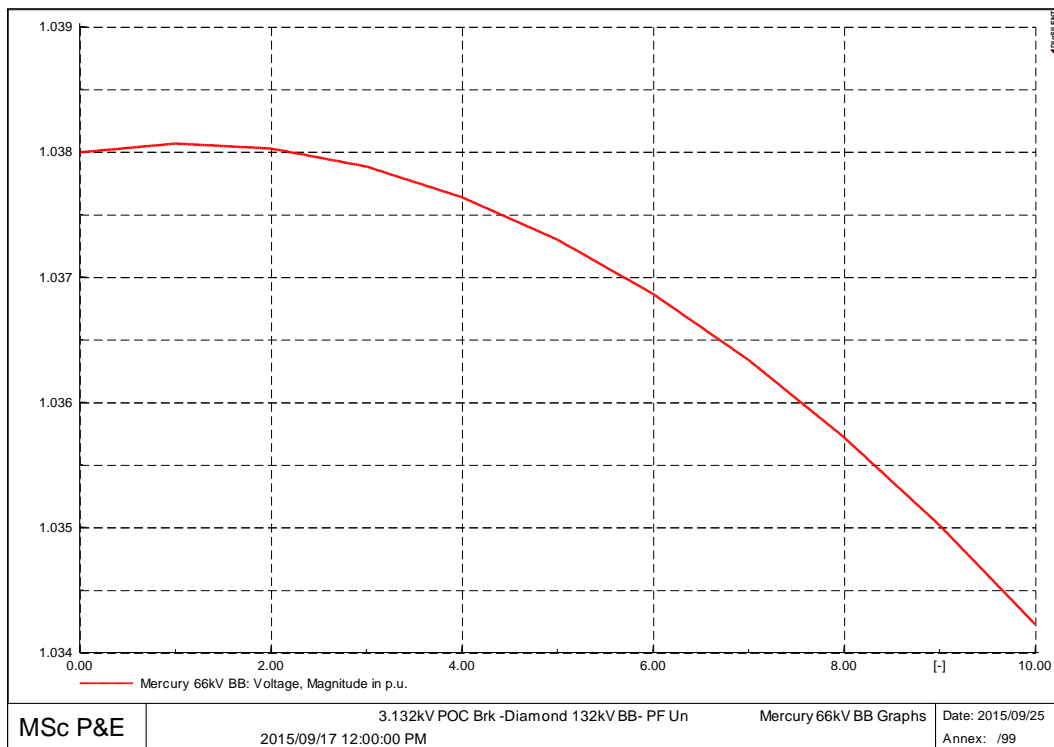
Figure 8-14 Voltage Variation Result of 66kV Earth Bus response to 89MW injection at 132kV Diamond Busbar

Figure 8-15 Voltage Variation Result of 66kV Mercury Bus response to 89MW injection at 132kV Diamond Busbar
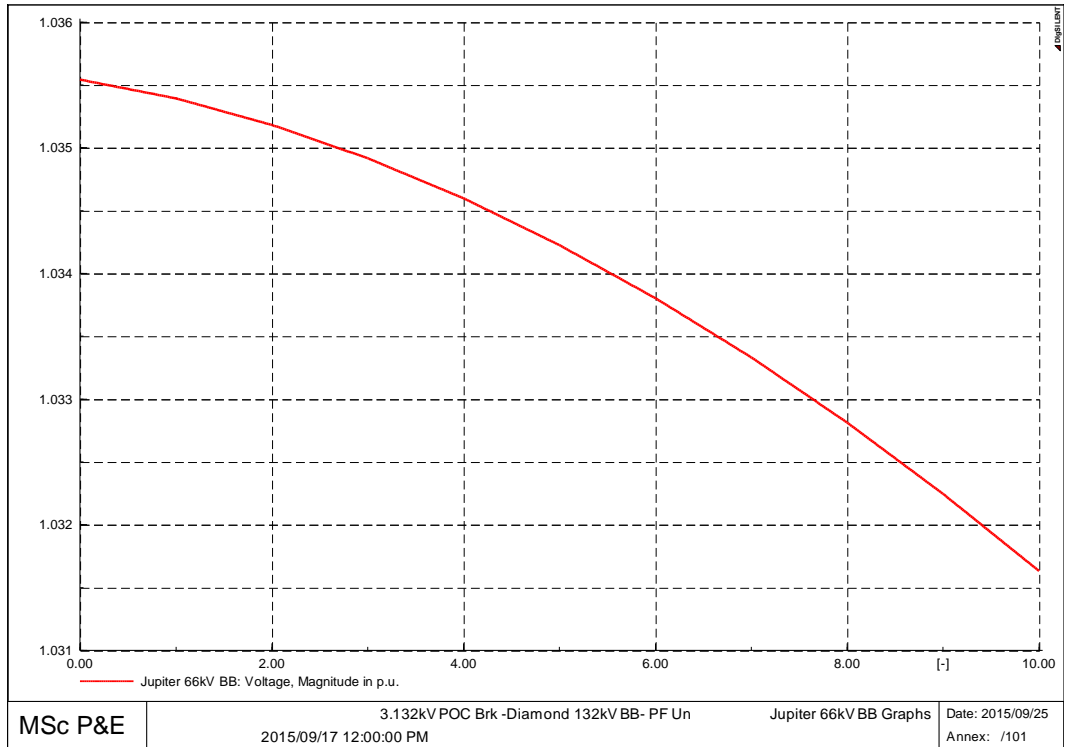
Figure 8-16 Voltage Variation Result of 66kV Jupiter Bus response to 89MW injection at 132kV
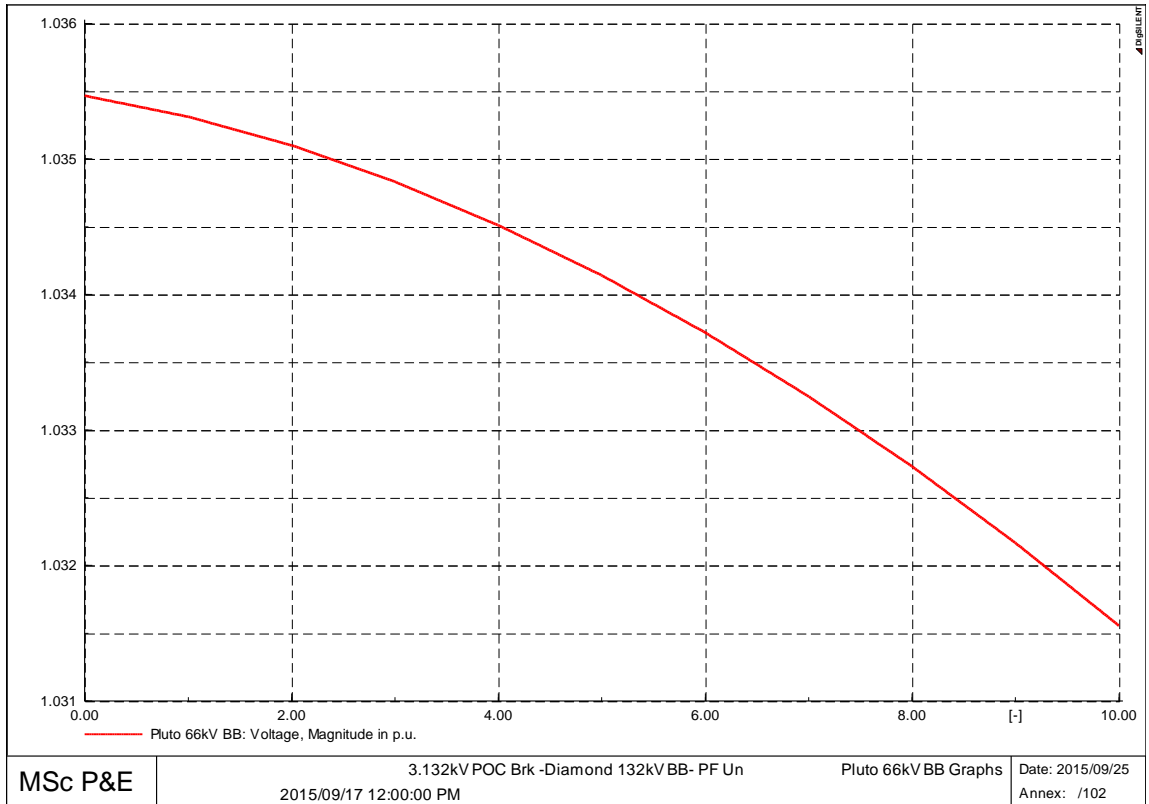Diamond Busbar

Figure 8-17 Voltage Variation Result of 66kV Pluto Bus response to 89MW injection at 132kV
Diamond Busbar

Voltage control by the source effects the entire downstream network and volt drops are exacerbated by line impedance.

8.5.1.3   Sub-transmission grid loss – post DG 132kV diamond

DG sizing at the 132kV diamond busbar shows an increase in grid losses of 98% for real power and 61% for reactive power. Solar power is not consumed at the 132kV Diamond bus. The effect of high levels on DG injection at non-load centre locations leads to increase in losses. Table 8-15 is extracted from the DPF grid summary report.

Table 8-15: Grid Loss Result after 98 MW of DG applied to 132kV Diamond bus

2015/09/17 12:00:00 PM
Grid Summary Post DG on 132kV Diamond 12pm
Grid Losses = 15.43 MW 30.17 Mvar

8.5.2   Basket 33kV busbar assessment for DG

8.5.2.1   Sub-transmission load flow – post DG 33kV Basket bus

Figure 8-18 and Figure 8-20 shows the pre- and post-DG real and reactive load flow profiles at the 33kV Basket bus. Comparison show the reduction in real power at the peak of the solar PV generation. Figure 8-19 shows the change in load profile as real power from solar PV is injected into the bus. This change in profile represents sub-optimal injection resulting in reverse power flow and increased losses.
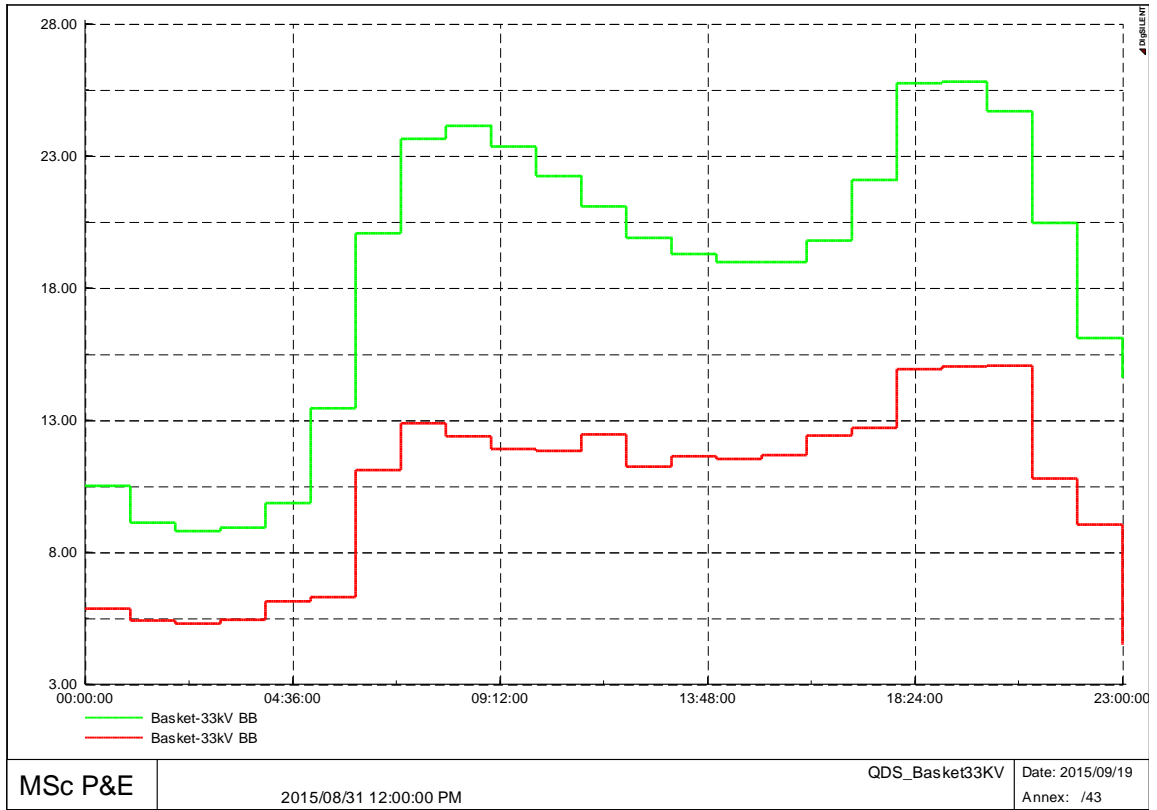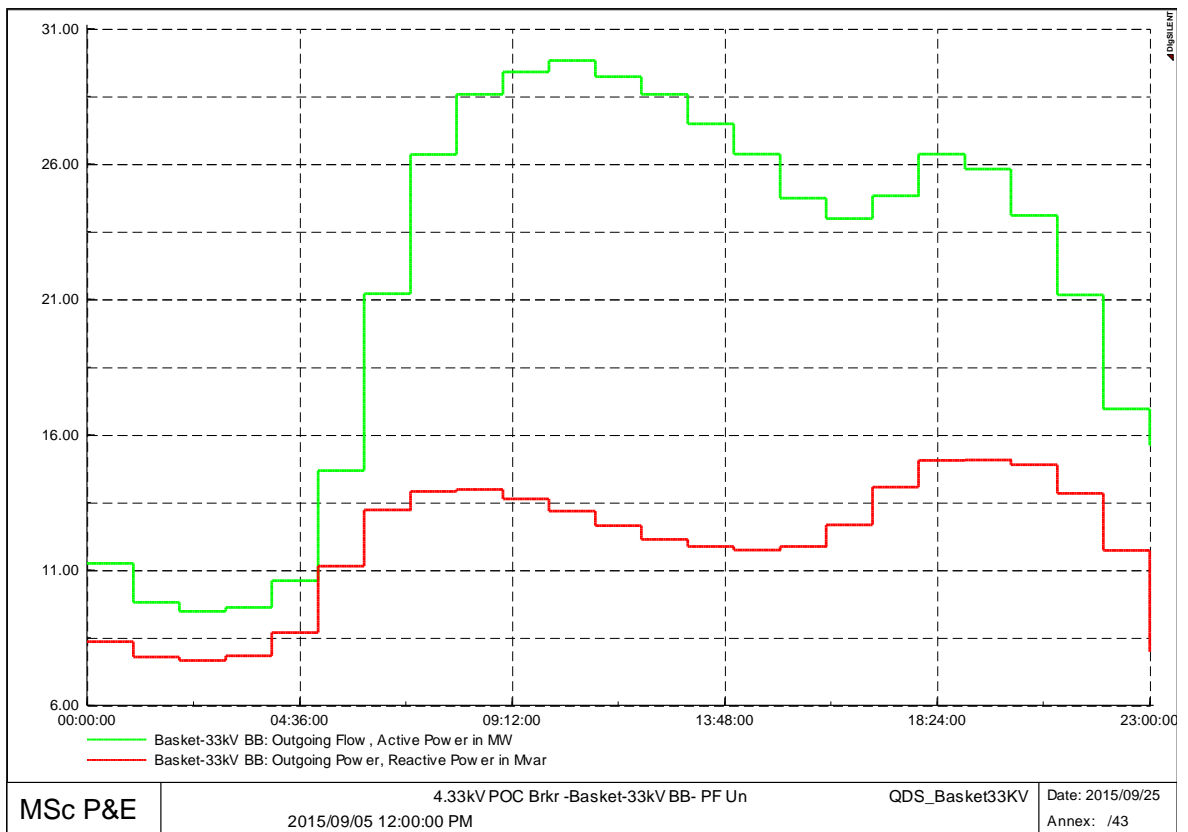
Figure 8-18 33kV Basket Busbar at 12PM – Pre–DG

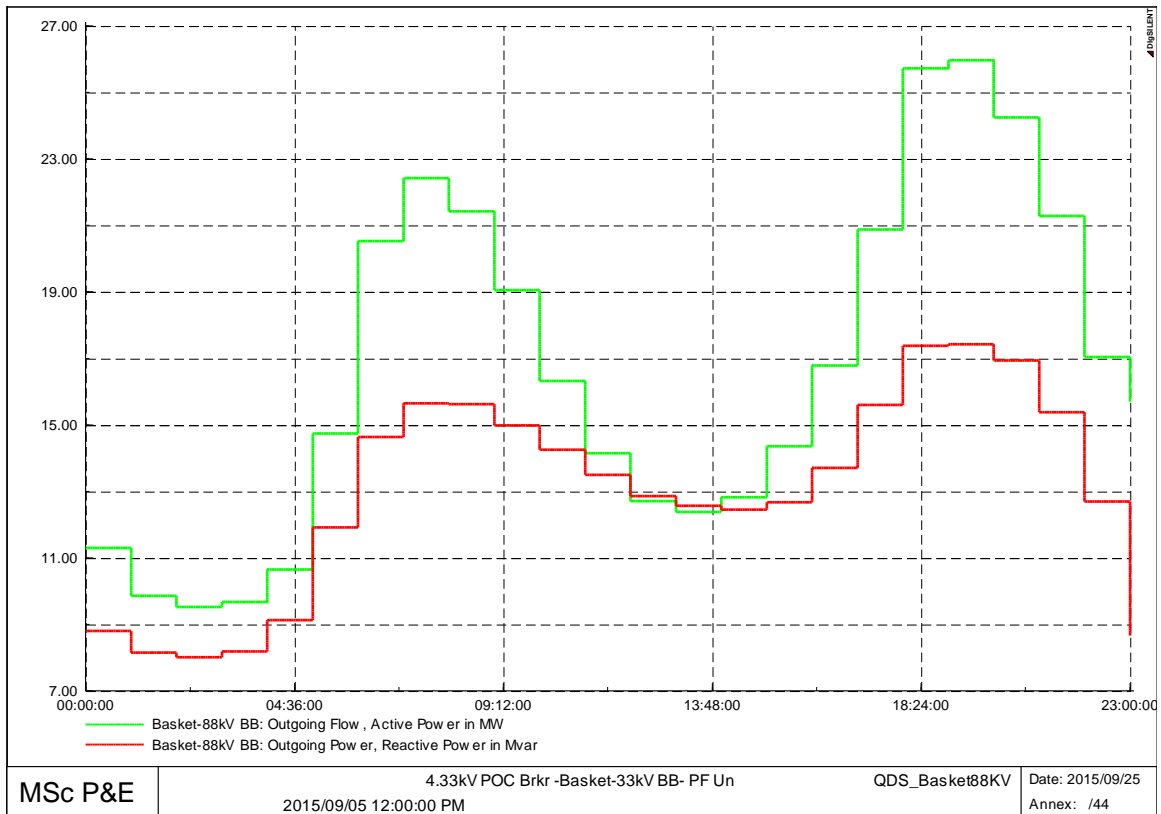Figure 8-19 33kV Basket Busbar at 12PM – Post–DG

Figure 8-20 88kV Basket Busbar at 12PM – Post–DG

The 88kV basket bus supplies the 33kV Basket busbar as shown in Figure 8-2. Solar PV injected into the 33kV Basket bus will have the effect of reducing the required real power from the 88V Basket busbar. The 88kV basket bus load flow demonstrates the reduction in load during the mid-day solar PV peak as confirmed by Figure 8-20 and Figure 8-18.

8.5.2.2   Voltage variation results – 33kV Basket busbar

The fault level at the 33kV Basket busbar is 4000 MVA. Sizing solar PV at 16MVA (16 MW, Cos θ = 1) for a maximum voltage variation of 3% yields the following results. Figure 8-21 to Figure 8-23, demonstrates voltage variation described in section 5.5. The voltage increases due to the injection of real power at 33kV basket busbar.

As real power is injected into the busbar the upstream demand reduces. The volt drop from sending to receiving bus reduces. This raises the voltage at the receiving end. The "bending" of the voltage over the injected load is attributed to the diminishing voltage rise.
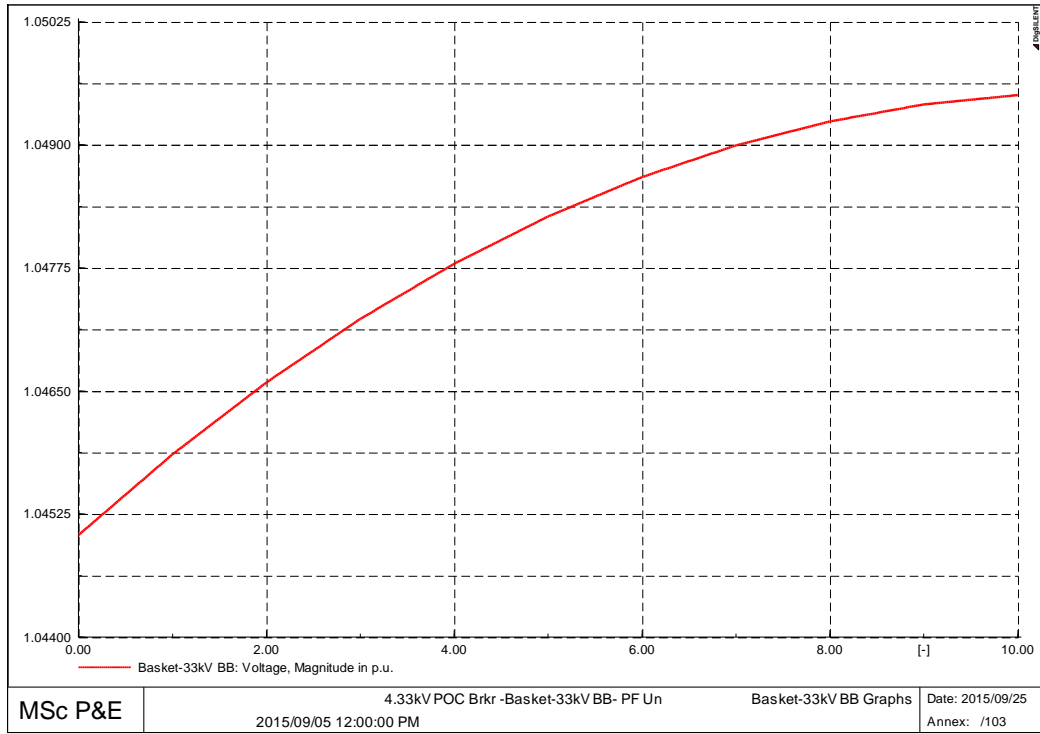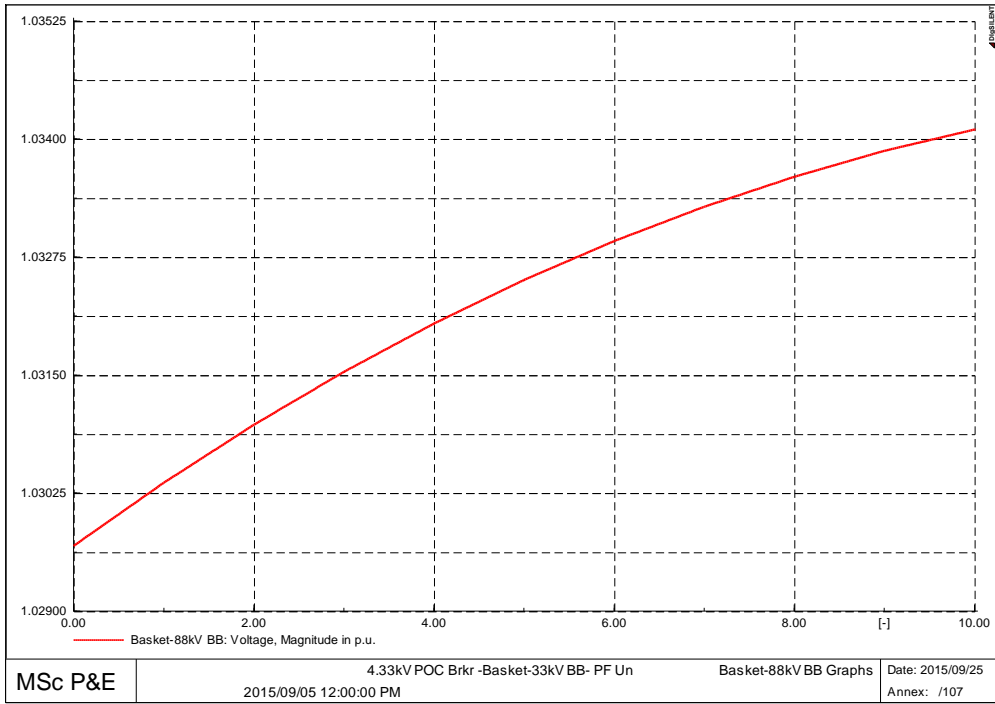
Figure 8-21 33kV Busbar Voltage Variation Result

Figure 8-22 Voltage Variation Result of 88kV Basket Bus response to 16MW injection at 33kV Basket Busbar
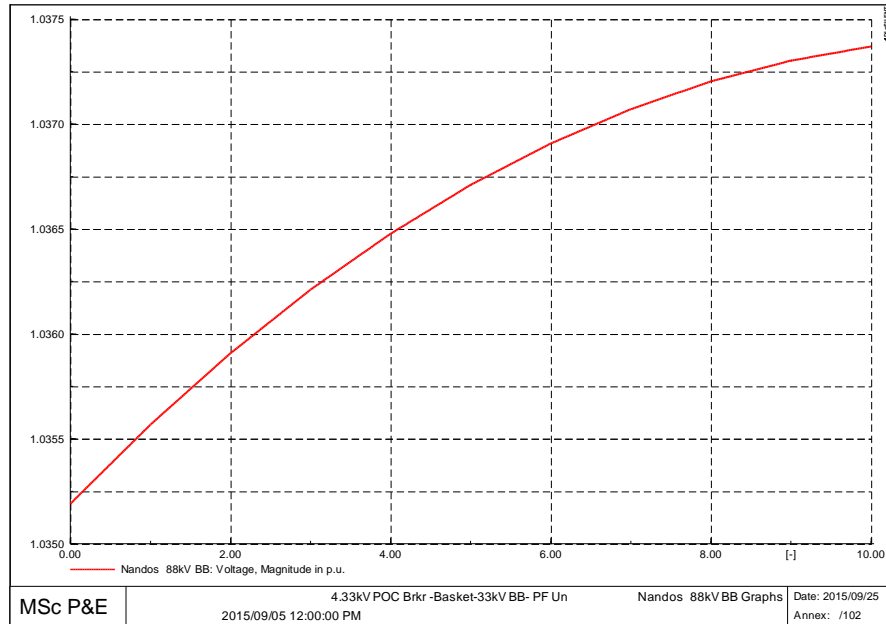
Figure 8-23 Voltage Variation Result of 88kV Nandos Bus response to 16MW injection at 33kV Basket Busbar

8.5.2.3 Sub-Transmission Grid Loss – Post DG 33kV Basket

Moderate sizing of DG can be located at the 33kV Basket busbar, due to its moderate fault level. Post-DG grid losses have reduced by 2.2% for real power and reduced by 18% for reactive power. The effect of moderate levels of DG can decrease grid losses when applied closer to the load centres. Table 8-16 shows the post-DG grid losses after 16MW of solar DG was applied to the 33kV Basket bus.

Table 8-16 Grid Loss Result after 16 MW of DG applied to 33kV Basket bus

2015/09/05 12:00:00 PM
Grid Summary Post DG on 33kV Basket 12pm
Grid Losses = 7.60 MW 15.26 Mvar

8.5.3   Phase angle results for post-DG connection to 11kV Earth busbar

Table 8-17: Phase angle results for post-DG connection to 11kV Earth Busbar

Row	Terminal i Busbar	Terminal j Busbar	Magnitude Terminal i in p.u.	Magnitude Terminal j in p.u.	Angle between Voltage and Current Terminal i in deg.	Angle between Voltage and Current Terminal j in deg.
1	ST1 Sub 132kV BB	Pearl 132kV BB	1.027748	1.005389	6.314307	-170.4446
2	Pluto 132kV BB	ST1 Sub 132kV BB	1.0037	1.027748	-167.7303	3.69474
3	Pearl 132kV BB	White 132kV BB	1.005389	1.003076	8.501927	-170.8422
4	White 132kV BB	Yellow132kV BB	1.003076	0.9989186	18.50217	-158.1779
5	Basket-88kV BB	Nandos 88 T-off	0.9969241	1.010594	-149.1568	30.19442
6	Nandos 88 T-off	Sub 88kV BB	1.010594	1.024336	-167.5946	12.52054
7	Nandos 88 T-off	Nandos 88kV BB	1.010594	1.008817	-20.54636	164.8663
8	Sub 88kV BB	LinkedIn 88kV BB	1.024336	1.024166	-22.86969	160.3484
9	Diamond 66kV BB	Ruby 66kV BB	1.045587	1.034764	21.35336	-151.4274
10	Diamond 66kV BB	Sapphire 66kV BB	1.045587	1.01379	13.55301	-164.4115
11	Diamond 66kV BB	Sapphire 66kV BB	1.045587	1.01379	13.55301	-164.4115
12	Diamond 66kV BB	Jade 66kV BB	1.045587	1.038284	-20.18636	-164.0658
13	Earth 66kV BB	Mercury 66kV BB	1.005205	1.010247	-113.6103	62.93881
14	Jupiter 66kV BB	Pluto 66kV BB	1.035028	1.035588	-157.3036	22.58795
15	Mercury 66kV BB	Jupiter 66kV BB	1.010247	1.035028	-148.1135	24.30095
16	Uranus 66kV BB	Pluto 66kV BB	1.034022	1.035588	-167.5469	11.47833
17	Pluto 66kV BB	Emerald 66kV BB	1.035588	1.033702	12.18063	-167.0296
18	Pluto 66kV BB	Topaz 66kV BB	1.035588	1.031932	4.694807	-156.0565
19	Sapphire 66kV BB	Earth 66kV BB	1.01379	1.005205	18.65493	-160.8706
20	Saturn 66kV BB	Pluto 66kV BB	1.024236	1.035588	-163.3155	10.04295
21	Basket-33kV BB	Orange 33kV-BB	1.040057	1.031197	45.05503	-135.0341
22	Basket-33kV BB	Pink 33kV BB	1.040057	1.031348	31.61128	-148.5787
23	Pink 33kV BB	Black-33kV BB	1.031348	1.029672	142.2174	-38.04894
24	Basket-33kV BB	Blou-33kV BB	1.040057	1.03614	7.448652	-172.6467
25	Yellow 33kV BB	Blou-33kV BB	1.037913	1.03614	97.02614	-83.08225
26	Orange 33kV-BB	Green-33kV BB	1.031197	1.029777	122.8762	-57.1396
27	White 33kV BB	Green-33kV BB	1.030409	1.029777	-7.611811	172.2921
28	Red 33kV BB	Yellow 33kV BB	1.027123	1.037913	-158.6626	20.81436
29	White 33kV BB	Black-33kV BB	1.030409	1.029672	-0.9320244	178.9975